Andrea Schmolzer

Characterization of a novel fluorescent label with potential for cell imaging

Supervisor from Technical University Graz: Dr Marcel Scheideler
Supervisor from Cranfield University: Prof Sergey Piletsky

October 2012

This thesis is submitted in partial fulfilment of the requirements for the degree of Dipl. Ing. Elektrotechnik

Statutory Declaration

I declare that I have authored this thesis independently, that I have not used other than the declared sources / resources, and that I have explicitly marked all material which has been quoted either literally or by content from the used sources.

Graz, ……. ……

date signature

ABSTRACT

Polyamidoamine (PAMAM) dendrimers were used as a grafting core in synthesis of fluorescent organic nanoparticles (NPs). The fluorescent labels used were fluorescent isoindole and fluorescein isothiocyanate. UV-initiated living polymerisation was performed from the surface of the dendrimers to give rise to the NPs that were fluorescent in the core or in the shell. Scanning electron microscope (SEM) showed that the size of the particles was around 30 nm. The modification steps were followed by dynamic light scattering measurements (DLS), in combination with fluorescent measurements. The synthesised nanoparticles were tested for their distribution across bladder cancer cells.

Keywords
PAMAM dendrimer, generation 4; fluorescent organic nanoparticles; fluorescent isoindole; fluorescein isothiocyanate; cancer cells;

ZUSAMMENFASSUNG

Für die Synthese von fluoreszierenden organischen Nanopartikeln (NPs) wurden Polyamidoamin (PAMAM) Dendrimere als innerer Kern für eine nachfolgende Polymerisation benutzt. Als Fluoreszenzmarker wurden fluoreszierendes Isoindol und Fluorescein-Isothiocyanat verwendet. Eine UV-initiierte kontrollierte/lebende radikale Polymerisation wurde durchgeführt, um NP entweder mit fluoreszierendem Kern oderfluoreszierender Schale herzustellen. Die Analyse mittels Rasterelektronen-Mikroskop (SEM) zeigte Partikel in der Größe von 30 nm. Die Modifikationsschritte wurden mittels dynamischer Lichtstreuungsmessung (DLS) und Fluoreszenz-Spektroskopie beobachtet und analysiert. Weiters wurden die synthetisierten Nanopartikel auf ihre Distribution in Blasenkrebszellen getestet.

Schlüsselwörter
PAMAM Dendrimer, 4 Generation; fluoreszierende organische Nanopartikel; fluoreszierendes Isoindol; Fluorescein-Isothiocyanat; Krebszellen;

ACKNOWLEDGEMENTS

I would like to thank and extend my appreciation and gratitude to the following people:

First and primary to my supervisors Prof Sergey Piletsky, Dr Sarah Morgan and Dr Marcel Scheideler for all their help, guidance and patience,

To the Cranfield chemistry group, for their help and support, especially Petya Ivanova-Mitseva, who showed me the fascinating world of polymer-chemistry and supported me under all circumstances, and Dr Michael Cauchi for his cooperation and for providing the fluorescent spectrometer,

To my parents, for making this year possible and for their care and support through rough times,

To my sister and my friends, who are too numerous to acknowledge individually, who were always there for me, in sickness and in thesis.

TABLE OF CONTENTS

LIST OF FIGURES

LIST OF TABLES

ABBREVIATIONS

100% modi	PAMAM dendrimer with 100% surface modification with CNDDA
2-ME	2-Mercaptoethanol
50% modi	PAMAM dendrimer with 50% surface modification with CNDDA
AMAH/FITC-shell	Nanoparticles with poly(*N*-(-3-aminopropyl) methacrylamide hydrochloride) and fluorescein isothiocyanate labelled shell
CNDDA	*S*-(carboxypropyl)-*N,N*-diethyldithiocarbamicacid
DLS	Dynamic light scattering
E_{ex}	Excitation wavelength
E_m	Emission wavelength
FII	Fluorescent isoindole
FITC	Fluorescein isothiocyanate
FNPs	Fluorescent organic nanoparticles
FRET	Förster resonance energy transfer/resonance energy transfer
GFP	Green fluorescent protein
HCL	Hydrochloric acid
IR	Infrared
MA/FII	Nanoparticles with poly(methacrylic) shell and fluorescent isoindole labelled dendrimer core
MA/FITC-core	Nanoparticles with poly(methacrylic) shell and fluorescein isothiocyanate labelled dendrimer core
MIPs	Molecularly imprinted polymers
NMR	Nuclear magnetic resonance spectroscopy
NPs	Nanoparticles
NTA	Nanoparticle tracking analysis
OPA	*o*-Phthalaldehyde
PAMAM	*P*oly(amido amine)
SA	Salicylic acid

SEM	Scanning electron microscopy
ST/FII	Nanoparticles with poly(styrene) shell and fluorescent isoindole labelled dendrimer core
UV	Ultraviolet

CHAPTER 1

INTRODUCTION

1. Introduction

Cell imaging has been and still is a major tool to improve the knowledge of micro-anatomic behaviour of living organisms. It has been used to develop a cell classification system based on the shape, and extracellular and intracellular organisation of cells in different tissues. This has increased the understanding of cell functioning, signalling and regulation. It has also made clinicians able to detect deviations from normal cell properties, which has had major influence on pathology. Different techniques have been developed to image cells and augment the possibility of intracellular signalling and behaviour. However, difficulties arise here due to the small scale at which these mechanisms occur. Improvement of imaging at a subcellular level is therefore encouraged.

This thesis presents the development of a new fluorescent label for cell imaging. For this purpose, two types of particles: poly(amido amine) dendrimers, generation 4, (PAMAM) conjugated with fluorescent isoindole and nanoparticles (NPs) with a fluorescent core and a fluorescent polymer–based shell were synthesised and tested as a tool useful for improving cell imaging. In fact, these types of fluorescent nanoparticles were found to be a promising method for labelling and imaging living cells.

This chapter reviews the theoretical background of cell imaging and the advances that have been made throughout the last decades. First, information about general cell imaging technologies is given. Then the principles of the fluorescent effect are explained. This is followed by a description of how fluorescence can be used for cell imaging and which fluorescent dyes are commonly used for this purpose. Since fluorescent dyes will be coupled to dendrimers to enable them to become incorporated in the cell, the basic design and synthesis of dendrimers will be explained. Next, the most important applications of these polymers in the area of biomedicine are reviewed with particular attention to fluorescent labelling. Finally, a short overview about nanotechnology, fluorescent organic nanoparticles (FNPs), polymerisation techniques and corresponding analytical methods is given.

1.1. Cell imaging technology

Cell imaging technologies are necessary tools to analyse and understand the structure and function of biological systems. The first imaging methods were based on light microscopy. Only non-living cells could be detected due to toxicity of most staining solutions as well as the fixation techniques used to attach cells to the microscopic slides. Over the years new methods and instruments for cell imaging have been developed, which improved the signal detection, resolution, and data collection.

For the purpose of imaging living cells and in vivo, new reagents such as vital dyes and intrinsically fluorescent proteins, such as green fluorescent protein (GFP), (Stephens, 2003; Wang et al., 1989) have been developed. These reagents do not damage the biological samples and have minimal toxicity.

1.1.1. Cellular staining

Cellular staining is used to improve the visualisation of cells and cell components under a microscope. To image different cell components, such as the nucleus or the wall of a cell, in one picture, different stains can be used simultaneously. As most of the stains are toxic the stain is often used on fixed or non-living cells. However, a few staining solutions can be used on living cells. These staining solutions are mostly fluorescent molecules which are classified in two groups. The first group contains biological molecules which exhibit internal fluorescence. The larger and more commonly used group contains the synthetic fluorescent dyes which can be exited using light of a specific wavelength to emit fluorescence.

Before the cells can be analysed, the sample has to be prepared. Five steps need to be performed in this preparation procedure. These are permeabilisation, fixation, embedding, mounting and staining.

1.1.1.1. Permeabilisation

Permeabilisation is used to dissolve the cell membranes in order to allow larger dye molecules to enter the cell. This step is only required when the staining solution requires access to the inside of the cell for a reaction with its analyte. This reaction is achieved by using a mild surfactant, such as Triton or Tween-20 (Abcam, 2011).

1.1.1.2. Fixation

The aim of the fixation step is to stabilise cellular tissue and preserve it for an increased lifetime outside its natural environment. During this process, the cellular

organelles are immobilised whilst the cellular structure is retained. The fixation process involves using chemical fixative, which creates chemical bonds between proteins. Commonly used fixatives are formaldehyde, ethanol and methanol, but the fixative used depends on the type of cells, stabilisation period, used imaging technique and purpose of the sample. Other procedures that can be used are heating or freezing.

1.1.1.3. Embedding

Embedding of a tissue sample is defined as converting the tissue into a solid form which can be sectioned. This step is mostly performed with a wax or gel-like component which is able to make cross-links between the different components in the samples. Mostly, paraffin or nitrocellulose is used for this purpose. After this step, the tissue can be sectioned by a microtome or ultramicrotome depending on the thickness of the sample slices that is desired. Cryomicrotomes are used for frozen samples.

1.1.1.4. Mounting

Mounting is a process in which the cells are transferred onto a glass or polymer slide for microscopy imaging. After the transfer of the cells, a coverslip slide is placed on the top of the cell sample. To present the cells near the coverslip, the slip has to be squeezed strongly to the microscope slide. However, the pressure on the sample needs to be controlled to prevent cell damage. To avoid this issue, cells can be grown directly on the glass slide.

1.1.1.5. Staining and negative staining

The process of staining is important to make a distinction between the analyte or organelle of interest and the remainder of the cell. This contrast can be increased by a negative staining of the surroundings. The process can be performed before or after fixation or mounting. Two major types of staining are recognised, i.e. direct staining and immunological staining. The purpose of direct staining is to give general information about the morphology of the cells in the sample. This can aid in

differentiating cell types and distinguishing pathological cell lines from their healthy counterparts. Direct staining can also be used for cell quantification. The best known type of direct staining is a haematoxylin-eosin staining. Haematoxylin is a blue stain used to visualise basophilic cell structures such as chromatine and ribosomes. Eosin stains the acidic structures with a red colour. Eosin can for example stain collagen and mitochondria. Immunological staining is used to provide information about the expression of proteins or other biomolecules. This is based on the visualisation of antibody-linked probes in which the probe can be an enzyme (immunochemical) or a fluorescent molecule (immunofluorescent). Immunological staining has a higher specificity compared to direct staining. The best resolution can be obtained by fluorescent staining. For this purpose, non-cytotoxic fluorophores are mostly used for living cell imaging (Baschong and Aebi, 2006; Greenwald and Brown, 2004).

1.2. Fluorescence

The phenomenon of the fluorescence effect was first described by Sir George Gabriel Stokes in 1852. He observed with a relatively simple experiment that a colourless quinine solution absorbs ultraviolet light (UV) and emits light in the visible range of the electromagnetic spectrum. Stokes used for his experiment blue glass from a church window as an excitation filter. This filter transmitted light from the sun with a wavelength below 400 nm. A yellow glass of wine was used as an emission filter and the quinine solution was placed between both filters. Stokes observed a blue colour near the surface of the quinine solution. This is due to the fluorescent emission of quinine at a wavelength of about 450 nm and the solution absorbed all of the UV light in the first millimetres. Stokes also found out that quinine exhibits the inner filter effect, which means that the light was “enfeebled” after passing through the solution and could no longer excite quinine (Lakowicz et al., 2008).In other words, when light is seen as a particle (photon), most of these particles are absorbed at the surface of the quinine solution. This makes light unable to excite quinine molecules which are further

away from the light source. The light that is emitted by the surface molecules can excite the bulk molecules. However, the energy of this excitation is lower, which reduces or impairs the possibility for fluorescent emission in the bulk solution.

1.2.1. Visible light spectrum

The visible light spectrum is the region that can be detect by the human eye. The resulting visible light is the electromagnetic radiation of a particle, which is visible to the human eye. Each colour is determined by a different length of the electromagnetic waves. The visible light spectrum ranges from near infrared (IR, around 700 nm) to near ultraviolet (UV, around 400 nm) (Starr et al., 2010).

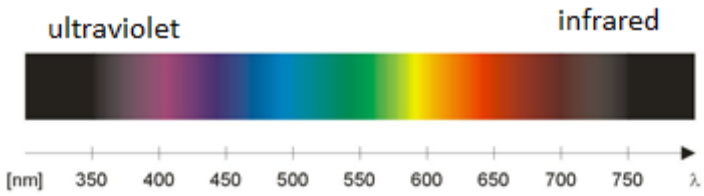

Figure 1.1: visible light spectrum from UV (300 nm) to IR (700 nm)

1.2.2. Appearance of the fluorescence light

The emission of light by any substance is called luminescence and occurs when the substance loses its energy as a photon while an electron returns from an excited state to the electronic ground state. Fluorescence as well as phosphorescence belongs formally to the family of luminescence. Fluorescence is defined as the emission of the light from a singlet excited state. In the singlet excited state all electrons in a molecule are spin-paired. The electron in the excited orbital is therefore paired to an electron with opposite spin in the ground state. Due to this pairing, the return of the excited electron to the ground state is allowed based on the laws of quantum mechanics. This relaxation occurs rapidly through the emission of a photon (Lakowicz, 2006).

Phosphorescence describes the emission of the light from a triplet excited state. One set of electron-spins is unpaired in this state (Lichtman et al., 2005). Since the excited electron has the same spin as the free electron in the ground state, transition to the ground state is forbidden. Therefore, the emission rate of excitation energy by phosphorescence is slow.

To obtain a better insight of the processes involved in the excitation and relaxation processes in a luminescent molecule, different schemes have been developed. One of the possibilities is the use of Jablonski diagrams.

1.2.3. Jablonski diagram

A Jablonski diagram is the most common way to schematically illustrate the process between the absorption and emission in a molecule. This diagram provides a way to determine which energy levels in different molecular orbitals are responsible for the phenomena of fluorescence and phosphorescence.

The following Figure (Figure 1.2) shows a typical Jablonski energy diagram. The diagram is drafted with electronic states divided into their different vibrational energy states. Further classification can be done on the rotational states between the vibration states; however these are not shown here for simplicity. In this Figure, the singlet ground, first and second electronic states are denoted by S0, S1 and S2 while the triplet electronic state is called T1. The energy level of this triplet state is between the ground state and the first electronic state. In every electronic or triplet state the fluorophore can exist in a number of vibrational energy levels indicated by 0, 1, 2, etc.

During excitation, a photon from excitation light source can interact with one of the valence electrons. After the light absorption the electrons of the fluorochrome can be excited from the ground electronic state to a higher electronic state and usually to a higher vibrational energy level. This transfer can however only occur when the energy

of the exciting photon is exactly equal to the difference in energy between two electronic or vibrational states (Resch-Genger, 2008). In the condensed phase the molecules can rapidly relax to the lowest vibrational level in the higher electronic state. This event is called internal conversion. The molecule returns then to the ground state typically in a higher excited vibrational energy level. At the ground state the molecules reaches thermal equilibrium. The type of energy that is released during this relaxation process is mostly heat, potential, collisional or luminescent. Energy is only released as fluorescence when the excited electron jumps from the lowest vibrational state of the S1 electronic state to the lowest vibrational state of the ground state.

Applied to phosphorescence: after absorption the electron has been excited to a higher electronic state, where it undergoes a spin conversion to the triplet electronic state. This process is called intersystem crossing. After reaching the triplet state the electron can return into the ground state. When it returns from the lowest vibrational energy level of the triplet state, phosphorescence occurs. In other occasions, the electron can be re-excited to a singlet state and then return to the ground state by the process of delayed fluorescence. Both phosphorescence and delayed fluorescence are however rare (Lakowicz et al., 2008).

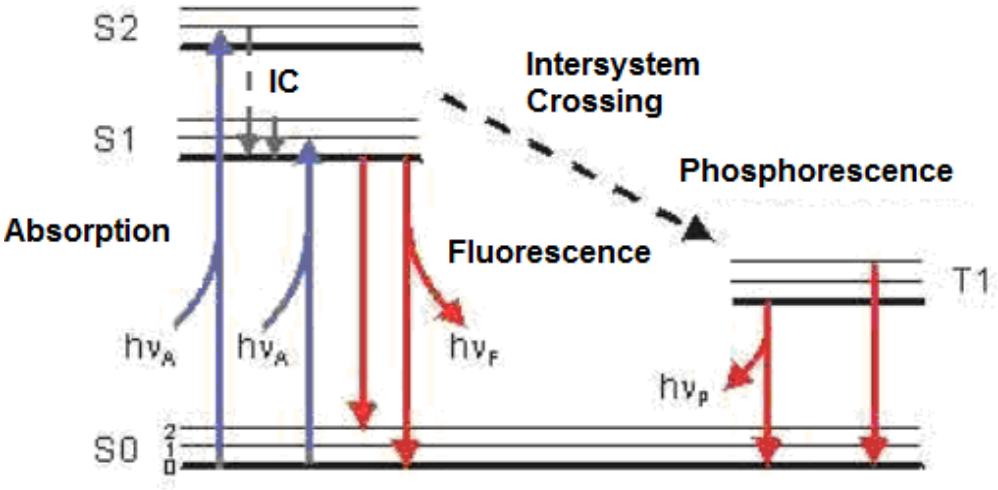

Figure 1.2 [source: (Lakowicz et al., 2008) **]:** typical Jablonski diagram; S_0, S_1 and S_2 are the singlet ground, first and second electronic states; T_1 is the triplet electronic state; 0,1,2 etc. are the vibrational energy levels; $h\upsilon_A$ is the absorption of an excitation photon, $h\upsilon_F$ is the energy of the fluorescence photon and $h\upsilon_P$ is the energy of the Phosphorescence photon; IC is the internal conversion and occurs when the molecule rapidly relax to the lowest vibrational level of S_1; Intersystem Crossing is the conversion of S_1 to T_1;

The energy that is released when the excited electron returns to the ground state is lower than the excitation energy itself. The difference between the excitation and emission energy is called the Stokes' shift and depends on the nature of the fluorescent molecule.

1.2.4. Stokes' shift

In 1852, the mathematician and physician Sir George Gabriel Stokes discovered that the emitted light of every fluorochrome has a bigger electromagnetic wavelength then the wavelength of the absorbed light. From this it follows that the radiated (fluorescent) light of every material shows a shift in wavelength towards a higher wavelength. This phenomenon normally occurs during the fluorescence effect and also in the Raman effect.

In the case of fluorescence, the Stokes' shift is the difference of the wavelength between the absorption and the emission spectra at their maxima (Figure 1.3). This difference occurs due to a loss of energy during the excitation and emission process. When the system absorbs a photon, it gains energy and enters into an excited state. The system will then try to relax and lose its energy. Most energy is released by the emission of heat. In another case, the excited system will collide with its surrounding and lose energy. In conductive environment, the excited energy can be released by transferring electrons to neighbouring molecules. With luminescence, the excitation energy is removed by emitting a photon. For fluorescence, the excited electron first has to be transferred to the lowest vibrational state of the first singlet state. Most electrons will however be in another state after excitation. The extra energy needs to be removed by other processes such as internal conversion. The loss of this energy gives rise to a lower energy of the resulting radiation compared to the incoming radiation. Based on Planck's law, energy is inversely proportional to the wavelength of light. The wavelength of the emission spectra therefore increases with regard to the excitation spectrum (Valeur, 2002).

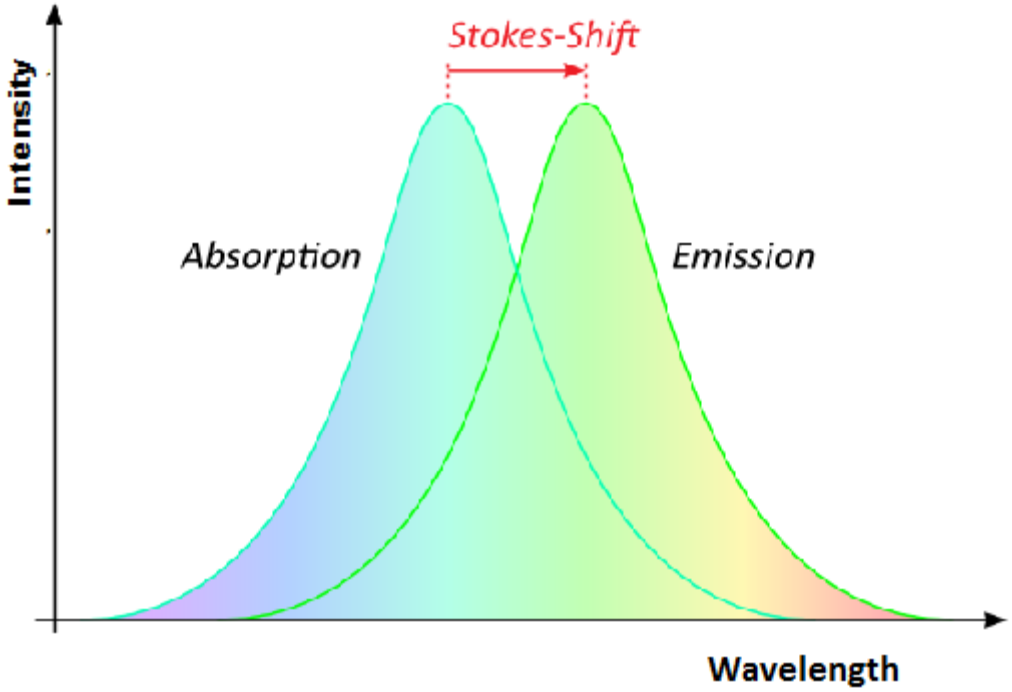

Figure 1.3 [source: (Niedermayr, 2011)**]:** shows an example of Stokes' shift within the fluorescence effect

1.2.5. Fluorescence lifetime and quantum yields

The most important characteristics of a fluorophore are probably the fluorescent lifetime and quantum yield. The lifetime of a fluorophore determines the available time of a fluorophore after the electron reaches the excited state to return to the ground state and give a fluorescent signal until the energy is radiated in form of a photon. The ratio of the number of emitted to the number of absorbed photons is called the quantum yield and describes the efficiency by which a fluorophore relaxes (Lakowicz, 2006).

As already quoted, a molecule will never solely release its excitation energy by fluorescence. Different processes take place which can reduce the intensity of the signal. These processes can occur within the excited molecule or between the

molecule and its environment. One of the most important intermolecular processes is fluorescence quenching.

1.2.6. Fluorescence quenching

Fluorescence quenching is a process which decreases the intensity of a fluorescence signal. It occurs due to several mechanisms such as collisional quenching, also called dynamic quenching, static quenching or because of a resonance energy transfer (FRET) reaction (Hof et al., 2005).

1.2.6.1. Collisional or dynamic quenching

The fluorescence intensity in collisional quenching decreases because the excited fluorophore collides with a quencher molecule. During this collision, the energy of the excited fluorophore will be transferred onto the quencher molecule and deactivate the excited molecule. The rate at which this deactivation occurs is faster than the rate of relaxation by fluorescence emission. Therefore, this process further decreases the fluorescence intensity by decreasing the fluorescence lifetime. A lower amount of excitable molecules will remain activated long enough to fluoresce. A higher ratio of quenching molecules to fluorophores increases this loss in intensity with time. The ratio does however not affect the possibility to observe the fluorescent process, as only the lifetime of the fluorophore is going to be reduced and not the fluorophores' ability to fluoresce (Caldin, 2001).

1.2.6.2. Static quenching

In the case of static quenching, the fluorophore builds a complex with a quenching molecule. This new complex is no longer fluorescent. Therefore, the fluorescence signal will either be decreased or extinguished. The concentration of the fluorophore and the quenching molecule plays an important role in this process as the number of

excited fluorophores is going to be reduced more significantly with a higher concentration of the quenching molecules (Goldys, 2009).

1.2.6.3. Resonance energy transfer quenching

The resonance energy transfer quenching also known as the Förster resonance energy transfer (FRET) is a mechanism which describes the energy transfer between two fluorophores. Here, a donor fluorophore transfers its energy to an acceptor fluorophore through a nonradiative dipole-dipole coupling. Due to this the intensity of the donor fluorophore decreases or becomes extinguished. For this process to occur, the donor and acceptor fluorophore have to be in close proximity of one another. The donor also has to be able to excite the acceptor with its emission spectrum. The closer the maximal absorption wavelength of the acceptor approximates the donor's maximal emission wavelength, the higher the energy transfer. This process can therefore be beneficial in specific circumstances were cell signalling or protein interactions need to be determined. One of the proteins of interest can be conjugated with the donor fluorophore and the other with an acceptor fluorophore. The sample can then be excited with the donor excitation wavelength. If the donor and acceptor are close to each other, resonance energy will be transferred and the acceptor molecule will be excited. This will then give rise to a fluorescent signal during the relaxation of the acceptor molecule. Interactions at the nanometer scale can be observed in this way if the fluorophores are chosen appropriately. The locus of interaction can also be determined using this process (Resch-Genger, 2008).

Another problem that needs much attention is photobleaching. This will be discussed in the next paragraph.

1.2.7. Photobleaching

The phenomenon of photobleaching describes the loss of the fluoresce ability of a fluorophore due to a photon-induced chemical damage and covalent modification. If the electron of a fluorophore transits from an excited singlet state to the excited triplet state, then the fluorophore can interact with other molecules and produce irreversible covalent modifications. As the triplet state is relatively long-lived, the excited molecules have much longer time to undergo a chemical reaction with the environment. Photobleaching of a fluorophore occurs after an average number of excitation and emission cycles and is depending on the molecular structure of the fluorophore and the local environment. Whereas some fluorophores are more robust and can undergo thousands or millions cycles before bleaching, are other fluorophores less stable and bleach quicker. Sometimes the fluorescence intensity drops so fast, that it is almost impossible to create a good picture (Pawley, 2006).

Photobleaching leads to a dramatic loss of fluorescence intensity of a fluorophore. In order to capture satisfied images of a specimen new dyes and fluorophore protection strategies have to be developed.

To avoid problems with fluorescence measurements, different dyes have been developed. This has also given the opportunity to use different dyes on the same sample to improve resolution and contrast. The major types of fluorescent dyes will be discussed in the next section.

1.2.8. Fluorescent dyes

The following chapter reviews commonly used fluorescent dyes. In particular the two dyes, fluorescent isonidole and fluorescein isothiocyanate, which were used in this thesis. Reactive fluorescent dyes are broadly used to label amino acids, proteins, oligonucleotides, and other biological molecules, while amine reactive dyes are most

often used to prepare the sample for immunochemistry, histochemistry, cell tracking and other applications.

1.2.8.1. Fluorone dyes

To the fluorone dyes belong dyes such as eosin, fluorescein, etc.

The fluorescent pink-red colour (excitation maximum: 520nm, emission maximum 540nm) of eosin results from the interaction of bromine with fluorescein. It is used to stain connective tissue, cytoplasm and other extracellular substances.

Fluorescein was first produced by Baeyer in 1871. He prepared a yellow powder by fusing a mixture of phthalic anhydride and resorcinol and by precipitating this mixture from alkaline solution using acids. When he crystallized the product from ethanol he created a dark red powder. While the red fluorescein has a quinoid structure and is more stable, the yellow fluorescein has a lactoid structure and is less stable. This means that the yellow fluorescein is transparent due to a closed ring-structure and the red fluorescein develops a colour do to an open ring–structure (Figure 1.3.). Both forms give the same derivate (Orndorff et al., 1927). Fluorescein is often used in fluorescent microscopy, forensics and serology to detect blood stains. It is soluble in water and alcohol. The excitation wavelength of FITC is 488 – 494 nm which occurs in an emission wavelength of 500 – 520 nm and give a green fluorescent colour.

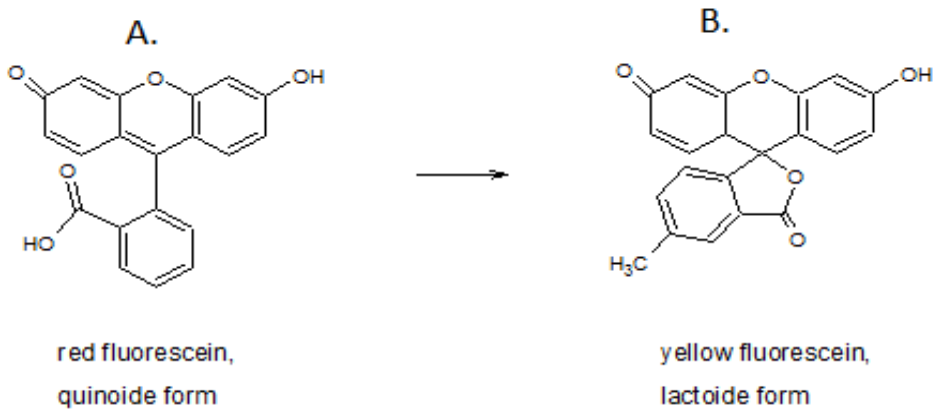

Figure 1.4: Chemical structure of A. red fluorescein with quinoide form, B. yellow fluorescein with lactoide form

1.2.8.2. Alexa fluor

Alexa fluor stains produce bright photostable conjugates for labelling proteins and other cell components. They are soluble in water and can be used over a broad pH range. Different types of Alexa fluorophores are produced ranging over the full visible emission spectrum. By combining the appropriate stains, good quality images with high intensity and contrast between different analytes of interest can be obtained. Besides this, it is possible to use these dyes for FRET measurements. All Alexa dyes are named after the region of their maximal excitation. An example of Alexa fluorescent dyes is the Alexa fluor 555. It is available in a yellow powder and gives a red fluorescence spectrum. Its excitation maxima lies at around 555 nm and the resulting emission maxima is 565 nm. In this thesis Alexa fluor 555 was used to stain the membrane of the cells.

1.2.8.3. Fluorescent isoindole (FII)

Fluorescent isoindoles are generated from the condensation reaction of *o*-phthalaldehyde (OPA) and 2-mercaptoethanol (2-ME) with a primary amine. Under the use of triethylamine as a catalyst, o-phthalaldehyde and 2-mercaptoethanol react to thioacetal. Thioacetal can then bind on a primary amine to react to fluorescent isoindole and give a fluorescent signal (Simons et al., 1978). The excitation wavelength of fluorescent isoindole is 330-390 nm which occurs in an emission wavelength of 430-480 nm and gives a blue fluorescent colour (E. V. Piletska, 2001).

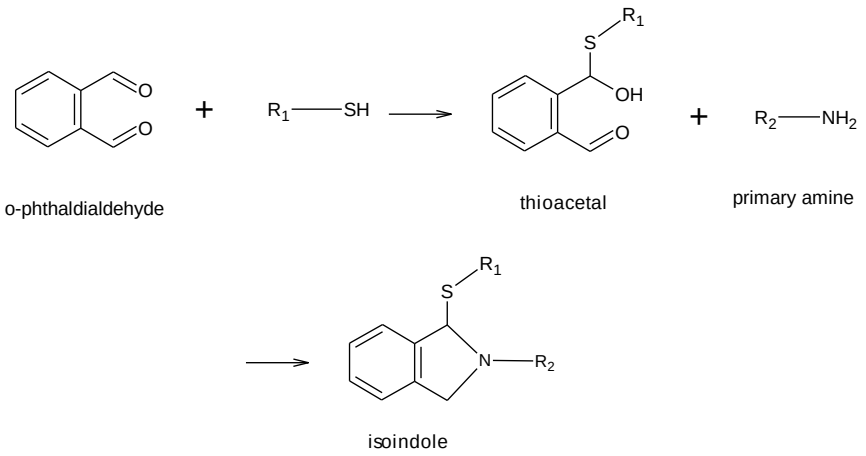

Figure 1.5: Scheme of the production of fluorescent isoindole is shown; OPA and 2-ME are generating in the presence of triethylamine thioacetal, which then reacts with a primary amine to fluorescent isoindole.

o-Phthalaldehyde (OPA) is a fluorescent reagent. In the presence of thiols it reacts specifically with primary amines. OPA is essentially non-fluorescent until it reacts with a primary amine in presence of mercaptan, such as 2-mercaptoethanol, then it forms fluorescent isoindole. It is well soluble, stable in water solution and sensitive to UV-light and air oxidation (DAI et al., 1997). 2-mercaptoethanol (2-ME) is used as a biological antioxidant and can reduce disulphide bonds. Its hydroxyl group offers high

solubility in water and lowers volatility. Triethylamine acts as a catalyst in condensation reactions.

1.2.8.4. Fluorescein isothiocyanate (FITC)

Fluorescein isothiocyanate (FITC) is one of the most common fluorescent dyes. To produce FITC the original fluorescein molecule is functionalized with an isothiocyanate reactive group. Fluorescein belongs to the family of fluorone dyes.

FITC primary targets amino groups and is used to label cells and track them under fluorescence microscope. It can be also attached to active molecules, such as antibodies, to specifically tag proteins or structures within cells.

The excitation wavelength of FITC is 488 – 494 nm which occurs in an emission wavelength of 500 – 525 nm and give a green fluorescent colour.

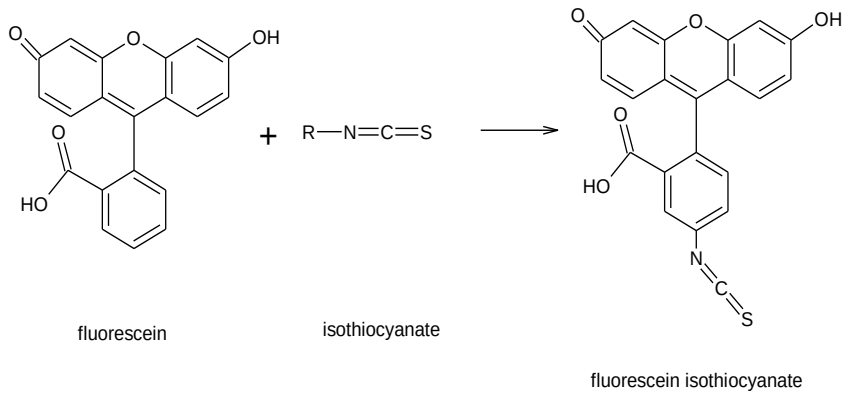

Figure 1.6: Scheme of the synthesis of fluorescein isothiocyanate

The properties of the aforementioned dyes and the principles of fluorescence have been used extensively in chemistry and biology. Two major tools that are still used frequently are fluorescence spectroscopy for analysis of (bio-) chemical structures and microscopy for analysis and visualisation of biological tissue on a subcellular scale.

1.2.9. Fluorescence spectroscopy

Fluorescence spectroscopy is an analytical tool which has obtained much attention in biochemistry, biophysics and material science. Besides this, it can be used in simple analytical assays in environmental and biomedical sciences.

In this thesis a FluoroMax–2 spectrofluorometer was used for the analyses of the fluorescence spectra. The spectrofluorometer uses a 150 W xenon lamp as excitation source. This lamp delivers monochromatic light to excite the fluorescent sample. A quartz beam splitter transfers 8% of this light to a reference diode and also acts as a transparent barrier to prevent dust from getting inside of the optical components. The emission spectrometer disperses the emitted light of the sample, which is then directed to a signal photomultiplier detector. After amplification of the signal, it is displayed on the computer screen.

1.2.10. Confocal laser scanning microscopy

One part of fluorescence spectroscopy is the use of fluorophores in microscopy. Two major types of fluorescence microscopy are performed. The basic and simpler approach is staining of the sample with one or more fluorescent dyes and applying the sample to a conventional microscope. This microscope consists of a light source in front of an excitation filter, an objective, emission filter and detector. The light source emits light from all wavelengths. The excitation filter then selects the appropriate wavelength and sends this light through the objective with a fluorescent sample. The fluorescent molecules are then excited and emit fluorescence, which is passed through the emission filter to improve resolution. The intensity of this signal is then detected and converted into an image (Caldin, 2001).

A conventional optical fluorescence microscope has the disadvantage that secondary fluorescence emitted by the specimen often “bleed” through the excited sample and

decreases the resolution of features that are in the sample's focal plane of interest. This problem is very significant in thicker specimens which exhibit high degrees of fluorescence. The loss of detail makes it difficult to obtain the information that one desires. With the confocal approach, this problem of out-of-focus light is reduced due to the use of pinholes. These pinholes are placed in front of the light source and detector, respectively. Besides this, the light source is changed from a conventional light source to a laser system which emits light from specific wavelengths. The laser system emits light through the pinhole aperture which is situated in a conjugate plane (i.e. confocal) with a scanning point on the specimen and a second aperture in front of the detection system. The laser light is deflected by a mirror system onto the specimen. The fluorescence emitted from the selected focal plane passes then back through this mirror system to the detector. Since only fluorescence from the selected plane can pass through the pinhole, out-of-focus light is reduced which leads to an increase in the resolution of the image (Goldman, 2006).

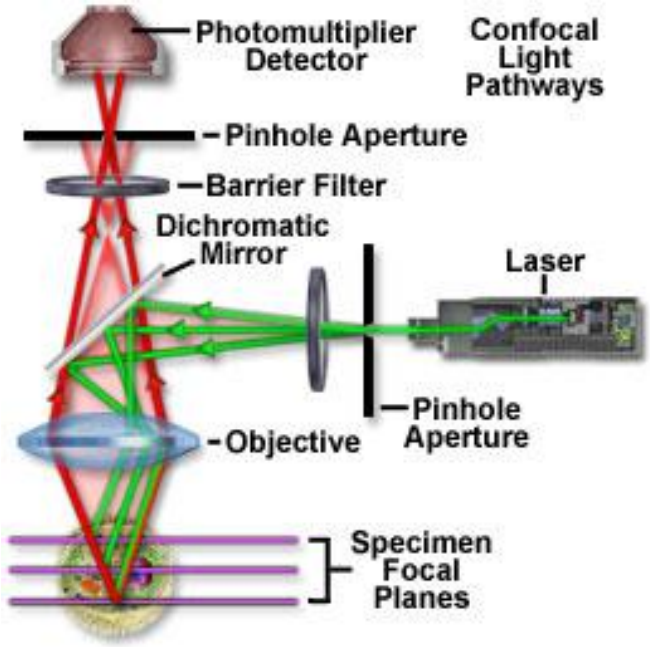

Figure 1.7 [source: (Olympus, 2011)**]**Schematic confocal microscope. Scattering of light is reduced in the confocal format due to the positioning of pinholes before the detector and light source.

Another advantage of the confocal system is the possibility to develop three-dimensional images from a specimen. This can be achieved by changing the focal plane in the z-axis and then scan every focal plane in the x- and y-direction. Data processing systems are able to collect all these data and combine them into one image. With this property, one is able to exactly localise an analyte of interest in the sample.

1.3. Dendrimers

Dendrimers are promising tools in the area of diagnostic and therapeutic. The name dendrimer stands for the Greek word dendron which means tree. In 1978 the dendrimer chemistry was first introduced by Fritz Vogtle (Buhleier et al., 1978). Although dendrimers belongs to the hyperbranched polymers, there are some differences between them. They are both polymerized from monomers and give a tree-like structure with exponential growth. While dendrimers are monodisperse, the normal hyperbranched polymers are polydisperse. Also the synthesis is different, as the synthesis of dendrimers requires absolute controlled steps (Pettersson, 1996).

1.3.1. Structure of a dendrimer

Typically dendrimers consist of a core from which branches extend in all three dimensions. Depending on the core which was used, the shape of the dendrimers can be more or less spherical or rod-shaped. The functionality of the core regulates the number of branches and typically the core is made of a polyfunctional molecule. While the tetrahedral core leads to a spherical polymer, a linear polymeric core gives a rod-shaped dendrimer (Grinstaff, 2002).

The branches of the dendrimer are built from monomers. These molecules typically consist of one reactive group of a certain species and two or more reactive groups of a

different type. As soon as a chain extender reacts with the core or an already-formed hyperbranched structure, a new branching point is created (Pettersson, 1996).

The dendritic polymer will then appear with a dense spherical structure containing a large number of reactive groups on its surface. Due to their synthesis strategy the density of the surface groups and the size of the dendrimer are controlled. With each generation and growing step of the dendrimer the density of the reactive groups on the surface increases.

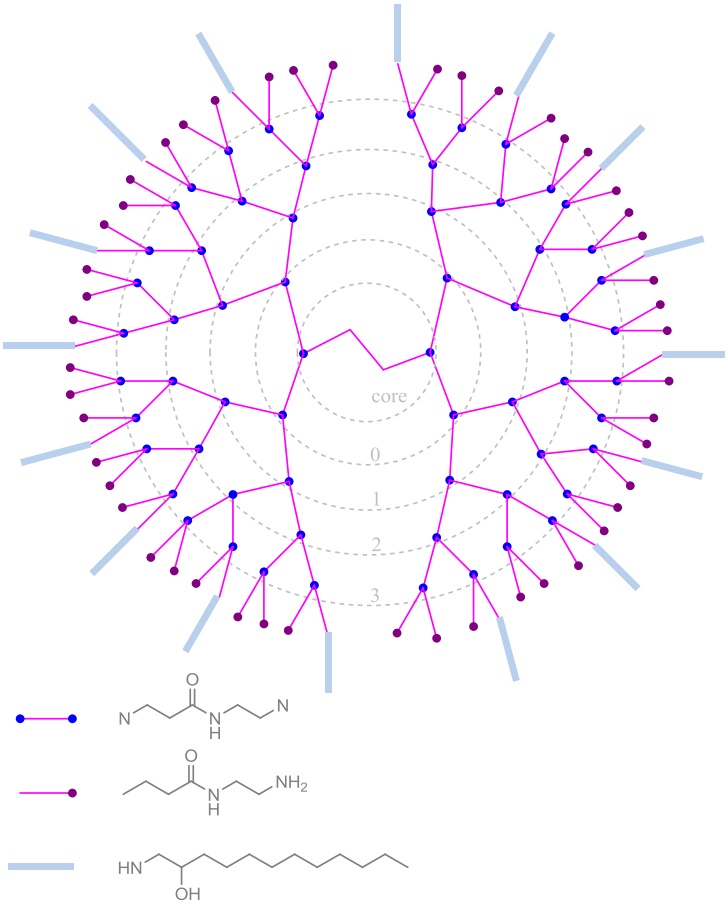

Figure 1.8: Schematic representation of the structure of PAMAM dendrimer, generation 3, 25% C_{12}, with ethylene diamine core.

The number of the monolayers in the dendrimer are called generation and are abbreviated with G0, G1, G2, etc. The term generation describes the size of the polymer and represents one repeating step. The number of peripheral functional groups doubles or triples with each layer of branching units. The abbreviation G0 represents the core (Cloninger, 2002).

Compared to other hyperbranched polymers dendrimers offer some unique characteristics. Whereas conventional polymers resulting in polymeric chains with a statistical distribution of molecular weight and size dendrimers can be synthesised with a precise molecular weight, shape, size, and numbers of functional surface groups. The diameter of one dendrimer ranges from 2 to 10 nm and results from the build generation (Dykes, 2001).

1.3.2. Synthesis strategy of dendrimer

The synthesis of dendrimers offers the opportunity to generate monodisperse, structure-controlled macromolecular architectures. The first synthesis of dendrimers had been performed by Denkewalter, Newkome and Tomalia. In general the dendrimer synthesis can be performed by two different methods. These methods are called convergent and divergent synthesis. Over the years the two strategies have been improved by using chemistries such as “Lego”, “click” and chemical ligation. The synthesis is repeated until the designated molecular weight, size and surface functionality is reached (Tomalia, 2005).

1.3.2.1. Divergent synthesis

The divergent approach was the first method which had been introduced by Tomalia. In this case the dendrons were built from the “inside out”. This means that the dendron is growing from the core site. Compared to the convergent synthesis the divergent method has several major advantages. The synthesis is fast and the growth is exponential, as well as it uses cheap reagents and it has the possibility to create large

dendrimers. However, the purification of compounds is more complicated, as the compounds of the desired product can be easily contaminated with deletion compounds. This deletion compounds can be dangerous because they can have very similar properties such as molecular weight, hydrophilicity, polarity, charge, etc. One limitation of the divergent method is that the steric resistance can prevent coupling of the building blocks (Boas et al., 2006).

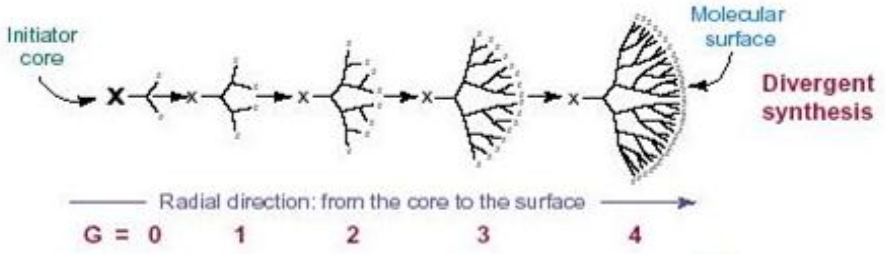

Figure 1.2 [source: (Mukesh et al., 2009)**]:** shows the divergent synthesis of dendrimer generation 4

1.3.2.2. Convergent synthesis

Conversely to the divergent method the convergent approach produces the dendrons growing from the "outside in". This means that first the branches are going to be produced which are then attached to the core. In this case also different types of dendrons can be attached to one dendrimer. The main advantages of the convergent method are that the purification and characterization of the product is easier as with the divergent method. The by-products are different enough in their properties that a successful purification can be achieved. The steric constraint is a limitation of the divergent synthesis as it could be important if larger dendrons have to be attached to the core (Boas et al., 2006).

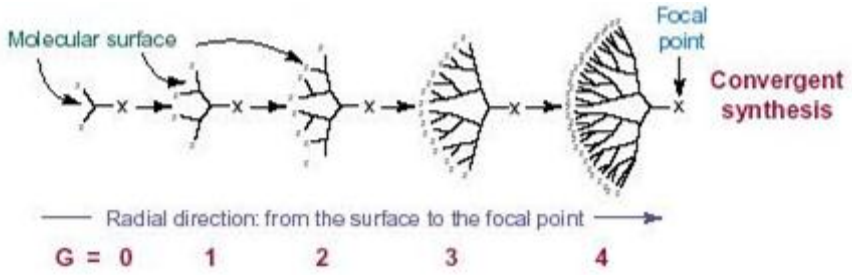

Figure 1.3 [source: (Mukesh et al., 2009)**]:** shows the convergent synthesis of dendrimer generation 4

1.3.2.3. Lego chemistry

Lego chemistry is used in general organic chemistry (Lubell et al., 2010) and for the straightforward synthesis of dendrimers (Villalonga-Barber et al., 2008). In this case small building blocks are used for the design and synthesis of any nanostructures. These blocks are called molecular Lego and have virtually any wanted shape. It is a simple method where the modules can be easily put together. Lego chemistry is a very fast method to create dendritic structures. Its limitation lies in the choice of monomers, as care must be taken to ensure selectivity (Börner, 2007).

1.3.2.4. Click chemistry

The dendrimer synthesis with click chemistry is one of the most promising methods. The method is quick, easy, reliable and based on nature. Click chemistry creates new elements by joining small modular units together. It is not based on a specific reaction. The reactions in this chemistry are highly modular, wide in scope, give very high chemical yields due to high thermodynamic driving force, generates only inoffensive byproducts, which can be removed by nonchromatographic methods. Click chemistry is also stereospecific (but not necessarily enantioselective) (Hartmuth C. Kolb, 2001). Click chemistry finds use not only in the synthesis of dendrimers and polymers; it finds also use in pharmacy, for bioconjugates and biomaterial as well as for the modification of structures in the scale of nanometer.

Click chemistry can however be toxic depending on the type of reaction used, e.g. when an alkyne group is couple to an azide, mostly a cupper intermediate is used as a catalyst. This could be harmful for biological samples (Prescher et al., 2005).

1.3.2.5. Chemical ligation

Chemical ligations are special cases of convergent methods and click chemistry. It is a technique which creates long peptides or protein chains by using chemoselective reactions (Schneider et al., 2010). Chemical ligation has been employed in many applications, such as activity-based proteosome profiling (Lemieux et al., 2003), fluorescent labelling of DNA (Weisbrod et al., 2008) and proteins (Watzke et al., 2006), and for labelling of cell-surface glycoproteins (Hangauer and Bertozzi, 2008).

Several different kinds of dendrimers are commercially available such as: poly(amidoamine) dendrimers (PAMAM), phosphorous dendrimers, polylysine dendrimers and poly(propylenimine) dendrimer (PPI). All these dendrimers are based on one of the synthesis strategies stated above. Commercialised dendrimers are conventionally categorised by their inner core, surface charge and generation (Hawker et al., 1990; Malik et al., 2000). Since the fourth generation of PAMAM dendrimers were used in this project, its characteristics are described in detail in the following section.

1.3.3. Characteristics of PAMAM dendrimer generation 4

In this thesis polyamidoamine (PAMAM) dendrimer generation 4 have been used as a grafting core to synthesise fluorescent organic nanoparticles (NPs). PAMAM dendrimers represents an exciting new class of macromolecular architecture. They are commercially available as a 10 wt. % methanol solution from Sigma Aldrich, Inc. and are normally synthesised by the divergent method. The PAMAM dendrimer consist of an ethylenediamine core, which has a tetrahedral structure and leads to a spherical

shaped polymer. While the half-generations have typically a carboxyl or methyl ester surface group, full-generations are having the amine terminal groups. These dendrimers, generation 4, are having 64 amine surface groups and possess a relatively high surface density. Their diameter ranges from 4-5 nm and molecular weight is 14,214.17 g/mol (Esfand et al., 2001).

The PAMAM dendrimers are having tertiary amine functional groups with ethylene bridges, an internal architecture of amide, are water-soluble and biocompatible. These remarkable hyperbranched polymers mimic the structure of proteins or peptide, which makes them highly interesting for biological applications (Talanov et al., 2006).

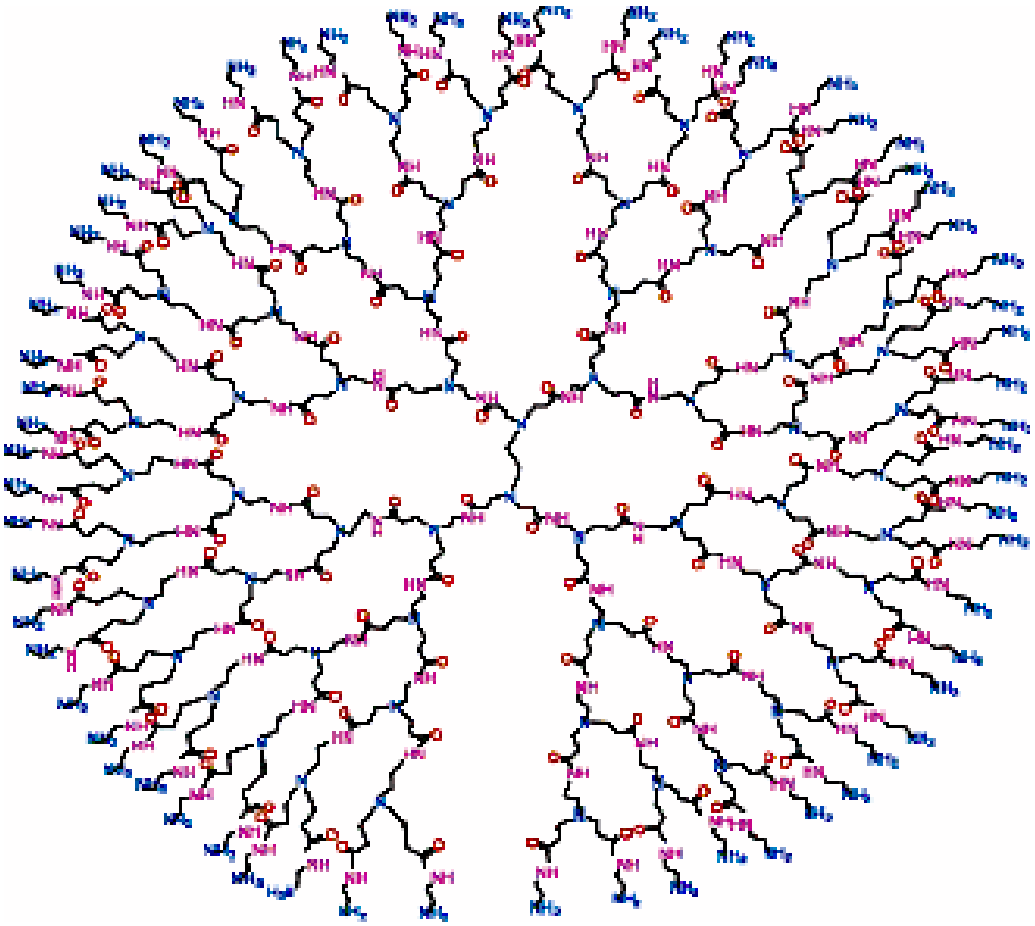

Figure 1.9 [source: (Diallo, 2006)**]:** structure of a PAMAM dendrimer generation 4, with ethylene diamine core and tertiary amine functional surface groups

1.3.4. Application of dendrimers

Dendrimers play a vital role in the field of medical nanotechnology, especially in the area of medical imaging. The functional surface groups of the dendrimer can be easily modified with contrast agents for nuclear medicine (Roberts et al., 1990), computed tomography (CT) (Fu et al., 2006), magnetic resonance imaging (MRI) (Kiessling et al., 2007; Kobayashi et al., 2001; Wiener et al., 1994) and optical imaging.

A wide range of papers have reported that the peripheral modification of dendrimers with various chromophores, such as azobenzen (Grebel-Koehler et al., 2003), dansyl sulfornate and cumarin (Vicinelli et al., 2002), provides a wide range of opportunities, such as light harvesting and sensing. Cross et al. attached naphthalene moieties to the PAMA dendrimer surface and observed an increase of energy transfer with higher generation, while the intensity of the fluorescence emission spectra decreased (Thornton et al., 1997). Crooks et al. modified PPI dendrimers with fluorescent pyrene moieties and observed the excimer formation of pyrene while the generations of the dendrimer increased (L. A. Baker et al., 2000). Wang et al. synthesised phenyl-shelled PAMAM dendrimers, which showed a decrease of the fluorescence emission while their excimer emission increased in the lower generations (G0-G3), whereas higher generations (G4, G5) showed a weaker and broader emission (B.-B. Wang et al., 2004).

For the purpose of medical imaging other optical imaging agents are required. It has been observed that PAMAM dendrimer with amine and carboxyl terminals have a detectable intrinsic fluorescence (Larson et al., 2001). Also a strong fluorescence emission from different dendrimers can be detected under acidic condition (D. Wang et al., 2004). The binding and uptake of fluorescein isothiocyanate (FITC) labelled PAMAM dendrimers into cells have been shown by Jevprasesphant et al. (Jevprasesphan et al., 2004). Thomas et al. also used FITC conjugated PAMAM dendrimers conjugated with antibodies to monitor the uptake of dendrimers due to the cell surface receptor CD14 (Thomas et al., 2004). Shi et al. linked dendrimer-entrapped gold nanoparticles with FITC to target and image cancer (Shi et al., 2007).

For the improvement of DNA microarray technology, Striebel et al. conjugated PAMAM dendrimers with Cy3-fluorophores and oligonuclide probes to detect the herpes virus using fluorescence (Striebel et al., 2004). By labelling PAMAM glycodendrimers with Alexa Fluor 594, Ibey et al. created a fluorescent glucose assay, which can nearly continuously detect the glucose level, as the binding is fully reversible (Ibey et al., 2005).

Dendrimers finds greater application as nanocarriers in drug delivery. Due to their multifunctional property, dendrimer can carry drugs and can be monitored while delivery. The drug can be delivered by the dendrimers either with a simple noncovalent encapsulation, covalent conjugation or electrostatic interaction. One example of noncovalent encapsulation is described by Sato et al. In this case PAMAM dendrimers showed to be an efficient deliverer of antisense DNA to protect DNA from degradation and target cancer cells (Sato et al., 2001). A more sufficient method to attach drugs to the surface of the dendrimers can be reached by a covalent conjugation. This method offers the opportunity to control drug loading and releasing. The improvement of an anticancer drug due to a covalently bound of the drug with a dendritic architecture has been shown by Ihre et al. The anticancer drug showed higher therapeutic efficiency and significantly reduced cytotoxicity (Ihre et al., 2002).

1.4. Nanotechnology and analytical techniques

The American physicist Richard Feynman (widely recognised as father of nanotechnology) gave a speech “There is Plenty of Room at the Bottom” in 1959 at an American Physical Society meeting, which outlined the basic principles of nanotechnology and various opportunities available in material science (Feynman, 1992). In his talk Feynman described the possibility of direct manipulation of individual atoms and molecules. Nanotechnology is a relatively new research area. It has the ability to create new and improved applications in the area of health and medical diagnostic, and therapeutic. Although it can be used in diagnosis and treatment of

many diseases, it can be also used as an environmental remediation technique to treat contamination of soil and water. Nanotechnology expands the boundaries of chemistry, physics and biology by understanding and controlling nanoscale materials, and conquers biological barriers (Fateh et al., 2011).

1.4.1. Organic nanoparticles and polymerisation

Nanoparticles (NPs) are most commonly defined as small molecules with dimension of 1 – 1000 nm. Compared to this a human hair has a diameter of 17 – 181 µm. “Nano” comes from the Greek work dwarf. One nanometer is around four times of the diameter of an atom, while the width of DNA ranges around 2.5 nm and proteins are having a size of 1 – 20 nm.

Fluorescent metal or inorganic semiconductor nanoparticles have been already comprehensively investigated. They have various potential applications such as photovoltaic cells (Hagfeldt et al., 1995), optical sensors (Wohltjen et al., 1998), light-emitting diodes (LEDs) (Schlamp et al., 1997) and also used as fluorescent biological labels (Bruchez Jr., 1998), whereas fluorescent organic nanoparticles (FONs) are at the moment at a very initial development stage. They provide a higher potential in biological application, as FONs allow much more flexibility and variability in synthesis and functional properties.

1.4.2. Living polymerisation

Polymeric nanoparticles can be synthesised via different kind of polymerisation, such as precipitation polymerisation, atomic transfer radical polymerisation, and mini- and micro emulsion polymerisation. These methods have several disadvantages. They can produce particles with irregular size and shape, decreased affinity and unpredictable number of binding sites. Most of the time, long polymerisation time and a high

temperature are required. Controlled living polymerisation overcomes these disadvantages.

The living polymerisation technique allows the synthesis of polymers with narrow molecular weight distribution and determined molecular weight.

1.4.3. Scanning electron microscope (SEM)

SEM pictures from the fluorescent nanoparticles have been taken to get detailed information about the surface, shape and size. Scanning electron microscope (SEM) is used for imaging and analysis of bulk specimens and nano–scale objects. It is a type of microscope that images the surface and composition of a sample by using a high-energy beam of electrons to scan the sample in a raster pattern across the surface. When the electron beam interacts with the sample it generates different signals. These signals give information about the morphology, topography, chemical composition and crystalline structure of the sample. The collected data of the sample surface creates a 2-dimensional image.

Before the sample can be analysed it has to be specially prepared, as the SEM works under vacuum. Before the sample can be placed in the SEM, all the water must be removed, as the water would vaporize in the vacuum. Moreover living cells and biological tissue require also a chemical fixation. While metals do not need any further preparation as they are already conductive, all non-metals need to be covered with a thin layer of conductive material. For this reason the sample is retained in a sputter coater, which uses an electric field and argon gas under vacuum. The sample can be either coated with gold or carbon. In the chamber the argon gas reacts with an electric field, an electron is removed from the argon and makes the atoms positively charged. The positively charged argon ions knock gold or carbon atoms from the foil and form a thin coating layer on the surface of the sample (Echlin, 2009).

After preparation the sample is ready for analysing and can be placed on a sample stage. At the top of the microscope an electron gun produces a beam of electrons, which then follows a vertical path through the microscope. The vacuum in the microscope holds the electron beam. The beam strikes the first condenser lens to form it and limit the current in the beam. At the condenser aperture some high-angle electrons are getting eliminated. The second condenser lens produces a thin, coherent and tight beam which then strikes an objective aperture to eliminate more high-angle electrons from the beam. The electron beam goes thru the scanning coils which are used to produce a deflection of the electron beam. This deflection is used to scan the beam across the surface of the sample in a raster pattern. The objective is the final lens and focuses the electron beam onto the specimen. When the electron-probe hits the specimen surface, two major interaction types occur: elastic and inelastic scattering of electrons. The final emission spectrum of the electrons therefore consists of the contribution of secondary electrons, Auger electrons and backscattered electrons. The final signal used for imaging is a combination of these emissions (Goldstein, 2003).

Two modes of detection can be used in SEM. If the distance between the specimen and the lowest border of the lens system is the electrons and quanta emitted can be recorded by detectors inside the specimen chamber. The magnetic field at the specimen surface therefore remains low and which increases the chromatic aberration, i.e. the distortion to focus all the light to the same convergence point is increased. An advantage is that large specimens can be determined.

The other detection mode is called the in-lens mode. Here, the lens excitation can be increased and the specimen can be placed in the lens system, this reduces aberrations and electron-probe diameter (Newbury, 1986).

A general advantage of SEM with respect to conventional light microscopy is the smallness of the scanning electron microscope aperture. The depth of focus is therefore larger in SEM which means that specimens with large depth variations can

be imaged much sharper than with light microscopy, even at low magnification (Reimer, 2011).

1.4.4. Dynamic light scattering (DLS)

Dynamic light scattering (DLS) is a non-invasive method to measure the size and size distribution of particles and molecules, in the submicron region, dispersed or dissolved in a liquid. It is an accurate, reliable, fast and repeatable analysing method for the size of particles and molecules (Berne et al. 2000). In this thesis DLS have been used to measure the size of the fluorescent nanoparticles.

The physical principle is based on the Brownian motion. The Brownian motion describes the motion of particles or molecules in a suspension, which have been induced by the bombardment by solvent molecules, which are moving due to their thermal energy. Due to this smaller particles move faster than bigger particles, as smaller particles are getting further kicked away (Maret et al. 1987).

This device uses a laser to illuminate the sample and measures the hydrodynamic diameter of the particles or molecules by detecting the intensity of the scattered light. The hydrodynamic diameter indicates how diffused a particle is in a fluid. The adjusted diameter of the device refers to the diameter of an ideal sphere that has the same diffusion coefficient as the measured particle. This coefficient depends on the size of the particle core, any surface structure, and the concentration and type of ions in the solution. Due to this, it can be that the measured size of the particles can be larger than the real size. Also coloured or fluorescent particles can occur bigger than they are, as the device uses a laser for illumination and measures the scattered light (Schmitz, 1990).

1.4.5. Nuclear magnetic resonance spectroscopy (NMR)

NMR has been used to confirm a successfully modification of the dendrimers with the UV-labile iniferter. Nuclear magnetic resonance (NMR) spectroscopy is a valuable tool for the analysis of organic components. It is one of the three conventional analysis techniques which are generally used for the determination of even the most complex organic molecules. NMR spectroscopy can be used for mapping the carbon-hydrogen framework of a component, whereas infrared spectroscopy and mass spectrometry are used for determining the functional groups and the molecular size and formula of the chemical, respectively. More advanced NMR techniques can be used in biological chemistry for protein structure determination (Ashurst et al. 1998).

For atoms to be useful for NMR, their nuclei have to be magnetisable by an external magnetic field B_0. All nuclei with an odd number of protons or neutrons show this behaviour. Only nuclei with an even number of both protons and neutrons cannot be magnetised. The most commonly used nuclei for NMR measurements are ^{1}H and ^{13}C, since organic components are basically carbon hydroxides. Further explanation will be based on the ^{1}H NMR spectroscopy, since this is used for determination of chemical structures in this project (Anderson et al. 2004).

In normal circumstances, the magnetic spin of nuclei is oriented randomly. When a sample containing ^{1}H nuclei is place in a strong magnetic field, however, a specific orientation is obtained. Nuclei can orientate their own magnetic field aligned with or against the external field. The aligned orientation has a lower energy level depending on the strength of B_0. This orientation is therefore favoured.

When the oriented nuclei are irradiated with electromagnetic radiation of appropriate physical properties, these nuclei can absorb the energy of this radiation. The lower-energy oriented atoms can therefore change their spin to the higher energy state. If this spin-flip occurs, the magnetic nuclei are in resonance with the applied radiation

and NMR occurs. The energy needed for the spin-flip to occur is proportional to the strength of B_0 (McMurry, 2008).

The absorption of the radiation energy is not only dependent on the strength of the electromagnetic radiation. When a molecule is placed in a magnetic field, the electrons in the molecular orbitals set up local magnetic fields of their own. These local fields act oppositely to the applied field. Therefore, the effective field felt by the nucleus is weaker than the applied field. This phenomenon is called shielding of the nuclei. This leads to the general framework of peaks that is obtained in NMR spectroscopy. The reduction of effective field to the applied field is measured relatively to a calibration peak. Mostly, tetramethylsilane is used as calibration solution (Sohár, 1984).

Some of the peaks for one ^{1}H nuclei on an NMR spectrum can be found as a combination of multiple peaks. This is due to the interaction or coupling of spins of neighbouring nuclei. The magnetic field produced by one nucleus affect the field felt by its surrounding nuclei. This phenomenon is also called spin-spin splitting. The amount of peaks that can be obtained for one ^{1}H nucleus depend on the amount of equivalent adjacent protons in the structure. A combination of these phenomena gives rise to a unique spectrum for every type of organic structure. This is the reason for the ubiquitous application of NMR in chemical synthesis as well as biochemistry (Smith et al. 1995).

1.5. Project aim

The main objective of this thesis is to develop nanoparticles with a fluorescent core as a possible new cell imaging method and observe their interaction with cells.

The first objective is to analyse the fluorescent spectra of fluorescent isoindole in conjugation with PAMAM dendrimer. Currently studies show that dendrimers can be easily labelled with a fluorophor. However, the literature often uses fluorophores, such as fluorescein and other amine-reactive fluorescein derivate. Several tests were performed to observe the changes of the fluorescent spectra in response to hydrochloride acid, changing the pH of the sample, and in response to salicylic acid. For this purpose a 3D and 2D analysis of the fluorescent spectra of all samples has been performed.

The second objective is to create organic nanoparticles with a size below 100 nm by using PAMAM dendrimers as a grafting core. Previous studies showed that the production of nanoparticles from dendrimer core is possible. The dendrimers were modified with a UV-labile iniferter and polymerised by using living polymerisation under UV-light. The produced nanoparticles should possess fluorescent core or fluorescent shell, as well as hydrophilic or hydrophobic properties.

The nanoparticles were stored at different temperature in different solutions to observe their shelf-life. The fluorescent spectra and size of the nanoparticles were analysed using Fluorescence Spectroscopy and dynamic light scattering.

In the last section the nanoparticles were applied to cells and observed by using confocal scanning microscopy and fluorescent microscopy.

CHAPTER 2

MATERIALS AND METHODS

2. Materials and methods

In this chapter a full description of materials and methods used in this thesis is reported, divided in three sections. In the first section the experiments performed for design, synthesis and characterisation of fluorescent nanoparticles (NPs) is reported. The second section describes the characterisation of the nanoparticles (NPs). Finally, the third section describes the materials and methods for cell culturing and application of the nanoparticles (NPs) in cell imaging.

2.1. Materials and methods for design, synthesis and characterisation of fluorescent nanoparticles (NPs)

2.1.1. Materials

The materials used were: PAMAM dendrimer generation 4, 10 wt. % in methanol (PAMAM, 25% C_{12}, 50% C_{12}), *o*-phthalaldehyde (OPA, 97%), 2-mercaptoethanol (2-ME, 98%), fluorescein 5(6)-isothiocyanate (FITC), ethanol (EtOH) and phosphate buffered saline (PBS) were all purchased from Sigma Aldrich (USA). Triethylamine (>99 %) and sodium hydroxide (NaOH, 100% pellets) were purchased from Fisher Scientific (UK). Amicon ultra centrifugation filter ultracel – 50k was purchased from Millipore (USA). Cell culture media RPMI 1640 was purchased from Gibco Invitrogen (USA).

2.1.2. Labelling of PAMAM dendrimers with fluorescent isoindole

o-Phthalaldehyde (OPA), 2-mercaptoethanol (2-ME) and triethylamine (5 µl) were mixed in methanol in a 3 cm^3 quartz cuvette. The concentrations of the components used were varied and are shown in Table 2.1. The above solution was mixed with 5 µl of 10 wt. % of commercially available PAMAM dendrimers, generation 4 (PAMAM, 25% C_{12}, 50% C_{12}). The periphery of PAMAM dendrimers, generation 4, was modified (50%

and 100%) with dithiocarbamate ester groups from *S*-(carboxypropyl)-*N,N*-diethyldithiocarbamicacid (CNDDA) (50% modi, 100% modi; discussed in section 2.2.2) and were used in the fluorescent labelling as described.

The fluorescence spectrum of the solution was recorded as a function of time (emission 300-700 nm, excitation wavelength E_{ex} = 275nm) with an interval of five minutes using a FluoroMax-2 fluorometer and Spex-3D fluorometer. The data and pictures were created by the program "viewSPECv1" created by Dr. Michael Cauchi®.

Table 2.1: Concentrations of the reagents used in fluorescent labelling of variety of dendrimers, generation 4 (PAMAM; PAMAM 25% C_{12}, PAMAM 50% C_{12}, 50% modi and 100% modi).

	PAMAM	25% C_{12}	50% C_{12}	50% modi	100 % modi
NH_2 [mol]	2.251×10^{-6}	1.193×10^{-6}	0.615×10^{-6}	2.251×10^{-6}	2.251×10^{-6}
OPA [mol]	2.251×10^{-4}	1.193×10^{-4}	0.615×10^{-4}	2.251×10^{-4}	2.251×10^{-4}
2-ME [mol]	2.251×10^{-4}	1.193×10^{-4}	0.615×10^{-4}	2.251×10^{-4}	2.251×10^{-4}

50% modi, 100% modi: PAMAM dendrimers with 50% and 100% surface modification with *S*-(carboxypropyl)-*N,N*-diethyldithiocarbamicacid (CNDDA);
NH_2: number of mol of surface primary amino groups in 5 µl 10 wt. % dendrimers;
OPA: *o*-pthalaldehyde;
2-ME: 2-mercaptoethanol.

2.1.2.1. Response of PAMAM dendrimer labelled with fluorescent isoindole to pH – change and presence of salicylic acid

o-Phthalaldehyde (2.251×10^{-6} mol), 2-mercaptoethanol (2.251×10^{-6} mol) and triethylamine (5 µl) were mixed in 3 ml methanol in a 3 cm^3 quartz cuvette. PAMAM dendrimer, generation 4 (10 wt. % in methanol, 5 µl) was added to this mixture and allowed to react for five minutes. The hydrochloric acid (1 M in water) was added to the sample of the labelled dendrimers in 10 µl aliquots every five minutes. The

fluorescence spectra of the solution were recorded using a FluoroMax-2 fluorometer and Spex-3D fluorometer.

For the response of isoindole labelled dendrimers to the weak salicylic acid, the sample was prepared as described above. Salicylic acid (62.26 M in methanol) was added to the dendrimer solution in 10 µl aliquots every five minutes. The fluorescence spectra of the sample were recorded using a FluoroMax-2 fluorometer and Spex-3D fluorometer.

2.1.3. Fluorescent labelling of PAMAM dendrimer with fluorescent isoindole and fluorescein Isothiocyanate

2.1.3.1. Fluorescent isoindole (FII)

The amino groups of PAMAM dendrimer 50% surface modified with dithiocarbamate groups (50% modi, 10 wt. % in methanol) were reacted with *o*-phthalaldehyde and 2-mercaptoethanol at a molar ratio of 1:10:10. PAMAM 50% modi dendrimer (1 ml, 10 wt. % in methanol) was mixed with *o*-phthalaldehyde, 2-mercaptoethanol and triethylamine. It was allowed to rect fifty minutes at room temperature.

The fluorescent labelled PAMAM dendrimers were purified as follows: The fluorescent labelled dendrimer solution was placed into a centrifuge filtration tube and was concentrated with 50% ethanol in water four times. The centrifuge tube with the purified dendrimers was then ultrasonicated for thirty minutes. In order to prepare the fluorescent labelled dendrimers for polymerisation, 1ml of DMF was added to the dendrimer solution and the water was evaporated *in vacuo*. Ethanol was used to form azeotrope with water.

2.1.3.2. Fluorescein isothiocyanate (FITC)

The amino groups of PAMAM dendrimer 50% surface modified with dithiocarbamate groups (50% modi) were reacted with fluorescein isothiocyanate (FITC) at a molar ratio of 1:1. Modified PAMAM dendrimers (1 ml) were mixed with FITC as follows: The appropriate amount of FITC was dissolved in ethanol, added to the modified PAMAM dendrimer, degassed with nitrogen and stirred for twelve hours at room temperature in the dark. The fluorescent labelled PAMAM dendrimers were purified as follows: The fluorescent labelled dendrimer solution was placed into a centrifuge filtration tube and was purified with 50% ethanol in water four times. The centrifuge tube with the purified dendrimers was then ultrasonicated for thirty minutes. In order to prepare the fluorescent labelled dendrimers for polymerisation, 1ml of DMF was added to the dendrimer solution and the water was evaporated *in vacuo*. Ethanol was used to form azeotrope with water.

The PAMAM dendrimer, 100% surface modified with dithiocarbamate groups (100% modi) were used as a graftable core to produce organic nanoparticle with a dendrimer core. After polymerisation they were placed into a centrifuge filtration tube and were concentrated with water/ethanol (50/50) three times. Sodium hydroxide solution (1 M in water) was added to the concentrated nanoparticles in volume ratio 1:1 for five minutes. The solution was filtered three times with 50% ethanol in water. The centrifugation tube with purified dendrimers was then ultrasonicated for thirty minutes. The appropriate amount of FITC was dissolved in ethanol, added to the modified PAMAM dendrimer nanoparticles, degassed with nitrogen and stirred for twelve hours at room temperature in the dark. In order to dissolve the unreacted FITC in the sample, the PAMAM dendrimer nanoparticles with fluorescent labelled shell were purified as follows: The fluorescent labelled dendrimer solution was placed into a centrifuge filtration tube and purified with 50% ethanol in water four times. The centrifugation tube with the purified dendrimers was then ultrasonicated for thirty minutes.

2.2. Materials and methods used in synthesis and characterisation of fluorescent nanoparticles (NPs)

2.2.1. Materials

PAMAM dendrimer, generation 4 (10 wt. % in methanol), extra dry acetonitrile, ethanol, extra dry dimethylformamid (DMF), methacrylic acid (MA, 98%), trimethylolpropane trimethacrylate (TRIM, 98%), ethylene glycol dimethacrylate (EDGMA, 98%) and aluminium oxide (Al_2O_3) were purchased from Sigma Aldrich (USA). 1-(3-dimethylaminopropyl)-3-ethyl-carboimide hydrochloride (EDC, 98%) was purchased from Argos Organics (UK). Trimethylolpropane trimethacrylate (TRIM) and ethylene glycol dimethacrylate (EDGMA) have been purified by filtering through Al_2O_3 column. S-(Carboxypropyl)-N,N-diethyldithiocarbamicacid (CNDDA) was synthesized (Ivanova-Mitseva et al., 2011).

2.2.2. Surface modification of PAMAM dendrimer with *S*-(Carboxypropyl)-*N,N*-diethyldithiocarbamicacid (CNDDA)

2.2.2.1. 50% surface modification of PAMAM dendrimer with CNDDA (50% modi)

PAMAM dendrimers, generation 4 (10wt. % in MeOH) were modified with (CNDDA, 0.225 x 10^{-3} mol, 0.049 g). A 50 ml round bottom flask, equipped with a magnetic stirring bar and argon atmosphere, was used as a reservoir for the reaction. *S*-(carboxypropyl)-*N*-diethyl-dithiocarbamic acid CNDDA (0.225 x 10^{-3} mol, 0.049 g) and 1- (3-dimethylaminopropyl)-3-ethyl-carboimide hydrochloride (EDC, 0.337 x 10^{-3} mol, 0.065 g) were mixed in 10 ml dry acetonitrile. PAMAM dendrimer, generation 4 (1ml, 10 wt. % in MeOH) was added to the mixture after thirty minutes stirring at room temperature in the dark. This mixture was stirred for three more hours at room temperature in the dark. The dendrimer solution was placed into a centrifuge filtration

tube and purified with 50% ethanol in water four times. The centrifugation tube with the purified dendrimers was then ultrasonicated for thirty minutes.

2.2.2.2. 100% surface modification of PAMAM dendrimer with CNDDA (100% modi)

PAMAM dendrimer with 100% surface modified with CNDDA was synthesised following, the same procedure as described above. The quantities used for CNDDA and EDC were 0.45 x 10^{-3} and 0.45 x 10^{-3} mol, respectively.

2.2.3. Synthesis of nanoparticles (NPs) with dendrimer core

2.2.3.1. Nanoparticles with fluorescent core

Methacrylic acid (MA, 0.905 x 10^{-3} mol, 77.52 x 10^{-3} g), trimethylolpropane trimethacrylate (TRIM, 0.27 x 10^{-3} mol, 91.4 x 10^{-3} g), ethylene glycol dimethacrylate (EDGMA, 0.45 x 10^{-3} mol, 89.2 x 10^{-3} g) and the PAMAM dendrimer, generation 4, (1 ml, 50% surface modified with CNDDA and 50% labelled with FITC, 10 wt. % in DMF) were mixed in 1 ml DMF. The mixture was degassed with nitrogen for 2 minutes and polymerised under UV radiation (Philips tube HB 171/A self-tanning UV lamp, fitted with four CLEO 15W UVA fluorescent tubes (Philips) with continues output in the region 300-400 nm, delivering 0.09 W cm^{-2} at a distance of 8 cm, Germany) for one minute in a closed glass bottle whilst stirring.

2.2.3.2. Nanoparticles with fluorescent shell

For the fluorescent shell nanoparticles, an identical procedure to the one described above, was used. As a monomer *N*-(-3-aminopropyl) methacrylamide hydrochloride (AMAH) was used instead of methacrylic acid. AMAH (0.901x 10^{-3} mol, 161 x 10^{-3} g), trimethylolpropane trimethacrylate (0.27 x 10^{-3} mol, 91.4 x 10^{-3} g), ethylene glycol

dimethacrylate (0.45 x 10^{-3} mol, 89.24 x 10^{-3} g) and the PAMAM dendrimer 100% surface modified with ENDDA (100% modi, 1 ml, 10 wt. % in DMF) were mixed as already described.

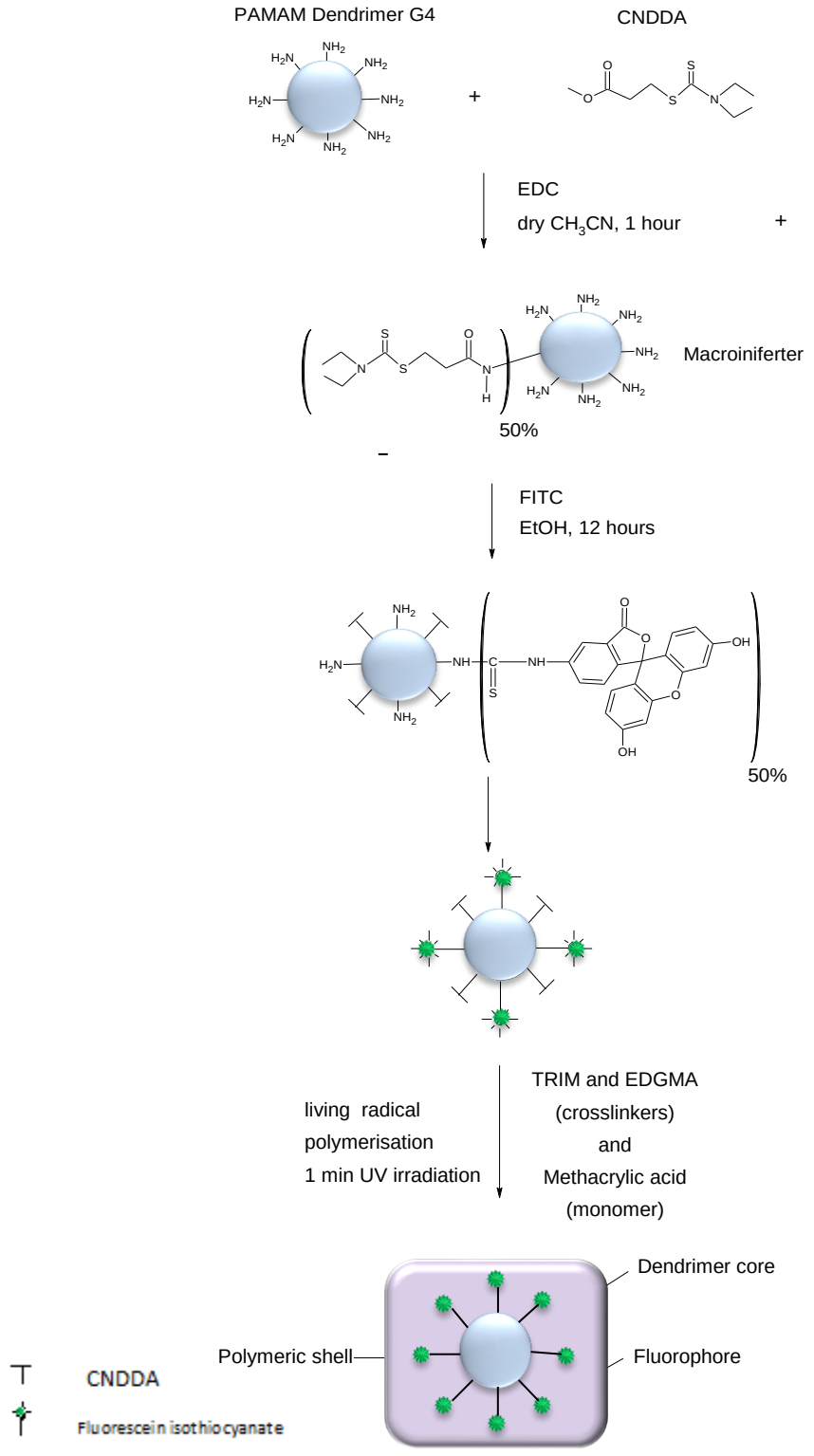

Figure 2.1: Schematic representation of the synthesis of NPs with fluorescent core. Starting with the reaction of *S*-(carboxypropyl)-*N,N*-diethyldithiocarbamic acid (CDNDDA) with the amine surface groups of the dendrimer via coupling reaction with EDC, to create a macroiniferter for the initiated living radical polymerisation to create NPs; dendrimers have been labelled with FITC.

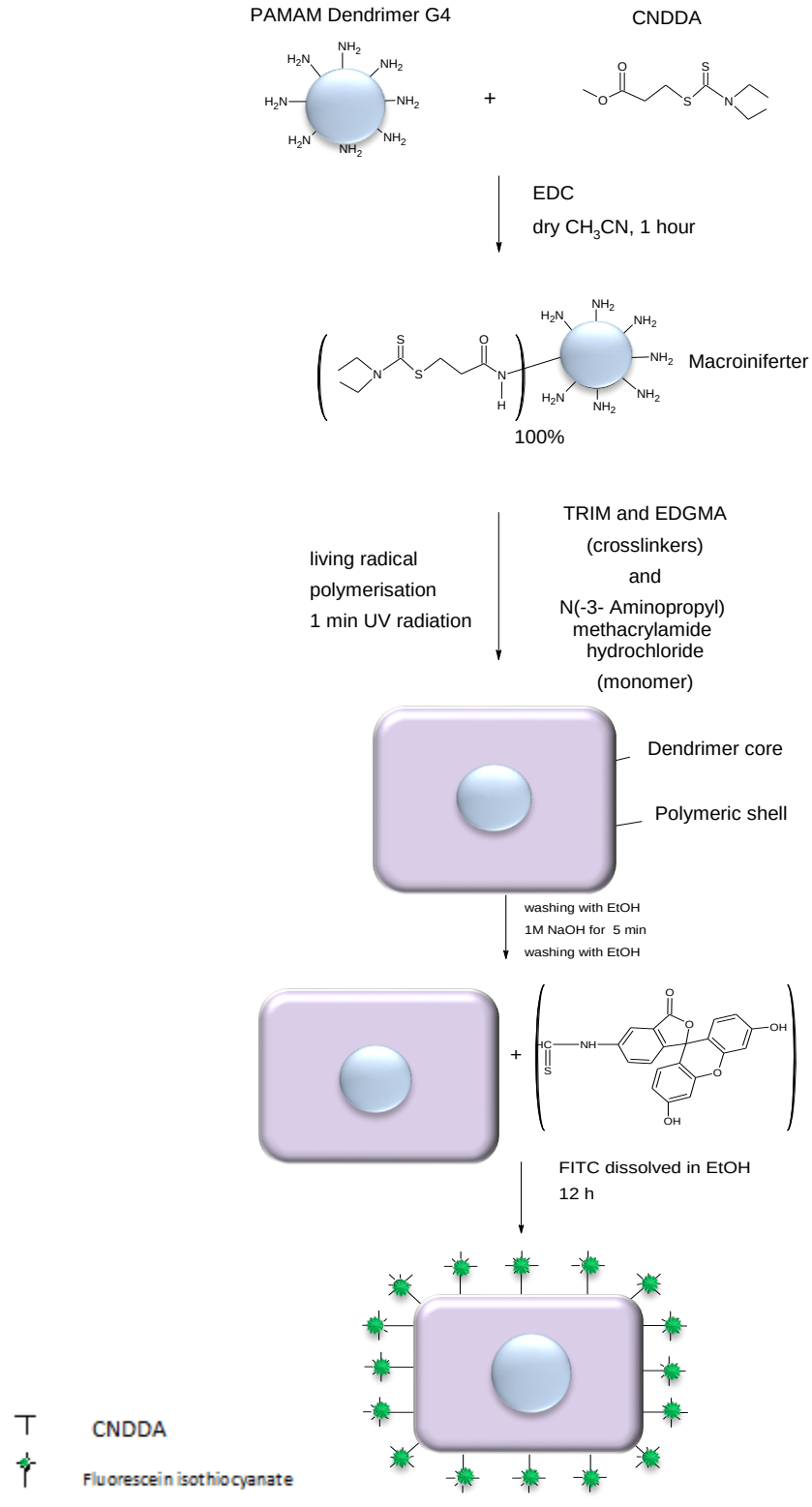

Figure 2.2: Schematic representation of the synthesis of NPs with fluorescent shell. Starting with the reaction of *S*-(carboxypropyl)-*N,N*-diethyldithiocarbamic acid (CDNDDA) with the amine surface groups of the dendrimer via coupling reaction with EDC, to create a macroiniferter for the initiated living radical polymerisation to create NPs; the shell have been labelled with FITC.

Furthermore two more different kinds of nanoparticles made of PAMAM 50% modi, were produced with either hydrophilic or hydrophobic properties of the shell. The dendrimers were labelled with fluorescent isoindole (50%). As monomers for the polymerisation, methacrylic acid (hydrophilic NPs) and styrene (hydrophobic NPs) were used.

2.2.3.3. Nanoparticles with hydrophilic properties of the shell

For the synthesis of the hydrophilic nanoparticles an identical procedure as above was used. A mixture of methacrylic acid (1.801×10^{-5} mol, 155×10^{-3}g), trimethylolpropane trimethacrylate (0.54×10^{-3} mol, 183×10^{-3} g), ethylene glycol dimethacrylate (0.90×10^{-3} mol, 179×10^{-3} g) and the PAMAM 50% modi dendrimer (1 ml, labelled with FII, 10 wt. % in DMF).

2.2.3.4. Nanoparticles with hydrophobic properties of the shell

For the synthesis of the hydrophobic nanoparticles the identical procedure to the one described above was used with a mixture of styrene (ST, 1.801×10^{-3} mol, 187×10^{-3}), trimethylolpropane trimethacrylate (0.54×10^{-3} mol, 183×10^{-3} g), ethylene glycol dimethacrylate (0.9×10^{-3} mol, 179×10^{-3} g) and PAMAM 50% surface modified with CNDDA (50% modi, 1 ml, labelled with FITC, 10 wt. % in DMF).

2.2.3.5. Preparation for storage of the fluorescent nanoparticles for further investigation

The fluorescent labelled PAMAM dendrimer core nanoparticles solution was placed into a centrifuge filtration tube and was purified with either phosphate buffered saline (PBS) or cell culture media (RPMI 1640) four times. The centrifuge tube with purified

dendrimers was then ultrasonicated for thirty minutes. The purified particles were stored for further analyses at different temperatures.

2.2.4. Scanning electron microscopy (SEM)

The surface nanostructures of the produced nanoparticles were analysed with a high resolution FEI XL30 SFEG analytical SEM. Four samples of nanoparticles with different properties have been prepared as follows: (1) the nanoparticles were suspended in PBS; (2) the sample solution was sonicated for five minutes; (3) the solution was dropped on a silicon support; (4) the sample was dried in air for twelve hours; (5) the samples were then coated with either carbon or gold/palladium alloy.

Poly(methacrylic acid) and poly(styrene) shell nanoparticles with a fluorescent isoindole labelled dendrimer core (MA/FII and ST/FII, respectively) were coated with carbon. Poly(methacrylic acid) shell NPs with fluorescent isothiocyanate dendrimer core (MA/FITC-core) and poly(AMAH) shell NPs with fluorescent isothiocyanate labelled polymeric shell (AMAH/FITC-shell) were coated with gold/palladium alloy.

2.2.5. Dynamic light scattering (DLS)

All size measurements were performed by Nano-S (Malvern Instruments, UK) at 25 °C in a 10 mm path length glass cuvette to analyse the different variation of the size of the samples by using dynamic light scattering (DLS). Preprogrammed parameters for the material PAMAM dendrimer 25% C_{12} generation 4 were used. For the parameter of the dispersants used (water and PBS) the following parameters were set: 78.5 dielectric constant, 0.343 m Pas viscosity and 1.33 refractive index. Three measurements were performed per sample, the measurement duration and the

numbers of runs were set to automatic. All samples were ultrasonicated for 5 min before analysis.

2.3. Materials and methods for cell culturing

3.5.1 Materials

One bladder transitional epithelium carcinoma cell line, RT-112/84 (ECACC No. 85061106) referred to as 'RT112' was used. RT 112 was maintained in Dulbecco's Modified Eagle Medium (DMEM) supplemented with HAMSF12, 10% fetal calf serum (FBS), penicillin-streptomycin solution (PS) and 1ml glutamine (complete media, purchased from Gibco Invitrogen, USA). They were passaged with trypsin and EDTA purchased from Sigma Aldrich, USA. Alex fluor 555 streptavidin conjugate purchased from molecular probes, Invitrogen USA.

3.5.2 Cell culture

Bladder cancer cells RT 112 was grown at 37°C in T-25 flasks in an atmosphere of 5% CO2 and 95% relative humidity. Cells were maintained by changing media every 3 – 4 days and passaging when cells reached 80% confluence.

3.5.3 Introduction of nanoparticles in bladder cancer cells RT 112/84

RT 112 was seeded onto an Ibidi 8 well chamber slide with 200 µl complete media (cell concentration per well 4 x 10^4). The cells were incubated for twenty-four hours prior to the addition the fluorescent core and fluorescent shell nanoparticles. Particles were suspended in sterile phosphate buffered saline (PBS) and were added in the ratio 25 µl, 50 µl, 100 µl per well, following an forty-eight hours incubation period.

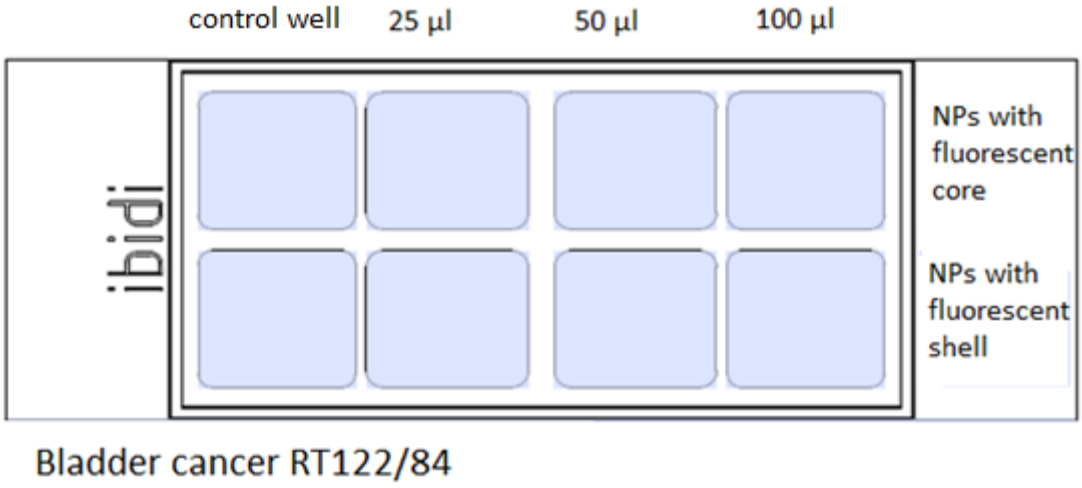

Figure 2.3: Ibidi µ-Slide 8 wells containing bladder cancer cells RT122/84 and different concentrations of NPs with either fluorescent core or shell.

3.5.4 Staining of bladder cancer cells RT 112/84 with Alexa fluor 555

To allow visualisation of the particles and cells, cells were fixed and counterstained with an Alex fluor 555 streptavidin conjugate (Molecular Probes, Invitrogen). After forty-eight hours incubation the RT 112 cells were twice rinsed with 200 µl per well cold sterile PBS pH 7.4, followed by fixation using 100 µl per well of cold methanol for five minutes. The Fixative was removed and the cells air dried for further five minutes. 50 µl of Alexa fluor 555 at a concentration of 5 µg/ml (in PBS) was added to each well and incubated for five minutes. Dye was then removed and wells were rinsed twice with PBS. For the mounting process 2 drops of the mounting media (aqueous-) vectormount (vector labs) were added per well. The cells were then observed by using Zeiss inverted laser scanning microscope LSM 510 Meta. The excitation wavelength of the channels was set as followed: Channel one argon laser set to 488 nm and channel two helium-neon laser was set to 543 nm.

CHAPTER 3

RESULTS

3. Results

This chapter concentrates on the results which were achieved and is divided into five sections starting with nuclear magnet resonance spectroscopy (NMR) to analyse the surface modification of dendrimers, followed by scanning electron microscope (SEM) pictures of the nanoparticles to determine their shape and size. After this, the results of the dynamic light scattering (DLS) analyses were presented and used to observe size changes of the nanoparticles. The fourth chapter focuses on the data generated by fluorescence spectroscopy measurements. The final section shows the results of the confocal scanning microscope.

3.1. Validation of coupling between dendrimer and iniferter

The PAMAM 50% modi dendrimers were analysed with Oxford NMR AS 400 to show successful modification of the periphery.

^{1}H and ^{13}C NMR spectroscopy (Figure 3.2 and 3.3, respectively) of the PAMAM dendrimer modified with *S*-(carboxypropyl)-*N*-diethyl-dithiocarbamic acid (CNDDA) was performed. All spectra were recorded in methanol-D_4. ^{1}H NMR showed additional peaks, compared to the unmodified dendrimers, at 4.01 ppm (A.) and 3.9 ppm (B.) due to the two signals from the methylene groups from the two ethyl groups, connected to the nitrogen from the dithiocarbamate residue. In the ^{13}C NMR spectra was observed an appearance of a peak at around 200ppm (C.), assigned dithiocarbamate thiocarbonly residue.

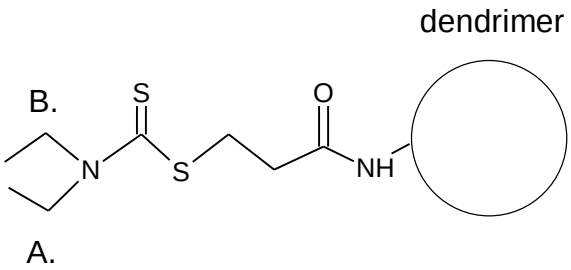

Figure 3.1: Schema of dendrimer modified with *S*-(carboxypropyl)-*N*-diethyl-dithiocarbamic acid (CNDDA). A. and B. methylene groups from the two ethyl groups, connected to the nitrogen from the dithiocarbamate residue

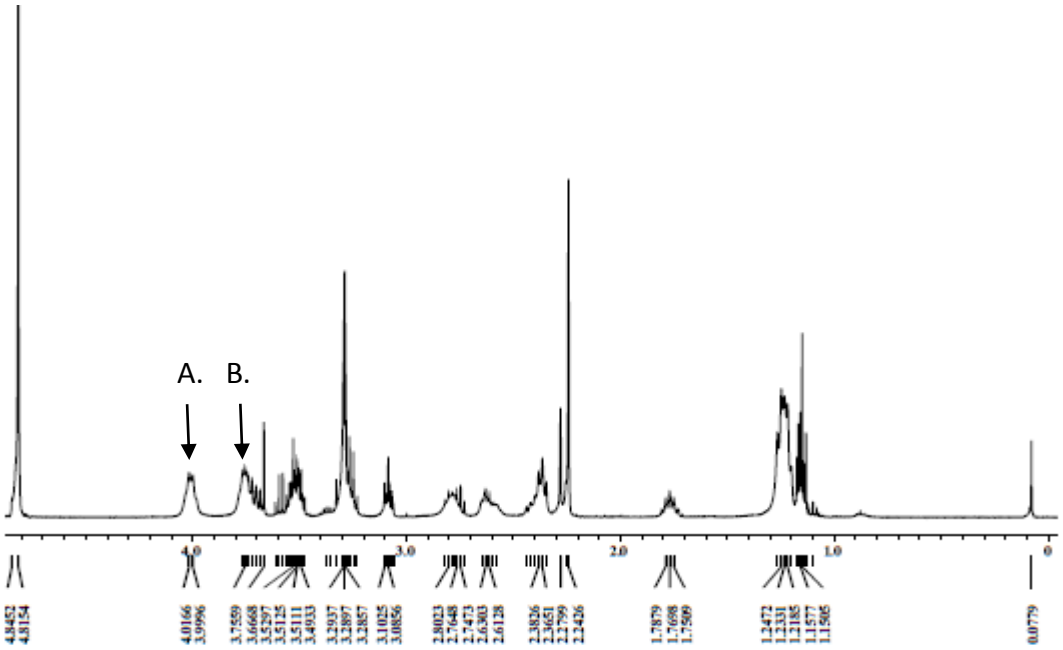

Figure 3.2: ^{1}H NMR spectra of the PAMAM dendrimer modified with *S*-(carboxypropyl)-*N*-diethyl-dithiocarbamic acid (CNDDA). A. and B. show the two signals of the methylene groups from the two ethyl groups, connected to the nitrogen from the dithiocarbamate residue.

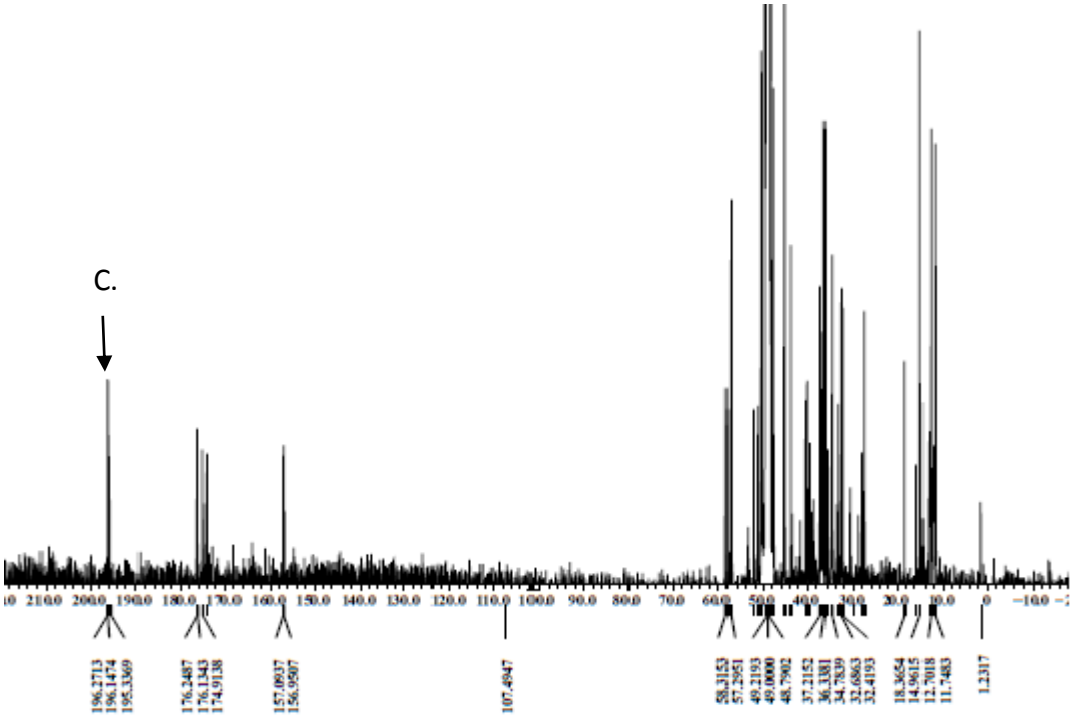

Figure 3.3: ^{13}C NMR spectra of the PAMAM dendrimer generation 4 modified with *S*-(carboxypropyl)-*N*-diethyl-dithiocarbamic acid (CNDDA). C. Peak at 200 ppm for the carbon from the dithiocarbamate residue.

Nuclear magnetic resonance spectroscopy showed the successfully modification of the PAMAM dendrimer with the *S*-(carboxypropyl)-*N*-diethyl-dithiocarbamic acid (CNDDA) group, which was used as an iniferter for the UV-initiated living polymerisation.

3.2. Characterisation of the nanoparticles shape and size

Scanning electron microscopy (SEM) was used to give detailed information for the structure of the produced nanoparticles. The following pictures give an impression about size and shape of the different NPs.

3.2.1. Nanoparticles shape and size of the with fluorescent isoindole labelled core

NPs with either methacrylic acid (MA) or styrene (ST) – shell and fluorescent isoindole (FII) labelled dendrimer-core were analysed with SEM. The pictures showed that these MA/FII NPs have cubic shape, whereas the ST/FII NPs have spherical shape. The size of both variations ranged between 90 nm – 115 nm.

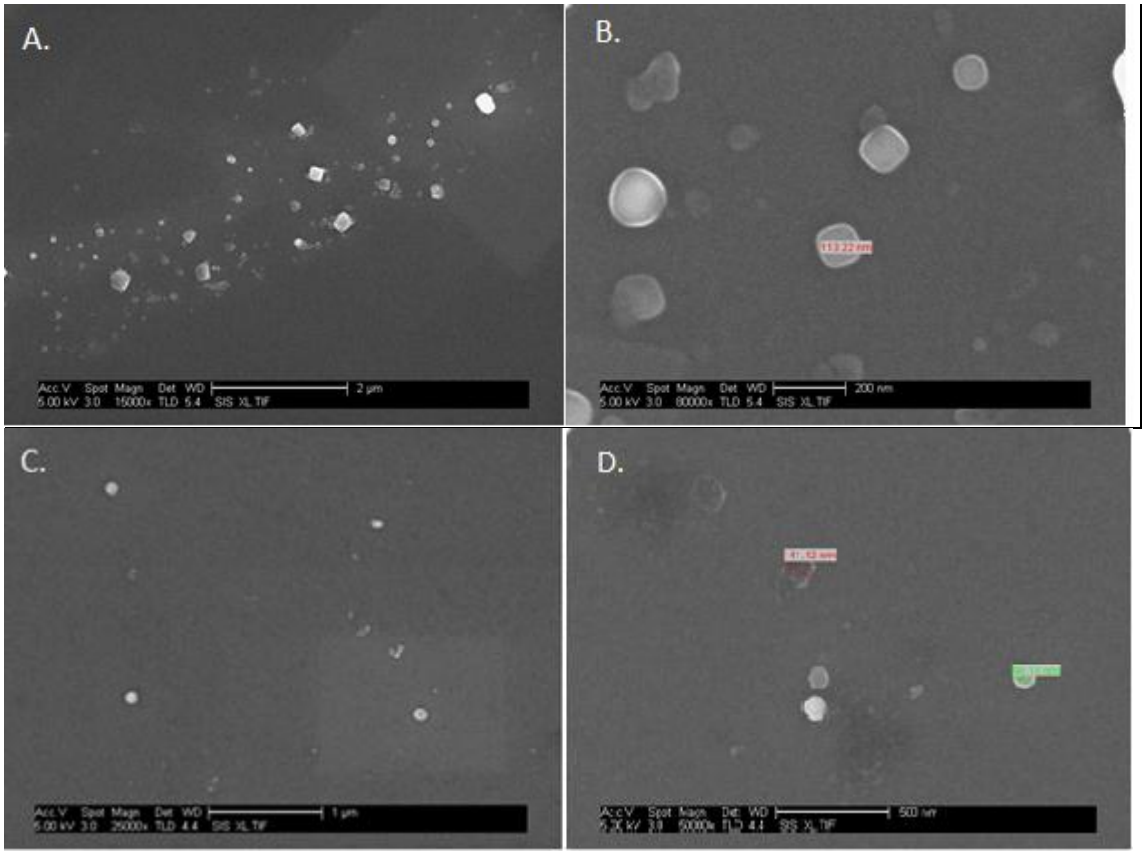

Figure 3.4: Scanning electron microscopy (SEM) pictures A. and B. of MA/FII NPs; C. and D. of ST/FII NPs.

3.2.2. Nanoparticles shape and size of the with fluorescent isothiocyanate labelled core and shell

SEM pictures have been taken from the particles with poly(methacrylic acid) (MA) shell and a fluorescent dendrimer core (FITC-core), and from the particles with poly(*N*-(3-aminopropyl) methacrylamide) (AMAH) shell and a fluorescent polymeric shell (FITC-shell). MA/FITC-core and AMAH/FITC-shell NPs were suspended in PBS. The analysed samples were found to contain cubic-shaped particles, similar to the shape of the MA/FII NPs, with the size ranging from 25 nm to 50 nm.

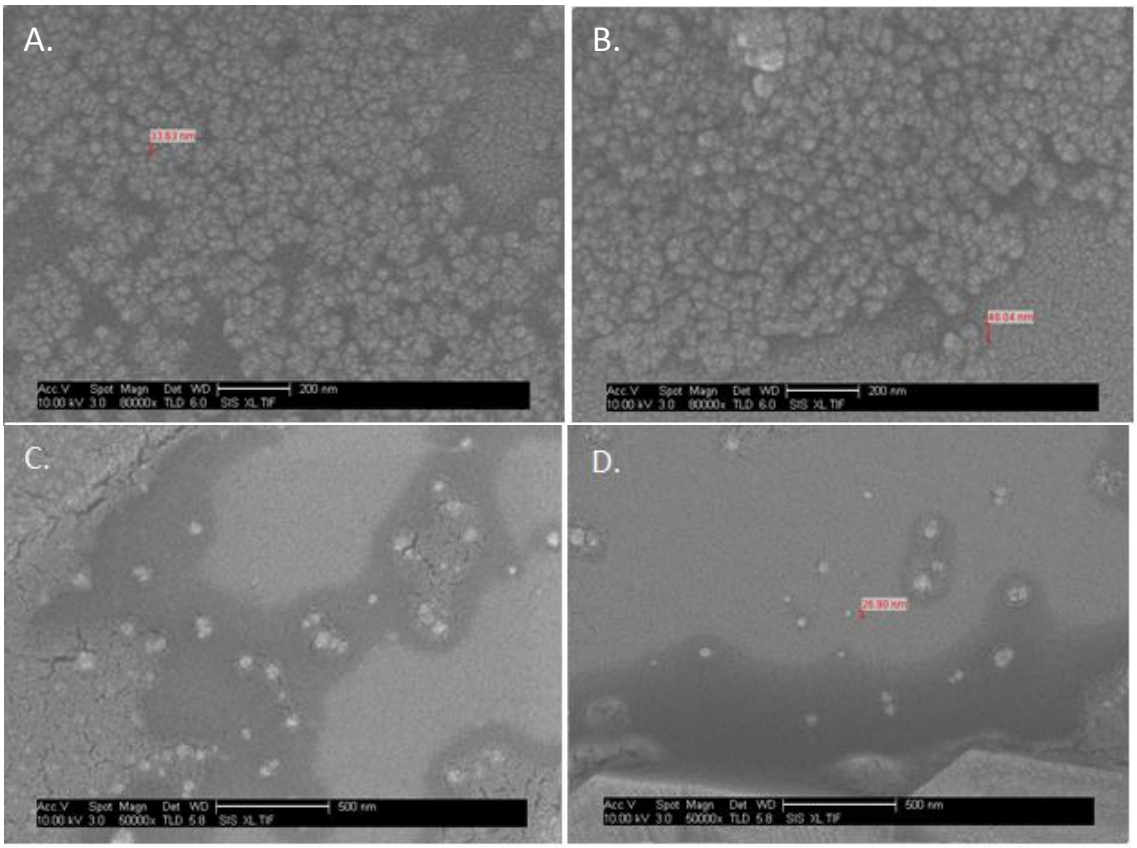

Figure 3.5: Scanning electron microscopy (SEM) pictures of A. and B. MA/FITC-core NPs; C. and D. MA/FITC-shell NPs.

3.3. Characterisation of the size of modified and unmodified dendrimers

To analyse the change of the hydrodynamic diameter of the different modified dendrimer, a Nano-S (Malvern Instruments, UK) was used, which is based on the principle of dynamic light scattering (DLS).

3.5.1 Modification of the dendrimers

The hydrodynamic diameter of PAMAM dendrimers (PAMAM, PAMAM 50% modi, PAMAM 100% modi and PAMAM FII labelled) were measured before and after each step of their surface modification as a qualitative measure for the successful conversions. Size measurement of the PAMAM dendrimers indicated hydrodynamic diameter of around 5 nm. After 50% surface modification with CNDDA the size increased with 1 nm. After 100% surface modification with CNDDA the size increased with another 1 nm. As expected the size increased further as the dendrimers were labelled with the FII fluorophore to a size of 9 nm.

Table 3.1: Average size of PAMAM dendrimer, generation 4 before and after modification with the iniferter as well as after modification with FII measured with Nano-S (Malvern Instruments, UK).

		PAMAM	50% modi	100% modi	50% modi +50% FII
PDL		0.395	0.960	0.121	0.437
Intercept		0.796	0.412	0.347	0.911
Peak 1	Size [nm]	5.13	6.34	7.51	9.30
	Intensity [%]	100	100	100	100
	Width [nm]	1.645	1.166	2.78	4.374

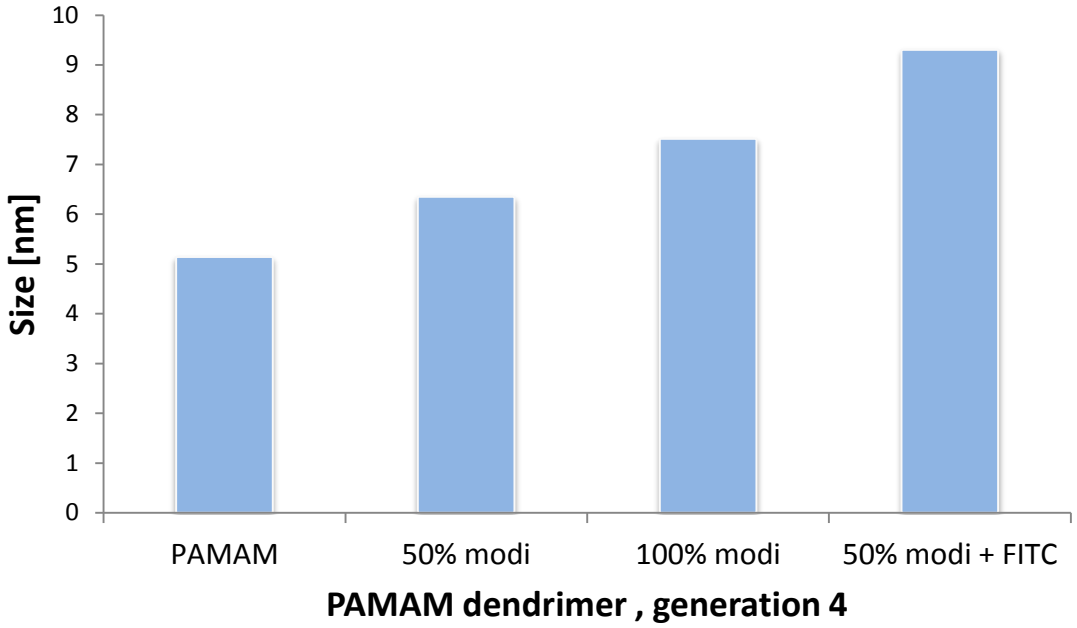

Figure 3.6. Hydrodynamic diameter of PAMAM, PAMAM 50% modi. PAMAM 100% modi. dendrimer with CNDDA ande PAMAM 50% modi labelled with FII fluorophore.

Furthermore, the change of the hydrodynamic diameter of the different nanoparticles (NPs) stored over time in different solutions were also analysed using the Nano-S, these results are summarised in Appendix A.

3.4. Assessment of the fluorescence characteristics

3.4.1. Fluorescence characteristics of the fluorescent isoindole (FII) labelled PAMAM dendrimers

The fluorescent spectra of the fluorescent isoindole (FII) labelled PAMAM dendrimers, with different surface modifications were analysed with FluoroMax-2 fluorometer and Spex-3D fluorometer. The FluoroMax-2 fluorometer parameter was set to an excitation wavelength of 275 nm.

The analyses indicated that the PAMAM dendrimer labled with FII have the highest intensity, followed by PAMAM 25% C_{12}, PAMAM 50% modi, PAMAM 50% C_{12} and PAMAM 100% modi dendrimers. This means, that the intensity of PAMAM 50% modi ranked between the intensity of the commercially available PAMAM 25% C_{12} and PAMAM 50% C_{12} dendrimers.

Table 3.2: Emission wavelength maximum (E_m) and the maximum intensity monitored during the reaction course of the modification of the surface primary amino groups of the PAMAM dendrimers with FII (excitation wavelength E_{xc} = 275 nm). Time-interval: Time used to couple the fluorophore to the dendrimer.

	E_m Wavelength [nm]	Intensity [cps]	Time-interval [min]
PAMAM	419	706490	0
25% C_{12}	424	59230	0
50% modi	425	33861	50
50% C_{12}	425	17758	0
100% modi	417	1231	60

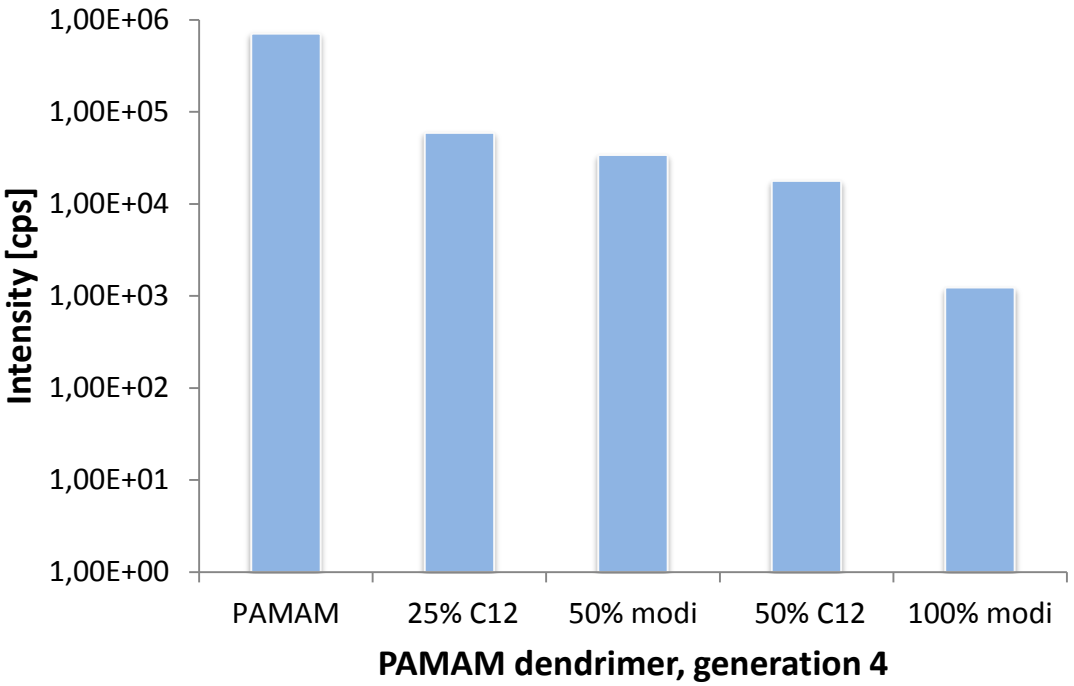

Figure 3.7: Maximum intensity of the fluorescent signal due to surface modification of the surface primary amino groups of the PAMAM, PAMAM 25% C_{12}, 50% modi, PAMAM 50% C_{12} and 100% modi dendrimers (E_{xc} = 275 nm in methanol).

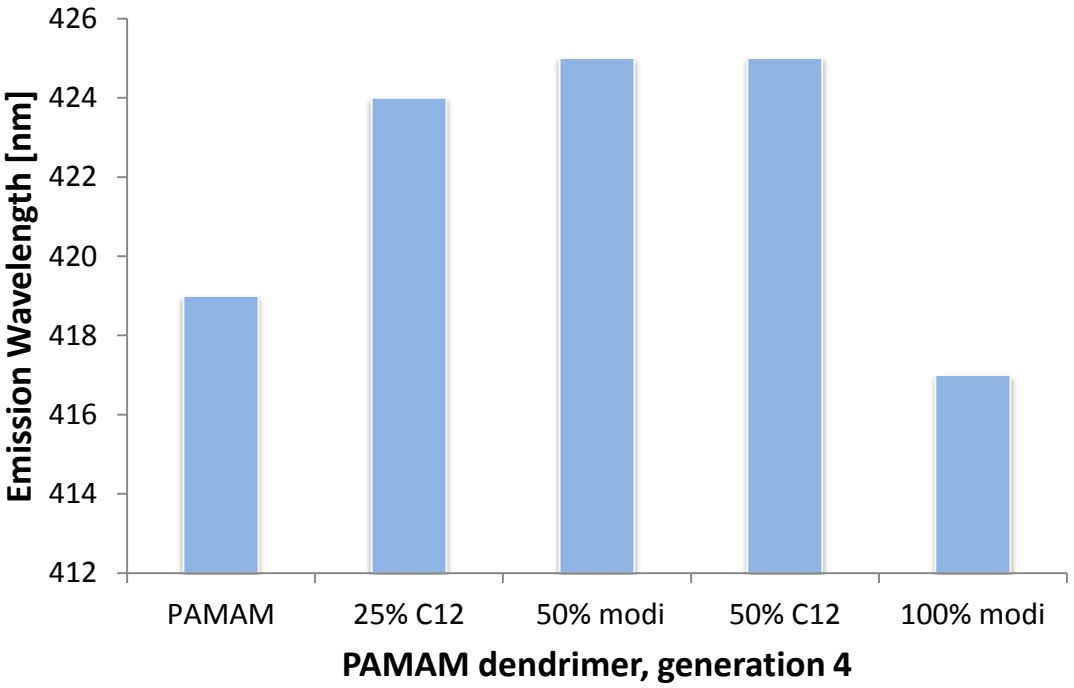

Figure 3.8: Emission wavelength maximum (E_m) of the different FII labelled PAMAM dendrimers (E_{xc} = 275 nm in methanol).

Besides, the fluorescence spectra of FII labelled PAMAM dendrimers were observed with Spex-3D fluorometer to determine the excitation wavelength.

The following figure (Figure 3.9) illustrates the 3D-fluorescence spectra of the FII labelled A. PAMAM dendrimer; B. PAMAM dendrimer, 50% C_{12} and C. PAMAM dendrimer, 25% C_{12}.

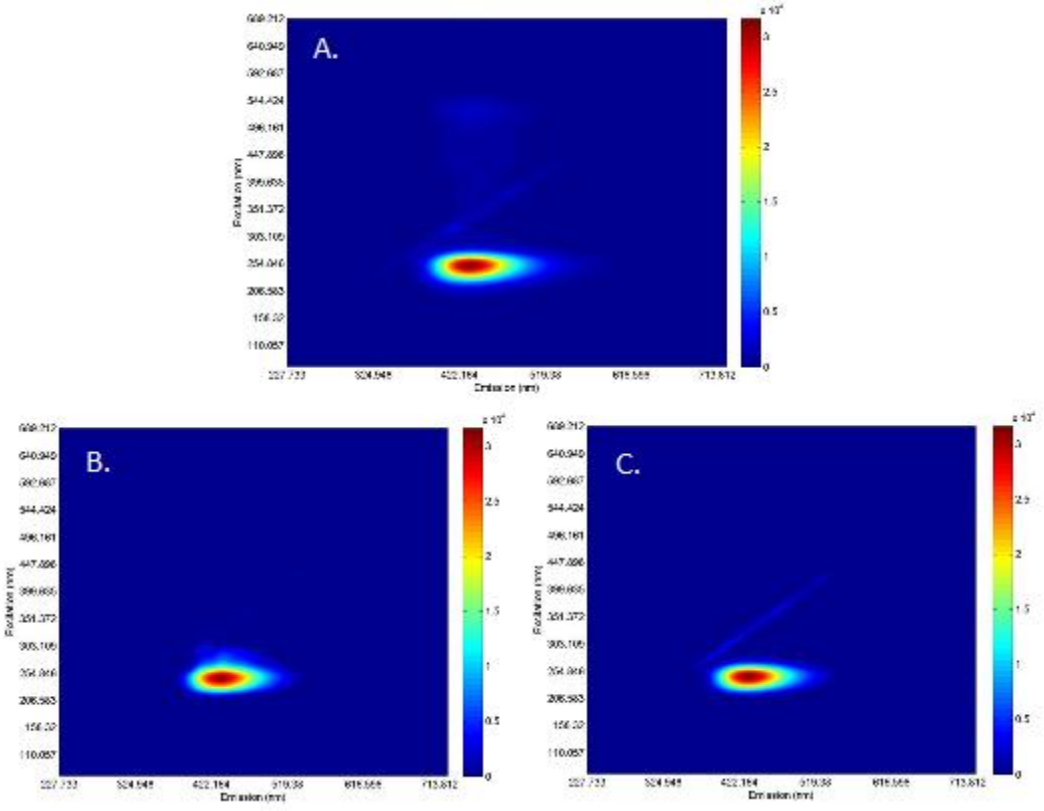

Figure 3.9: 3D-fluorescence spectra of FII labelled: A. PAMAM; B. PAMAM 50% C_{12} and C. PAMAM 25% C_{12}, dendrimers.

3D-fluorescence spectra analysis showed an excitation wavelength between 230 nm and 310 nm with a resulting emission wavelength between 375 nm and 540 nm. For this reason an excitation wavelength maximum was chosen to be set to 275 nm for all the experiments unless stated otherwise.

3.4.2. Fluorescence spectra of the fluorescent isoindole labelled PAMAM dendrimers at different pH and in presence of salicylic acid

To see the effect of pH change on the fluorescence spectra of the fluorescent isoindole (FII) labelled PAMAM dendrimers, hydrochloric acid (HCL) was used. Solution of 1 M HCL in 10µl aliquots was added to the sample every five minutes. The excitation wavelength was set to 275 nm for all experiments.

Fluorescence measurements showed that the fluorescence intensity of the FII labelled dendrimers decreased fast and a red shift was observed in the emission wavelength maximum whiles the pH changed from almost neutral to low acidic pH. After total addition of 50 µl 1 M HCL, a pH of 5.0-6.0 was reached, the fluorescence intensity signal significantly decreased and the emission wavelength maximum shifted to the near infrared region. It could be observed that whilst the concentration of HCL increased the emission wavelength shifted more and more into the infrared-region.

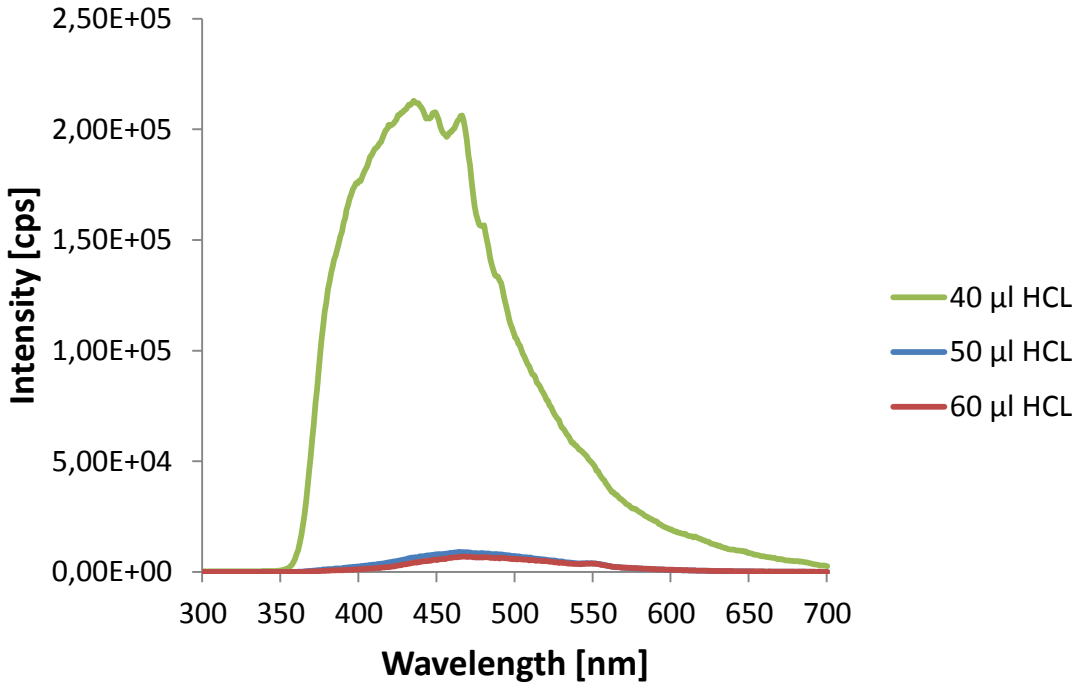

Figure 3.10: Emission spectra of dendrimers labelled with FII while the pH decreases (E_{xc} = 275 nm in methanol).

As PAMAM dendrimers were frequently used as nanocarriers in drug delivery they often can serve also as hosts to incorporate different guest molecules in their inner cavities. The FII labelled PAMAM dendrimers could serve as fluorescent sensors by themselves if a difference in the fluorescence is observed when guest molecule is incorporated. As a guest molecule salicylic acid (SA) was chosen, not only due to its size but also because it does not contain any primary amino groups which would react with the excess of the thioacetal presented in the mixture. The fluorescence spectra of the FII labelled PAMAM dendrimers was recorded during the addition of SA (62.26 M) in 10 µl aliquots in five minutes intervals (E_{xc}=275 nm in methanol).

The fluorescence spectra analyses showed that due to the injection of 10 µl and 20 µl aliquot of SA (62.26 M) the fluorescence intensity highly increased and the emission wavelength shifted to the UV region. Whereas a higher concentration of SA leaded to a slowly decreasing of the fluorescence intensity while the emission wavelength maximum did not change.

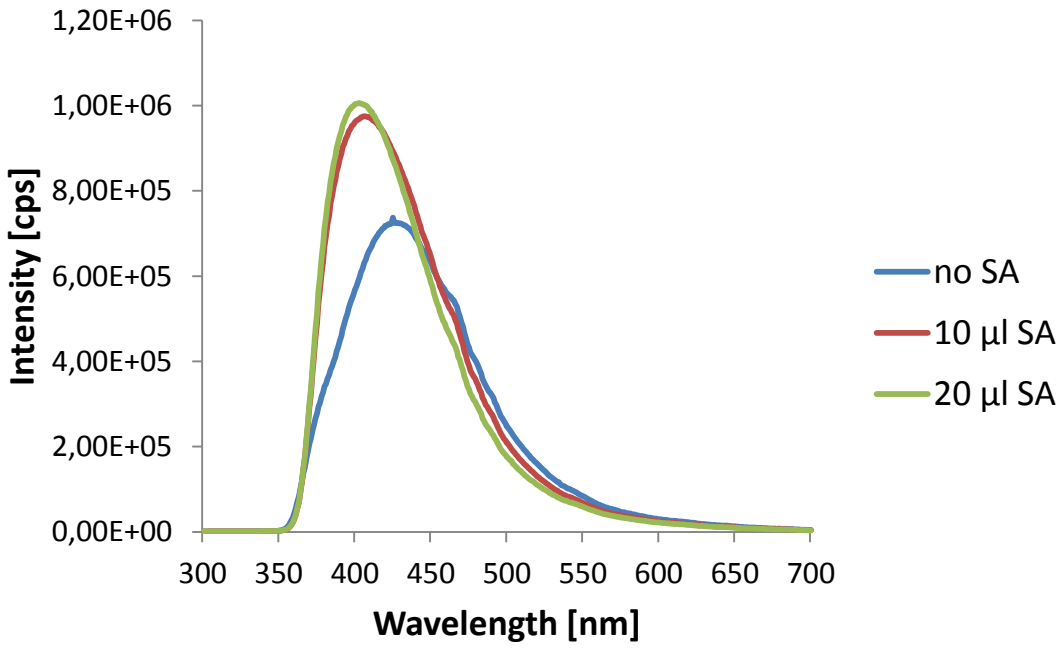

Figure 3.11: Emission spectra of dendrimers labelled with fluorescent isoindole while adding salicylic acid (SA), highest intensity was reached after the addition of 20 µl (62.26 M) of SA (E_{xc} = 275 nm, in methanol).

Table 3.3: Highest fluorescent intensity and their associated emission wavelength for fluorescent isoindole labelled PAMAM dendrimer in cooperation with increasing concentration of A. hydrochloride acid (HCL) and B. salicylic acid (SA) (E_{xc} = 275 nm, in methanol).

B. HCL	E_m Wavelength [nm]	Intensity [cps]
Dendrimer FII	430	759570
10 µl HCL	434	472870
20 µl HCL	436	323400
30 µl HCL	436	250800
40 µl HCL	435	212950
50 µl HCL	467	8975
60 µl HCL	467	6983
70 µl HCL	466	6347
80 µl HCL	466	5621
90 µl HCL	469	5005

A. SA	E_m Wavelength [nm]	Intensity [cps]
Dendrimer FII	425	737580
10 µl SA	406	975 240
20 µl SA	402	1005300
30 µl SA	402	965990
40 µl SA	403	984660
50 µl SA	403	959100
60 µl SA	403	920050
70 µl SA	403	867510
80 µl SA	404	822810
90 µl SA	403	790 800

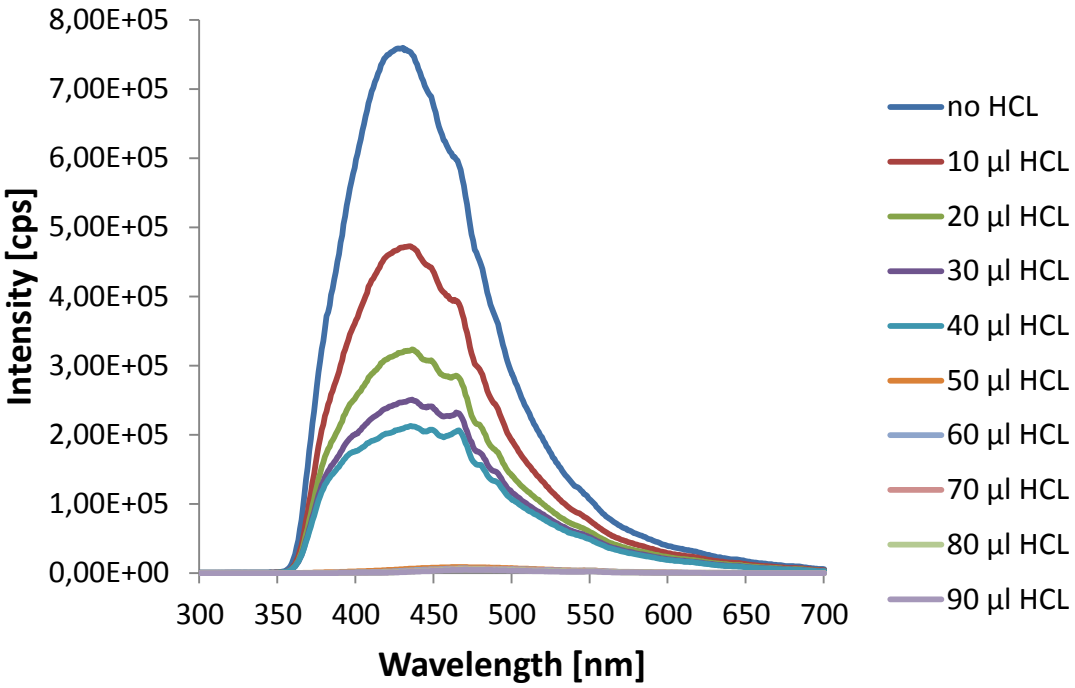

Figure 3.12: Fluorescence intensity of the fluorescent isoindole labelled PAMAM dendrimers while the pH-value changes due to an increasing ratio of hydrochloride acid (HCL) (E_{xc} = 275 nm, in methanol).

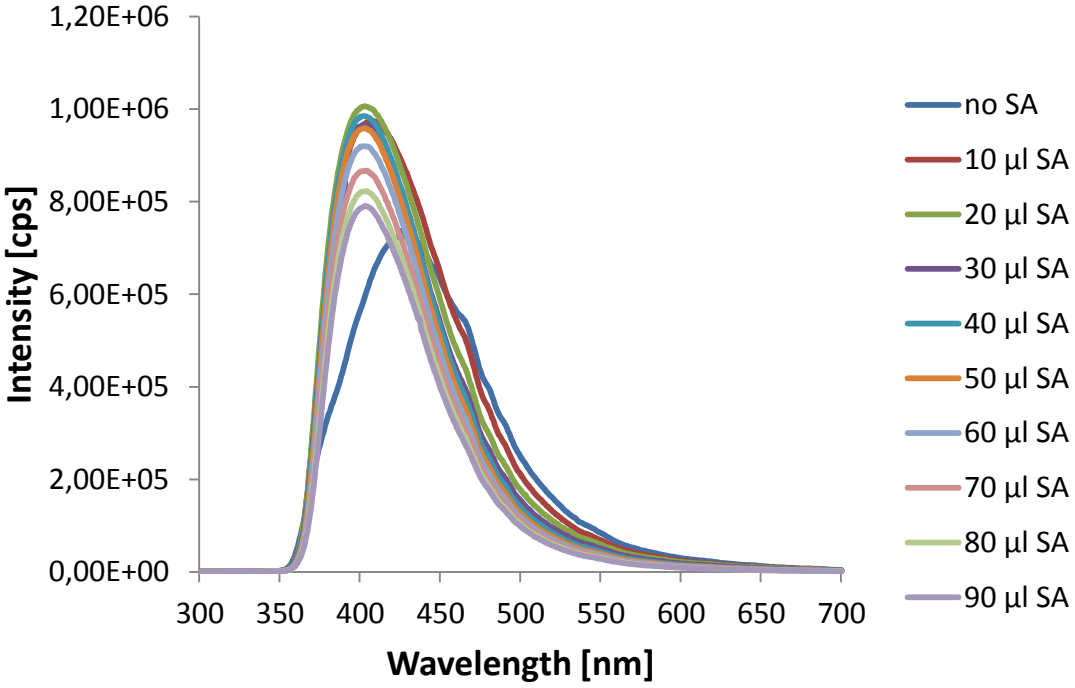

Figure 3.13: Fluorescence intensity of the fluorescent isoindole labelled PAMAM dendrimers while the concentration of salicylic acid (SA) have been increased (E_{xc} = 275 nm, in methanol).

3.4.3. Monitoring of changes in wavelength and intensity of the fluorescence spectra of the fluorescent isoindole labelled nanoparticles over time

Furthermore the fluorescence spectra of the NPs with a fluorescent isoindole (FII) labelled dendrimer core and different polymeric shells (hydrophobic poly(styrene), ST/FII and hydrophilic poly(methacrylic acid), MA/FII) were analysed and their fluorescence intensity were measured over a period of four weeks. The NPs were transferred into PBS, stored in the fridge at 4°C and measured once per week. To analyse the fluorescence intensity of the NPs 3 ml methanol and 5 µl of the NP solution (10 wt. % in PBS) were inserted in a quartz cuvette.

Table 3.4: Fluorescence intensity maximum and corresponding emission wavelength of MA/FII and ST/FII NPs in PBS (E_{xc} = 275 nm, in methanol)

After synthesis		MA/FII	ST/FII
Peak 1	E_m wavelength [nm]	304	304
	Intensity [cps]	19 601	705 520
Peak 2	E_m wavelength [nm]	427	448
	Intensity [cps]	5160	261 010
Peak 3	E_m wavelength [nm]	444	551
	Intensity [cps]	5 251	444 730
Peak 4	E_m wavelength [nm]	551	583
	Intensity [cps]	250 940	358 740
Peak 5	E_m wavelength [nm]	607	605
	Intensity [cps]	8 957	402 570

Table 3.5: Fluorescence intensity and emission wavelength of MA/FII and ST/FII NPs after A. one week and B. four weeks in PBS at 4°C (E_{xc} = 275 nm, in methanol).

A. After 1 week	MA/FII	ST/FII
E_m wavelength [nm]	338	304
Intensity [cps]	64 123	437 030
E_m wavelength [nm]	444	449
Intensity [cps]	15 304	352 460
E_m wavelength [nm]	551	550
Intensity [cps]	213 060	392 950
E_m wavelength [nm]	582	583
Intensity [cps]	4 795	220 160
E_m wavelength [nm]	607	603
Intensity [cps]	10 292	240 720

B. After 4 weeks	MA/FII	ST/FII
E_m wavelength [nm]	339	304
Intensity [cps]	53 943	72 895
E_m wavelength [nm]	510	457
Intensity [cps]	162 48	158 760
E_m wavelength [nm]	551	551
Intensity [cps]	105 230	202 210
E_m wavelength [nm]	581	582
Intensity [cps]	4 566	45 884
E_m wavelength [nm]	607	602
Intensity [cps]	7 927	45 066

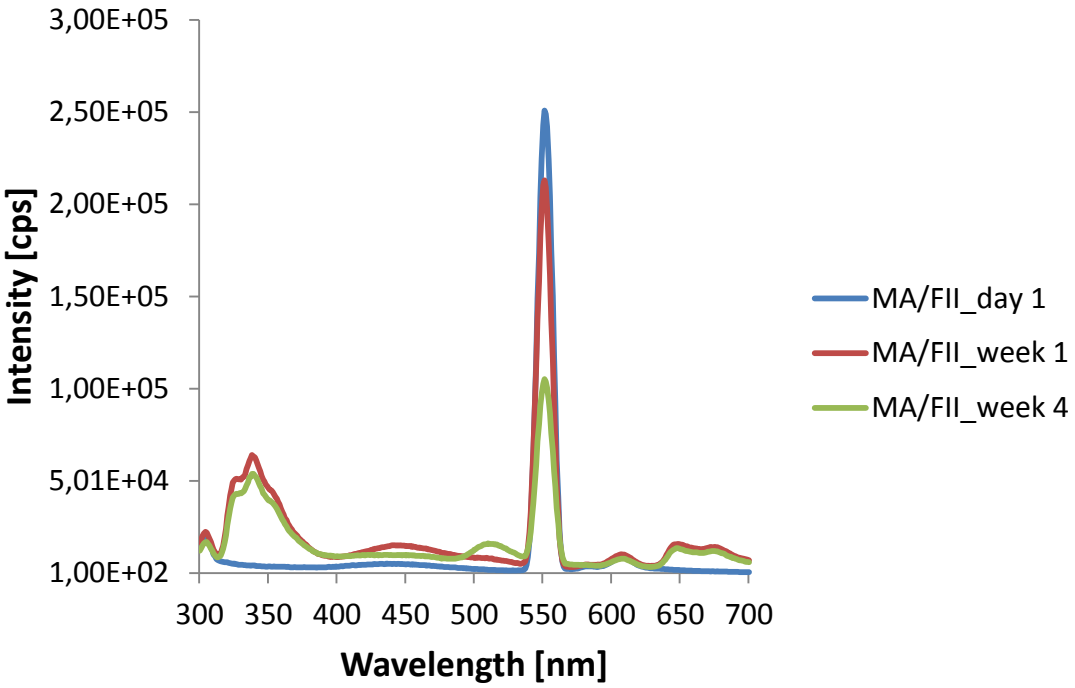

Figure 3.14: Emission spectra of the MA/FII NPs after one day, one week and four weeks (E_{xc} = 275nm, in methanol).

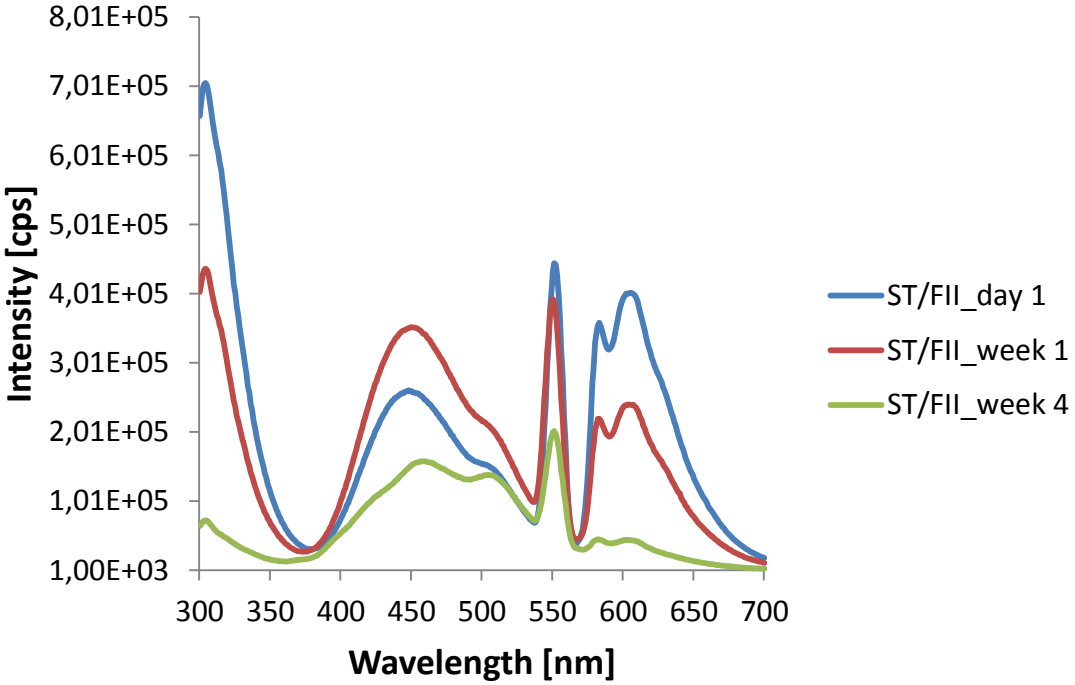

Figure 3.15: Emission spectra of the ST/FII NPs after one day, one week and four weeks (E_{xc} = 275 nm, in methanol).

The fluorescence spectra of the MA/FII and ST/FII NPs showed for each type of NPs five significant intensity maxima. MA/FII compared to ST/FII showed similar intensity maxima at certain wavelength.

3.4.3.1 MA/FII NPs

The fluorescence spectra analyses of the MA/FII NPs over time showed that the first peak at around 304 nm shifted to 338 and increased its intensity, whereas the peak at 551 nm decreased its intensity and did not shift. The emission spectra of MA/FII after four weeks showed a new intensity maximum at 510 nm. The intensity maxima at higher wavelength (607 nm) slightly decreased over time.

3.4.3.2 ST/FII NPs

Fluorescence measurement of the ST/FII NPs over time showed a rapidly decreasing intensity at 304 nm. The second fluorescence maximum increased after one week while the emission wavelength did not shift. After four weeks the peek shifted to a higher wavelength. The fluorescence intensities in the higher regions (551 nm, 583nm, 603 nm) decreased over time.

Although MA/FII compared to ST/FII NPs showed similarity in emission wavelength, its maximum of highest intensity shifted. The highest intensity of MA/FII NPs is at 551 nm, whereas the highest intensity of the ST/FII NPs is at the beginning at 304 nm, these peaks did not change their emission wavelength. Furthermore, the emission spectra in the overall showed that the intensity of the fluorescence signal of the ST/FII NPs is higher than of the MA/FII NPs.

Besides an excitation wavelength of 355 nm were chosen and their resulting emission spectra of the NPs have been observed with Exc = 355 nm. The measurement of the MA/FII and ST/FII NPs displayed only one significant emission wavelength at an excitation wavelength of 355 nm. ST/FII NPs showed the highest intensity maximum at

441 nm, whereas the highest intensity maximum of the emission spectra for MA/FF NPs was 404 nm.

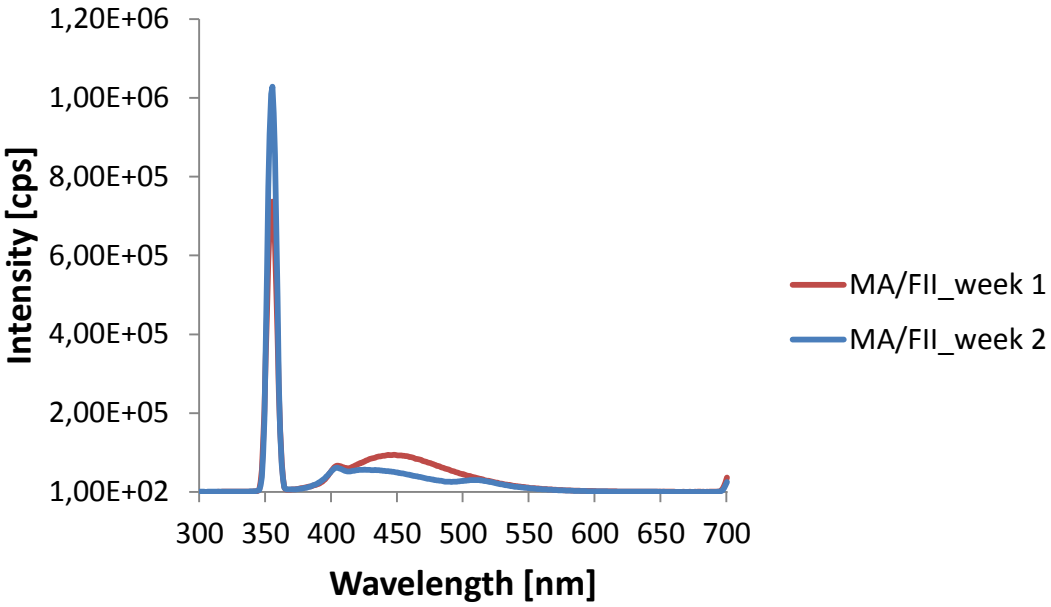

Figure 3.16: Fluorescence spectra of MA/FII NPs with an excitation wavelength at 355 nm after one week and four week.

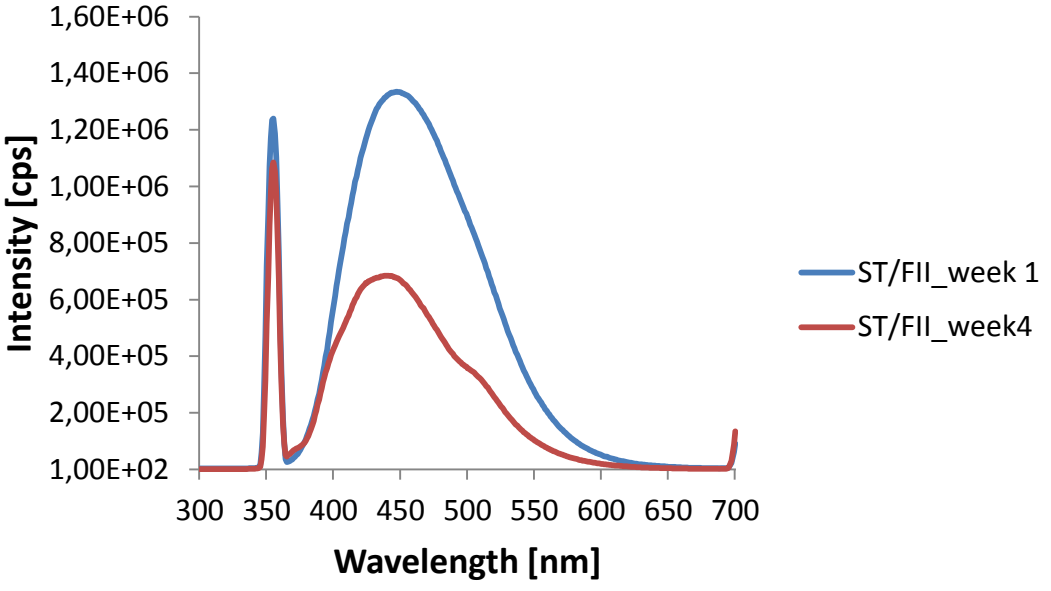

Figure 3.17: Fluorescence spectra of ST/FII NPs with an excitation wavelength at 355 nm after week one and week four.

3.4.4. Fluorescence characteristics of the fluorescein isothiocyanate (FITC) nanoparticles

The fluorescent spectra of the nanoparticles with fluorescein isothiocyanate (FITC) labelled dendrimer core (MA/FITC-core) or labelled polymeric shell (AMAH/FITC-shell) were analysed with FluoroMax-2 fluorometer and Spex-3D fluorometer. The FluoroMax-2 fluorometer parameter was set to an excitation wavelength of 488 nm.

The emission spectra of FITC dissolved in methanol showed a red shift compared to the spectra of the NPs labelled with FITC. A significant blue shift was observed in the case of the NPs with the florescent core as well as a significant quenching of the intensity of the signal.

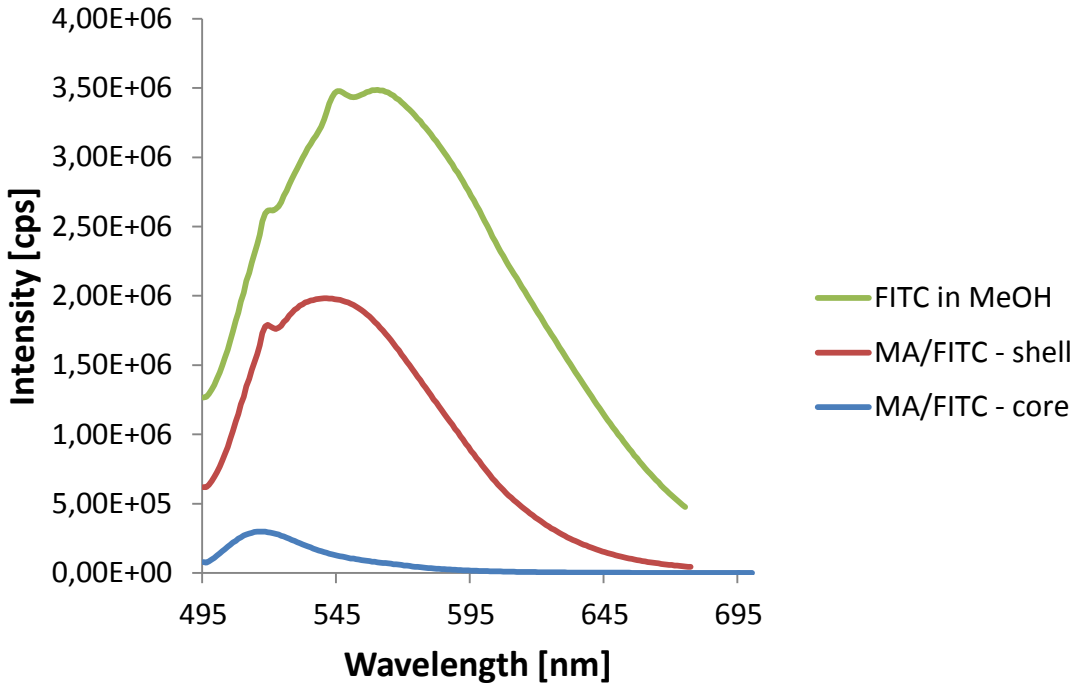

Figure 3.18: Emission spectra of FITC dissolved in MeOH compared to MA/FITC-core and AMAH/FITC-shell NPs.

Table 3.6: Fluorescence intensity maximum and corresponding emission wavelength maximum of FITC dissolved in MeOH compared to MA/FITC-core and MA/FITC-shell NPs. (E_{xc} = 488 nm in methanol)

	Emission wavelength [nm]	Intensity [cps]
MA/FITC-core	516	298 560
AMAH/FITC-shell	569	1 849 900
FITC dissolved in MeOH	608	1 885 500

3.4.4.1 MA/FITC - core NPs

The fluorescence measurements of the MA/FITC-core NPs over time stored at different temperatures (4 °C, 24 °C, 37 °C) in PBS showed for all samples a decrease of the fluorescence intensity. The intensity of the samples stored at 4 °C and 37 °C decreased slower, then the intensity of the sample stored at 24 °C. The emission wavelength stayed stable at around 515 nm.

3.4.4.2 AMAH/FITC – shell NPs

The measured fluorescence intensity of the AMAH/FITC-shell NPs samples stored at different temperatures in PBS show at all temperatures a slowly decrease in the intensity over time. In contrast to the MA/FITC-core NPs shifted the emission wavelength of the AMAH/FITC-shell NPs from 570 nm to 540 nm in the following weeks.

Table 3.7: Highest fluorescence intensity and their corresponding emission wavelength from **A.** MA/FITC-core NPs and B. AMAH/FITC-shell NPs over time (E_{xc} = 488 nm, in methanol).

A. MA/FITC-core		Em wavelength [nm]	Intensity [cps]
after 1 week	4 °C	516	267 700
	24 °C	516	325 840
	37°C	516	318 460
After 2 weeks	4 °C	511	242 610
	24 °C	509	220 120
	37°C	510	245 220
After 3 weeks	4 °C	517	243 250
	24 °C	516	182 730
	37°C	515	222 680

B. AMAH/FITC-shell		Em wavelength [nm]	Intensity [cps]
After 1 week	4 °C	571	1 874 100
	24 °C	570	1 885 800
	37°C	569	1 877 900
After 2 weeks	4 °C	568	1 870 200
	24 °C	558	1 871 700
	37°C	565	1 870 700
After 3 weeks	4 °C	555	1 862 800
	24 °C	541	1 865 900
	37°C	554	1 863 200

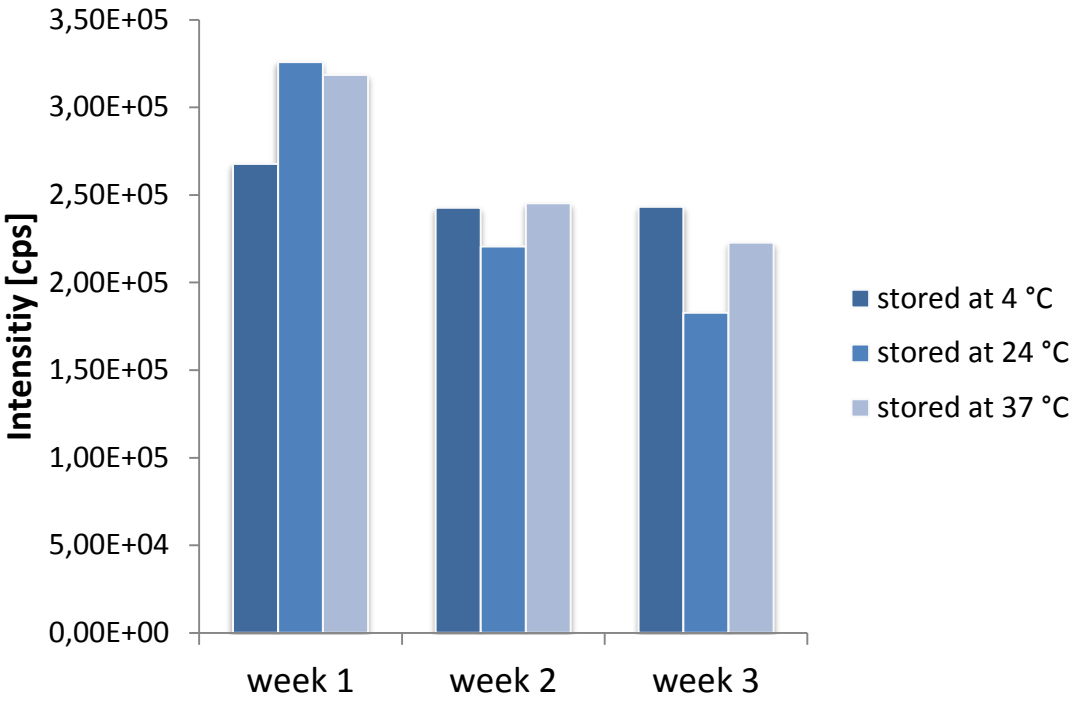

Figure 3.19: Highest fluorescence intensity of the MA/FITC-core NPs, which were stored at different temperature (4 °C, 24 °C, 37 °C) in PBS measured over three weeks

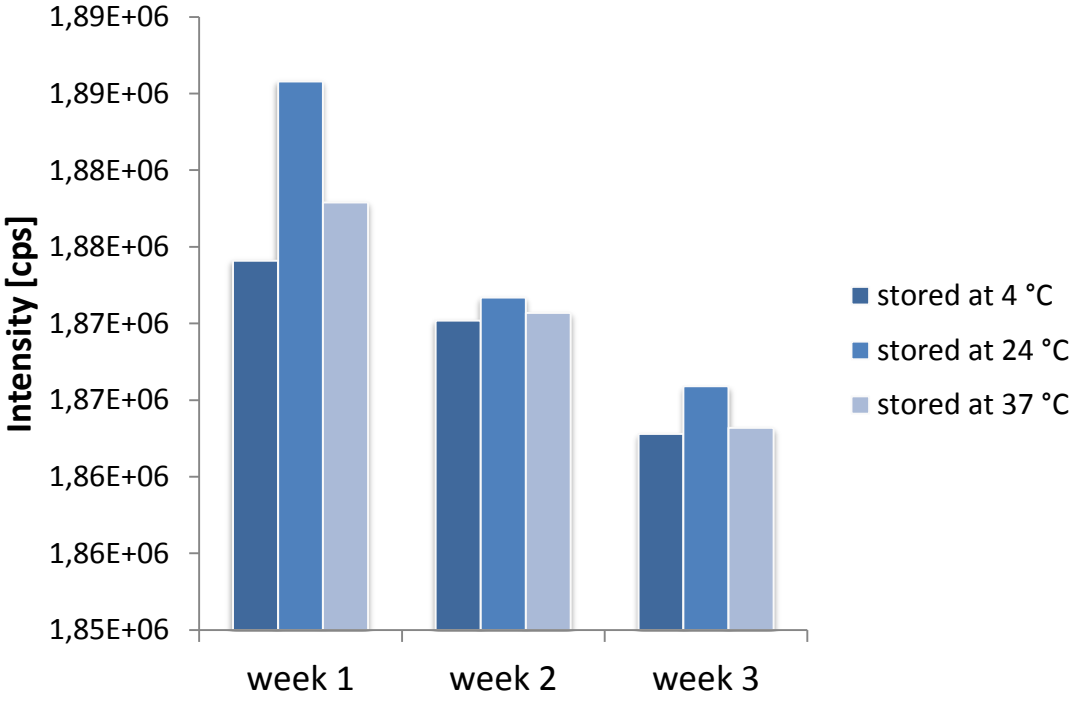

Figure 3.20: Highest fluorescence intensity of the AMAH/FITC-shell NPs, which were stored at different temperature (4 °C, 24 °C, 37 °C) in PBS measured over three weeks

3.5. Nanoparticles detection with confocal microscopy

3.5.1 Nanoparticles detection without cells

The MA/FITC-core and AMAH/FITC-shell NPs have been observed under a Zeiss inverted confocal scanning microscope LSM 510 Meta. Sample of NPs was prepared and excited with an argon laser at 488 nm and was detected with a band-pass filter at 505-550 nm. The cell membrane of bladder cancer cells were stained with Alex 555 streptavidin conjugate and excited with a helium-neon laser at 543 nm. They were detected with a long-pass filter at 560 nm.

The NPs have been observed under the fluorescence microscope of the LSM 510 Meta. Observation showed that the MA/FITC-core NPs and AMAH/FITC-shell NPs have the same intensity. The ascertained size ranged below 50 nm for both types of NPs and showed high monodispersity. The NPs showed also high solubility. The green shadowing shown in the background of Figure 3.21 was seen to be background noise, while the intense fluorescent points were proven to be the NPs. The particles have been permanently excited under the confocal microscope and showed a longer lifetime then FITC background noise.

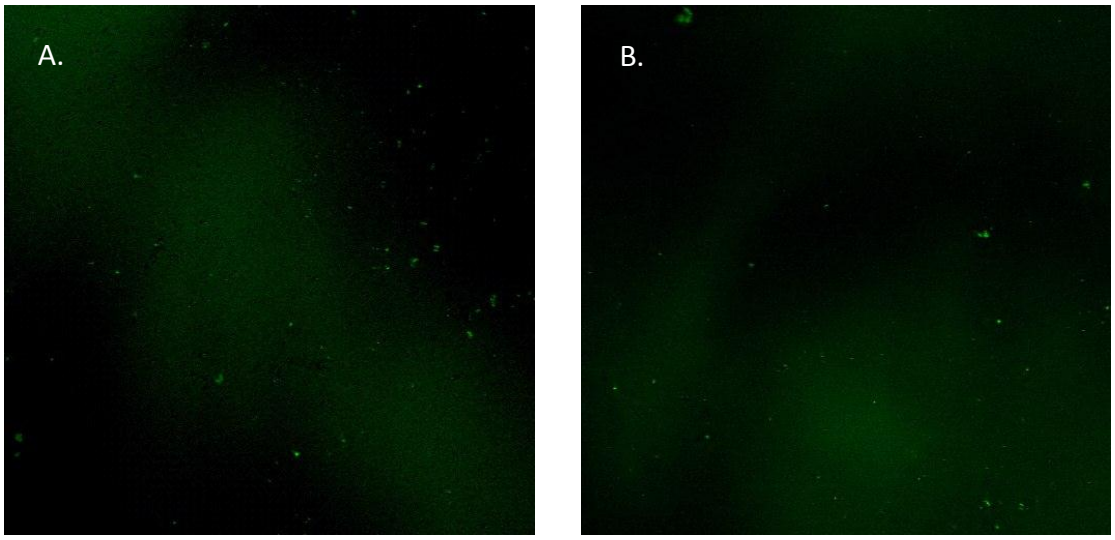

Figure 3.21: Confocal microscopy pictures of the A. MA/FITC-core and B. AMAH/FITC-shell NPs.

3.5.2 Nanoparticles detection after cell incubation

Bladder cancer cells were treated with the fluorescent nanoparticles and after forty-eight hours analysed with confocal and non-confocal microscopy. Due to device failure no confocal microscope pictures of the nanoparticles on the cells could be taken. Nevertheless observation by eye through the fluorescence microscope LSM 510 Meta showed that the NPs interacted with the cell membrane. We detected on the red channel the cells, on the green channel the nanoparticles and detected green spots on the red labelled cells but not on the background. This indicates that either the NPs have attached outside on the cell membrane or have been in cooperated inside the bladder cancer cells. Without confocal microscopy no clear statement can be given concerning their position within the cells. Furthermore it could be observed that there was no influence on cell growth as the cells treated with the fluorescent nanoparticles showed a normal growing behaviour.

CHAPTER 4

DISCUSSION

4. Discussion

In this project a new materials for cell imaging have been studied. Fluorescent core-shell nanoparticles have been produced, which gives the possibility to direct specific target biological material, prevents fluorescent dyes from leaking and increases the lifetime of fluorescent dyes.

This chapter gives a better understanding of the accomplished results. It deals with the problems which have been investigated during the thesis and discusses the NP shape, size measurement technologies, fluorescence experiments and the interaction of the NPs with bladder cancer cells.

4.1. Synthesis strategy

The NPs were synthesised by a UV initiated living radical polymerisation using an iniferter attached to the dendrimer periphery. EDC was used to introduce the iniferter (CNDDA) onto the surface of the dendrimers. During polymerisation TRIM and EDGMA acted as cross-linkers and were copolymerised with the used monomer to build out a crosslinked polymeric shell around the dendrimer core. The thickness of the shell can be controlled by varying the amount of monomers and cross-linkers as well as by the polymerisation time and the intensity of the UV source.

4.2. Size and shape evaluation

Scanning electron microscopy (SEM) pictures of the nanoparticles have been taken to identify their shape and size. However, SEM cannot be used to investigate the size of the sample stored at different temperature and different solutions over time, as SEM requires a dehydration of the sample. Bigger particles could be coated with carbon, whereas the smaller particles needed a gold/palladium coating due to decreased

contrast. Carbon coating gives a better resolution for small objects than gold/palladium coating but is less conductive and could not provide good contrast. Gold/palladium coating could be seen as small granules that are covering the sample due to the bigger size of the coated particles. This would lead to masking surface of the NPs.

The shape of the NPs investigated by SEM showed a cubic shape for the samples with a hydrophilic MA-shell of the NPs and a spherical shape for the hydrophobic ST-shell of the NPs. The different shape of the particles can be explained by the hydrophilic and hydrophobic properties of the polymeric shells. All types of NPs were dispersed in PBS media, which is water based or hydrophilic.

As the principal of dynamic light scattering (DLS) is based on Brownian motion and uses a laser to irradiate the particles in the sample it can cause problems while measuring the size of coloured or fluorescent samples. The mathematical model uses an ideal sphere to calculate from the back scattered light the size of the particles. The monochromatic light of the laser causes a Doppler shift when it hits a moving particle, this leads to a change of the wavelength of the reflected light. This change can be detected and is related to the size of the measured particle. However, not only the wavelength is depending on the size and shape of the molecule, but also depends on the detection angle, frequency and the intensity of the scattered light (Berne et al. 2000).

DLS measurements of the dendrimers before and after each modification step were recorded. The analysis showed clear difference between the samples which indicated a successful surface modification. When samples labelled with FITC were analysed, a significant increase of the hydrodynamic diameter was observed. This increase could not be real since these data contradict not only due to the possible outcome of preparation procedure but also from the SEM analysis, which shows much smaller sizes. DLS measurement of coloured or fluorescent sample changes the scattered wavelength due to multiple absorption of the exposed light - wavelength. For this

reason other analysing technologies such as nanoparticle tracking analysis (NTA) are more appropriate. NTA uses the same principle as DLS, but analyses the Brownian motion of the particles by video. It tracks the position changes of every single particle in two dimensions and determines the particles diffusion, from which the hydrodynamic diameter can be defined (Filipe et al. 2010).

Nevertheless, SEM pictures showed the right size of the particles but this technique is not convenient for observation of the particles behaviour in a solution. Atomic force microscopy (AFM) showed to be a capable technique to analyse size and shape of particles in aqueous or other fluid environment (Neto et al., 1999). It gives information about surface structure, size and shape of a sample either dried or in a liquid. Whereas SEM requires an electrically conductive sample, AFM does not require any coatings. This means no dehydration of the sample is required and samples can be imaged in their hydrated state. ATM has a non-contact mode, which offers the opportunity to investigate soft samples and not damage them (Morita et al. 2009).

DLS measurements showed that the NPs where likely to agglomerate, as after longer sonication the measured size decreased and smaller sizes have been observed. For this reason a zeta potential analyses would have been interesting. The zeta potential gives information about materials stability and liability of agglomeration in a solution. It is defined as the electrical potential which is located close to the surface of the particle. A high zeta potential indicates a low attraction between the particles, which means that the particles in the sample are highly dispersed. In contrast, a low zeta potential denotes large agglomeration of the particles, as they attracted each other (Hosokawa, 2007).

Transmission electron microscopy (TEM) would give higher resolution for small NPs and a clearer picture of their shape and morphology.

4.3. Fluorescence characteristics

4.3.1 Fluorescent isoindole (FII)

The fluorescence analysis of the different modified PAMAM dendrimers displayed that the PAMAM dendrimers with 100% free surface amino groups, labelled with FII had the highest intensity. The fluorescence intensity changes depending on the number of the available surface amino groups available for modification. The commercially available PAMAM 25% C_{12} dendrimers have 75% free surface amino groups ready to be labelled with FII, while the 50% C_{12} have only 50% free groups. The 50% modified dendrimers were analysed by labelling with FII to prove that the iniferter modification of the PAMAM dendrimers ranged between 25% and 50% of the surface groups. The fluorescence analysis confirmed that the 50% modification of the PAMAM dendrimer was successful and ranked between 25% and 50% of the amine surface groups of the PAMAM dendrimers.

As expected, a decrease in the fluorescence intensity of FII labelled dendrimers accompanies decrease in the pH of the sample. Hydrochloric acid was used to change the pH from neutral to acidic. This change acted as a quencher of the fluorescence. While the intensity of the fluorescence spectra decreased, it shifted the emission wavelength towards the red–region. It is reported that solvent polarity has a large effect on the isoindole fluorescence spectra. Whereas an aqueous solution with a low pH causes quenching, low concentration and non-aqueous solutions stabilise the fluorescence intensity of fluorescent isoindole (Simons et al. 1978).

Interestingly, the experiment with dendrimers in combination with fluorescent isoindole and the weak salicylic acid, showed an increase of the fluorescence intensity. This can serve as a model for the investigation of the effect of a guest drug binding to the host FII labelled PAMAM dendrimers. Salicylic acid due to its size would serve as a guest in the dendrimers cavities (Saboktakin, 2008) and does not contain any free primary amino groups that would react with the excess of the isoindole presented in

the reaction mixture. Salicylic acid in cooperation with FII labelled dendrimers at an excitation wavelength of 275 nm in methanol showed a shift of the emission wavelength from 420 nm to 400 nm. Salicylic acid in combination with methanol forms an ester, known as methyl salicylate, which is a natural product of many plants. Also methyl salicylate is reported to develop fluorescence with similar excitation and red shifted emission wavelength maximum (Lopez-Delgado et al. 1981), compared to the fluorescent dendrimer. Due to the inherited fluorescent signal of salicylic acid or rather methyl salicylate the intensity of FII labelled dendrimers increased. The blue shift could be due to the guest-host interaction as the emission maxima of the salicylic acid would be red shifted compared to the FII labelled dendrimers.

Fluorescent measurement of the NPs with an FII labelled dendrimer core gives information on their fluorescence behaviour due to the shell properties. The results show, that the intensity slowly decreased and the emission wavelength into the UV region shifted over time. The excitation wavelength of 275 nm was chosen as most appropriate based on the 3D fluorescent measurements. The literature reports an excitation wavelength for FII at 355 nm; measurements of the NPs were also taken at this wavelength (E V Piletska et al., 2001).The literature shows an emission maximum at 430 nm for a thioacetale–containing polymer. However, the FII NPs showed a corresponding emission wavelength for MA/FII and ST/FII at around 400 and 445 nm. Interestingly measurement of the dendrimers labelled with FII at an excitation wavelength of 275 nm showed a resulting emission wavelength also in this area but with lower intensity.

4.3.2 Fluorescein isothiocyanate (FITC)

The fluorescence shelf life of MA/FITC–core and AMAH/FITC–shell NPs was observed. The results showed that over time the fluorescence intensity slowly decreases. The AMAH/FITC–shell NPs showed a high intensity. As these particles have been observed under the confocal microscope it was impossible to see the discrete particles, as there were too small. After photobleaching of the background noise, the NPs bulk could still

be seen, which indicates, that the lifetime of the particles increased. Under the confocal microscope AMAH/FITC–shell particles seemed to be as bright as the MA/FITC–core particles which mean that the light penetrates through the shell.

4.4. Nanoparticle detection with fluorescence microscopy

4.4.1. Fluorescent isoindole (FII)

The nanoparticles containing FII labelled dendrimer core could not be imaged with the confocal microscope, as the used Zeiss LSM 510 Meta did not possess the right laser for an excitation wavelength at 275 nm or 355 nm. However, NPs have been observed by eye using the microscope in combination with a xenon lamp. The observation showed bright blue particles.

4.4.2. Fluorescein isothiocyanate (FITC)

The nanoparticles with either FITC labelled dendrimer core or polymeric shell could be excited using argon laser at an excitation wavelength of 488 nm. Although MA/FITC–core NPs have a negatively charged surface and the AMAH/FITC–shell NPs have a positively charged surface, a difference in cell uptake for these materials was negligible, as both types of nanoparticles within the bladder cancer cells showed to bind to the cell membrane in the same way.

For the purpose of imaging NPs and cells together, the bladder cancer cells have been stained, which means that the entire medium was removed and cells were washed. All now remaining NPs were bound to the cells. Under the microscope while switching between red and green channel either the cells or the NPs could be observed by eye. So it could be confirmed, that particles were still presented interacting with the cell membrane. A possible explanation why the nanoparticles could not be pictured is that

they are too small to build out a big layer on the cell membrane. The confocal microscope LSM 510 Meta is not build to picture particles in the nanometer size.

The particles showed also high solubility as no bigger agglomeration could be observed. A higher concentration of nanoparticles was not easy to create. Millipore amicon ultra centrifugal filter, used to purify the nanoparticles required at least one millilitre of medium. To have 1 ml concentrated solution of NPs more dendrimers have to be labelled and polymerised.

Neither the MA/FITC–core nor the AMAH/FITC–shell nanoparticles showed to influence the cell viability at low concentration. Although the cells seemed to have a normal cell growth a toxicity effect cannot be excluded. Further investigation in this area has to be done by using cell viability assays such as MTT–assay and neutral red. The MTT–test is a very commonly used test to determine the viability and proliferation of cells and a possible cytotoxicity effect outgoing from materials, such as nanoparticles. Another possible cell viability assay is the neutral red uptake assay. This assay is based on the ability of the cells to bind on a supravital dye in the lysosomes, to estimate the number of viable cells in a culture. It is generally used as a cytotoxicity test for many environmental and biomedical applications (Repetto et al., 2008).

CHAPTER 5

CONCLUSION AND FUTURE WORK

5. Conclusion and Future work

Fluorescent core/shell organic nanoparticles have been designed, synthesised and tested over a period of three month. Two different labels were used during this work, FITC and FII. FII has never been used as a fluorescent label for dendrimers or for NPs. FII NPs with hydrophobic and with hydrophilic polymer shell were developed. NPs labelled with FII could not be used in the cell imaging due to excitation maximum restrictions in the technique used for the analysis (confocal microscopy). FII labelled dendrimers have been studied for their fluorescence stability, pH sensitivity and drug interaction, as a possible new fluorescent sensor.

In this work PAMAM dendrimers, generation 4, were used as a grafting core for the synthesis of core/shell organic nanoparticles. The power of these core/shell particles labelled with fluorescent dyes is threefold. The possible advantages of fluorescent core NPs are that a dye leaking can be prevented and also by encapsulating the fluorescent dye with an organic polymeric shell, their performance (e.g. brightness and stability) can be enhanced. At last, the fluorescent core architecture allows creating multiple functions, such as fluorescent ability, drug encapsulation and specific targeting. Developing fluorescent shell NPs can be advantageous as the fluorescent signal is higher in intensity and no quenching was observed due to the polymer shell formation as is the case of the florescent core NPs.

Although the nanoparticles in the cells could not be imaged by the confocal microscope, it could be observed that there was no leaking and no impact on cell growth from the NPs. Further work on imaging of the nanoparticles has to be done by using a higher concentration of the nanoparticles. As it was possible to produce these fluorescent nanoparticles with two different kind of fluorescent dyes and showed similarity in increasing fluorescent lifetime, it is assumed that the fluorescent nanoparticles can be produced with every kind of fluorophore.

Further work has to be done to estimate toxicity, as no cell viability assay has been performed.

The organic polymeric shell offers the opportunity to imprint their surface, to mimic natural antibodies. Molecularly imprinting is a technology, where a polymer has been polymerized in the presence of a template. This template has similar properties of the chemical structure as the targeting molecule. These polymers are called molecularly imprinted polymers (MIPs) and have the ability to bind specific target molecules.

In conclusion, the fluorescent core/shell nanoparticles are a promising tool for specific targeting and can be used as a new specific label for cell imaging. Furthermore it has been proven, that the shell of the nanoparticles increases the fluorescent lifetime of the fluorescent dyes.

References

Abcam. (2011). Immunostaining. (Abcam, Ed.). Cambridge. Retrieved from http://www.abcam.com/

Anderson, R. J., Bendell, D. J., & Groundwater, P. W. (2004). *Organic spectroscopic analysis*. Cambridge: Royal Society of Chemistry.

Anja Niedermayr. (2011). Fluoreszenzmikroskopie. (Universität Göttingen, Ed.). Retrieved from https://lp.uni-goettingen.de/get/text/6741

Ashurst, P. R., & Dennis, M. J. (1998). *Analytical methods of food authentication*. London: Blackie Academic {&} Professional.

BUHLEIER, E., WEHNER, W., & VÖGTLE, F. (1978). "Cascade"- and "Nonskid-Chain-like" Syntheses of Molecular Cavity Topologies. *Synthesis*, *1978*(02), 155-158. doi:10.1055/s-1978-24702

Baker, L. A., & Crooks, R. M. (2000). Photophysical Properties of Pyrene-Functionalized Poly(propylene imine) Dendrimers. *Macromolecules*, *33*(24), 9034-9039. doi:10.1021/ma001379c

Baschong, W., & Aebi, U. (2006). Negative Staining. *Solutions*, 1-3.

Berne, B. J., & Pecora, R. (2000). *Dynamic light scattering: With applications to chemistry, biology, and physics* (Dover.). Mineola, N.Y: Dover Publications.

Boas, U., Christensen, J. B., & Heegaard, P. M. H. (2006). *Dendrimers in medicine and biotechnology*. Cambridge: RSC.

Bruchez Jr., M. (1998). Semiconductor Nanocrystals as Fluorescent Biological Labels. *Science*, *281*(5385), 2013-2016. doi:10.1126/science.281.5385.2013

Börner, H. G. (2007). Functional Polymer-Bioconjugates as Molecular LEGO{\circledR} Bricks. *Macromolecular Chemistry and Physics*, *208*(2), 124-130. doi:10.1002/macp.200600559

Caldin, E. (2001). *The mechanisms of fast reactions in solution*. Amsterdam and , Washington, DC: IOS Press.

Cloninger, M. J. (2002). Biological applications of dendrimers. *Current opinion in chemical biology*, *6*(6), 742-748.

DAI, F., BURKERT, V., SINGH, H., & HINZE, W. (1997). Update and Evaluation of the Effectiveness of Different Thiols and Micellar Media in Roth's Fluorimetric Method for the Determination of Primary Amino Compounds. *Microchemical Journal*, *57*(2), 166-198. doi:10.1006/mchj.1997.1529

Diallo, M. S. G. W. A. R. J. L. (2006). Cellular Uptake and Toxicity of Dendritic Nanomaterials: An Integrated Physicochemical and Toxicogenomics Study. (EPA UNited States Environmental Protection Agency, Ed.). Retrieved from http://cfpub2.epa.gov/ncer_abstracts/index.cfm/fuseaction/display.abstractDetail/abstract/7857/report/2006

Dykes, G. M. (2001). Dendrimers: a review of their appeal and applications. *Journal of Chemical Technology {&} Biotechnology*, *76*(9), 903-918. doi:10.1002/jctb.464

E. V. Piletska, S. A. P. S. S. K. K. A. P. F. T. (2001). A new reactive polymer suitable for covalent immobilisation and monitoring of primary amines, *8*(42), 3603-3608. doi:10.1016/S0032-3861(00)00739-4

Echlin, P. (2009). *Handbook of sample preparation for scanning electron microscopy and x-ray microanalysis*. New York and , London: Springer.

Esfand, R., & Tomalia, D A. (2001). Poly(amidoamine) (PAMAM) dendrimers: from biomimicry to drug delivery and biomedical applications. *Drug discovery today*, *6*(8), 427-436.

Fatehi, L., Wolf, S. M., Ramachandran, G., & Kuzma, J. (2011). Introduction: designing nanobiotechnology oversight. *Journal of Nanoparticle Research*, *13*(4), 1341-1343. doi:10.1007/s11051-011-0231-4

Feynman, R. P. (1992). There's plenty of room at the bottom (data storage). *Journal of Microelectromechanical Systems*, *1*(1), 60-66. doi:10.1109/84.128057

Filipe, V., Hawe, A., & Jiskoot, W. (2010). Critical Evaluation of Nanoparticle Tracking Analysis (NTA) by NanoSight for the Measurement of Nanoparticles and Protein Aggregates. *Pharmaceutical Research*, *27*(5), 796-810. doi:10.1007/s11095-010-0073-2

Fu, Y., Nitecki, D., Maltby, D., Simon, G., Berejnoi, K., Raatschen, H.-J., Yeh, B., et al. (2006). Dendritic iodinated contrast agents with PEG-cores for CT imaging: synthesis and preliminary characterization. *Bioconjugate chemistry*, *17*(4), 1043-1056. doi:10.1021/bc060019c

Goldman, R. D. (2006). *Basic methods in microscopy: Alaboratory manual*. New York: Cold spring harber laboratory press.

Goldstein, J. (2003). *Scanning electron microscopy and x-ray microanalysis* (3rd ed.). New York: Kluwer Academic/Plenum Publishers.

Goldys, E. M. (2009). *Fluorescence applications in biotechnology and life sciences*. Wiley-Blackwell. Retrieved from http://books.google.de/books?id=4Lu_Fsspx9YC

Grebel-Koehler, D., Liu, D., Feyter, S. de, Enkelmann, V., Weil, T., Engels, C., Samyn, C., et al. (2003). Synthesis and Photomodulation of Rigid Polyphenylene Dendrimers with an Azobenzene Core. *Macromolecules*, *36*(3), 578-590. doi:10.1021/ma021135n

Greenwald, S. E., & Brown, A. G. (2004). Histology and Staining. *Histochemie*, 16-1 - 16-25.

Grinstaff, M. W. (2002). Biodendrimers: new polymeric biomaterials for tissue engineering. *Chemistry (Weinheim an der Bergstrasse, Germany)*, *8*(13), 2839-2846.

Hagfeldt, A., & Graetzel, M. (1995). Light-Induced Redox Reactions in Nanocrystalline Systems. *Chemical Reviews*, *95*(1), 49-68. doi:10.1021/cr00033a003

Hangauer, M. J., & Bertozzi, C. R. (2008). A FRET-based fluorogenic phosphine for live-cell imaging with the Staudinger ligation. *Angewandte Chemie International Edition*, *47*(13), 2394-2397. Retrieved from http://www.ncbi.nlm.nih.gov/pubmed/18306205

Hartmuth C. Kolb, M. G. F. K. B. S. (2001). Click Chemistry: Diverse Chemical Function from a Few Good Reactions. *Angewandte Chemie International Edition*, *June 1, 20*(Volume 40, Issue 11), 2004-2021.

Hawker, C. J., & Frechet, J. M. J. (1990). Preparation of polymers with controlled molecular architecture. A new convergent approach to dendritic macromolecules. *Journal of the American Chemical Society*, *112*(21), 7638-7647. doi:10.1021/ja00177a027

Hof, M., Hutterer, R., & Fidler, V. (2005). *Fluorescence spectroscopy in biology: Advanced methods and their applications to membranes, proteins, DNA, and cells*. Berlin and , New York: Springer.

Hosokawa, M. (2007). *Nanoparticle technology handbook*. Elsevier. Retrieved from http://books.google.de/books?id=6rcfIEclo7IC

Ibey, B., Beier, H., Rounds, R., Cote, G., Yadavalli, V., & Pishko, M. (2005). Competitive binding assay for glucose based on glycodendrimer-fluorophore conjugates. *Analytical chemistry*, *77*(21), 7039-7046. doi:10.1021/ac0507901

Ihre, H. R., Padilla Jesús, O. L. de, Szoka, F. C., & Fréchet, J. M. J. (2002). Polyester Dendritic Systems for Drug Delivery Applications:~ Design, Synthesis, and Characterization. *Bioconjugate Chemistry*, *13*(3), 443-452. doi:10.1021/bc010102u

Ivanova-Mitseva, P. K., Fragkou, V., Lakshmi, D., Whitcombe, M. J., Davis, F., Guerreiro, A., Crayston, J. A., et al. (2011). Conjugated Polymers with Pendant Iniferter Units : Versatile Materials for Grafting. *Macromolecules*, 110314100149046. doi:10.1021/ma102692h

Jevprasesphant, R., Penny, J., Attwood, D., & D'Emanuele, A. (2004). Transport of dendrimer nanocarriers through epithelial cells via the transcellular route. *Journal of Controlled Release*, *97*(2), 259-267. doi:10.1016/j.jconrel.2004.03.022

Kiessling, F., Morgenstern, B., & Zhang, C. (2007). Contrast agents and applications to assess tumor angiogenesis in vivo by magnetic resonance imaging. *Current medicinal chemistry*, *14*(1), 77-91.

Kobayashi, H, Kawamoto, S., Saga, T., Sato, N., Hiraga, A., Ishimori, T., Konishi, J., et al. (2001). Positive effects of polyethylene glycol conjugation to generation-4 polyamidoamine dendrimers as macromolecular MR contrast agents. *Magnetic resonance in medicine : official journal of the Society of Magnetic Resonance in Medicine / Society of Magnetic Resonance in Medicine*, *46*(4), 781-788.

Lakowicz, J. R. (2006). *Principles of fluorescence spectroscopy* (3rd ed.). New York: Springer.

Lakowicz, J. R., & Masters, B. R. (2008). *Principles of Fluorescence Spectroscopy, Third Edition* (Vol. 13). doi:10.1117/1.2904580

Larson, C. L., & Tucker, S. A. (2001). Intrinsic Fluorescence of Carboxylate-Terminated Polyamido Amine Dendrimers. *Applied Spectroscopy*, *55*(6), 679-683. doi:10.1366/0003702011952596

Lemieux, G. A., De Graffenried, C. L., & Bertozzi, C. R. (2003). A fluorogenic dye activated by the staudinger ligation. *Journal of the American Chemical Society*, *125*(16), 4708-4709. Retrieved from http://www.ncbi.nlm.nih.gov/pubmed/12696879

Lichtman, J. W., & Conchello, J.-A. (2005). Fluorescence microscopy. *Nature Methods*, *2*(12), 910-919. doi:10.1038/nmeth817

Lopez-Delgado, R., & Lazare, S. (1981). Fluorescence properties of methyl salicylate in vapor, liquid, and solution. *The Journal of Physical Chemistry*, *85*(7), 763-768. doi:10.1021/j150607a009

Lubell, W. D., Meldal, M., Tornøe, C. W., Nielsen, T. E., Diness, F., Le Quement, S. T., Christensen, C. A., et al. (2010). Ralph F. Hirschmann award address 2009: Merger of organic chemistry with peptide diversity. *Biopolymers*, *94*(2), 161-182. doi:10.1002/bip.21344

Malik, N., Wiwattanapatapee, R., Klopsch, R., Lorenz, K., Frey, H., Weener, J. W., Meijer, E. W., et al. (2000). Dendrimers: relationship between structure and biocompatibility in vitro, and preliminary studies on the biodistribution of 125I-labelled polyamidoamine dendrimers in vivo. *Journal of controlled release : official journal of the Controlled Release Society*, *65*(1-2), 133-148.

Maret, G., & Wolf, P. E. (1987). Multiple light scattering from disordered media. The effect of brownian motion of scatterers. *Zeitschrift f*  *r Physik B Condensed Matter*, *65*(4), 409-413. doi:10.1007/BF01303762

McMurry, J. (2008). *Organic chemistry* (7th ed.). Belmont, CA: Thomson Brooks/Cole.

Morita, S., Giessibl, F. J., & Wiesendanger, R. (2009). *Noncontact Atomic Force Microscopy*. Springer. Retrieved from http://books.google.de/books?id=kuNTEWKAVacC

Mukesh, C. G., & Rajesh, K. P. (2009). Dendrimer: an overview. (Pharmainfo.net, Ed.). Retrieved from http://www.pharmainfo.net/reviews/dendrimer-overview

Neto, C., Aloisi, G., Baglioni, P., & Larsson, K. (1999). Imaging Soft Matter with the Atomic Force Microscope:˜ Cubosomes and Hexosomes. *The Journal of Physical Chemistry B*, *103*(19), 3896-3899. doi:10.1021/jp984551b

Newbury, D. E. (1986). *Advanced scanning electron microscopy and X-ray microanalysis*. New York: Plenum Press.

Olympus. (2011). Confocal Microscopy. *2004-2009*. Retrieved from http://www.olympusfluoview.com/theory/index.html

Orndorff, W. R., & Hemmer, A. J. (1927). FLUORESCEIN AND SOME OF ITS DERIVATIVES. *Journal of the American Chemical Society*, *49*(5), 1272-1280. doi:10.1021/ja01404a016

Pawley, J. B. (2006). *Handbook of biological confocal microscopy*. Springer. Retrieved from http://books.google.de/books?id=E2maxdEXFNoC

Pettersson, B. (1996). Hyperbranched polymers: unique design tools for multi-property control in resins and coatings. *Pigment {&} Resin Technology*, *25*(4), 4-14. doi:10.1108/eb043185

Piletska, E V, Piletsky, S A, Subrahmanyam, S., Karim, K., & Turner, A. P. F. (2001). A new reactive polymer suitable for covalent immobilisation and monitoring of primary amines. *Polymer*, *42*(8), 3603-3608. doi:10.1016/S0032-3861(00)00739-4

Prescher, J. A., & Bertozzi, C. R. (2005). Chemistry in living systems. *Nature Chemical Biology*, *1*(1), 13-21. doi:10.1038/nchembio0605-13

Reimer, L. (2011). *Scanning electron microscopy: Physics of image formation and microanalysis* (3rd ed.). Berlin [u.a.]: Springer.

Repetto, G., Del Peso, A., & Zurita, J. L. (2008). Neutral red uptake assay for the estimation of cell viability/cytotoxicity. *Nature Protocols*, *3*(7), 1125-31. Nature Publishing Group. doi:10.1038/nprot.2008.75

Resch-Genger, U. (2008). *Standardization and Quality Assurance in Fluorescence Measurements: Techniques*. Springer. Retrieved from http://books.google.de/books?id=kZvTX1QEhE8C

Roberts, J. C., Adams, Y. E., Tomalia, D., Mercer-Smith, J. A., & Lavallee, D. K. (1990). Using starburst dendrimers as linker molecules to radiolabel antibodies. *Bioconjugate chemistry*, *1*(5), 305-308.

Saboktakin, M. R. ; M., Abel; Ramazanov, Mohammad Ali. (2008). Poly(amidoamine)(PAMAM) /CMS Dendritic nanocomposite for controlled drug delivery. *The Journal of American Science*, *4*(1), 48 - 52.

Sato, N., Kobayashi, H, Saga, T., Nakamoto, Y., Ishimori, T., Togashi, K., Fujibayashi, Y., et al. (2001). Tumor targeting and imaging of intraperitoneal tumors by use of antisense oligo-DNA complexed with dendrimers and/or avidin in mice. *Clinical cancer research : an official journal of the American Association*, *7*(11), 3606-3612.

Schlamp, M. C., Peng, X., & Alivisatos, A. P. (1997). Improved efficiencies in light emitting diodes made with CdSe(CdS) core/shell type nanocrystals and a semiconducting polymer. *Journal of Applied Physics*, *82*(11), 5837. doi:10.1063/1.366452

Schmitz, K. S. (1990). *An introduction to dynamic light scattering by macromolecules*. Boston: Academic Press.

Schneider, J., Tiefenbrunn, T. K., & Dawson, P. E. (2010). Chemoselective ligation techniques: Modern applications of time-honored chemistry. *Biopolymers*, *94*(1), 95-106. doi:10.1002/bip.21337

Shi, X., Wang, S., Meshinchi, S., Van, A., Bi, X., Lee, I., & Baker, J. (2007). Dendrimer-entrapped gold nanoparticles as a platform for cancer-cell targeting and imaging.

Small (Weinheim an der Bergstrasse, Germany), *3*(7), 1245-1252. doi:10.1002/smll.200700054

Simons, S. S., & Johnson, D. F. (1978). Reaction of o-phthalaldehyde and thiols with primary amines: formation of 1-alkyl(and aryl)thio-2-alkylisoindoles. *The Journal of Organic Chemistry*, *43*(14), 2886-2891. doi:10.1021/jo00408a030

Smith, I. C. P., & Blandford, D. E. (1995). Nuclear magnetic resonance spectroscopy. *Analytical Chemistry*, *67*(12), 509-518. doi:10.1021/ac00108a037

Sohár, P. (1984). *Nuclear magnetic resonance spectroscopy*. Boca Raton, Fla: CRC Pr.

Staining, W.-G. (2000). Staining of Cells. *Cytometry*, 4-7.

Starr, C., Evers, C. A., & Starr, L. (2010). *Biology: Concepts and Applications*. Cengage Learning. Retrieved from http://books.google.de/books?id=_16xbB2Py_UC

Stephens, D. J. (2003). Light Microscopy Techniques for Live Cell Imaging. *Science*, *300*(5616), 82-86. doi:10.1126/science.1082160

Striebel, H.-M., Birch-Hirschfeld, E., Egerer, R., Foldes-Papp, Z., Tilz, G., & Stelzner, A. (2004). Enhancing sensitivity of human herpes virus diagnosis with DNA microarrays using dendrimers. *Experimental and molecular pathology*, *77*(2), 89-97. doi:10.1016/j.yexmp.2004.05.004

Talanov, V. S., Regino, C. A. S., Kobayashi, Hisataka, Bernardo, M., Choyke, P. L., & Brechbiel, Martin W. (2006). Dendrimer-Based Nanoprobe for Dual Modality Magnetic Resonance and Fluorescence Imaging. *Nano Letters*, *6*(7), 1459-1463. doi:10.1021/nl060765q

Thomas, T., Patri, A., Myc, A., Myaing, M., Ye, J., Norris, T., & Baker, J. (2004). In vitro targeting of synthesized antibody-conjugated dendrimer nanoparticles. *Biomacromolecules*, *5*(6), 2269-2274. doi:10.1021/bm049704h

Thornton, A., Bloor, D., Cross, G. H., & Szablewski, M. (1997). Novel Functionalized Poly(amido amine) (PAMAM) Dendrimers:~ Synthesis and Physical Properties. *Macromolecules*, *30*(24), 7600-7603. doi:10.1021/ma9704119

Tomalia, Donald A. (2005). Birth of a new macromolecular architecture: dendrimers as quantized building blocks for nanoscale synthetic polymer chemistry. *Progress in Polymer Science*, *30*(3-4), 294-324. doi:10.1016/j.progpolymsci.2005.01.007

Valeur, B. (2002). *Molecular fluorescence: Principles and applications*. Weinheim and , New York: Wiley-VCH.

Vicinelli, V., Ceroni, P., Maestri, M., Balzani, V., Gorka, M., & VÖGTLE, F. (2002). Luminescent Lanthanide Ions Hosted in a Fluorescent Polylysin Dendrimer. Antenna-Like Sensitization of Visible and Near-Infrared Emission. *Journal of the American Chemical Society*, *124*(22), 6461-6468. doi:10.1021/ja017672p

Villalonga-Barber, C., Micha-Screttas, M., Steele, B. R., Georgopoulos, A., & Demetzos, C. (2008). Dendrimers as Biopharmaceuticals: Synthesis and Properties. *Current Topics in Medicinal Chemistry*, *8*(14), 1294-1309. doi:10.2174/156802608785849012

Wang, B.-B., Zhang, X., Jia, X.-R., Luo, Y.-F., Sun, Z., Yang, L., Ji, Y., et al. (2004). Poly(amidoamine) dendrimers with phenyl shells: fluorescence and aggregation behavior. *Polymer*, *45*(25), 8395-8402. doi:10.1016/j.polymer.2004.10.015

Wang, D., & Imae, T. (2004). Fluorescence Emission from Dendrimers and Its pH Dependence. *Journal of the American Chemical Society*, *126*(41), 13204-13205. doi:10.1021/ja0454992

Wang, Y.-L., & Taylor, D. L. (Eds.). (1989). *Fluorescence Microscopy of Living Cells and Culture*. San Diego [etc.]: Academic Press.

Watzke, A., Köhn, M., Gutierrez-Rodriguez, M., Wacker, R., Schröder, H., Breinbauer, R., Kuhlmann, J., et al. (2006). Site-selective protein immobilization by Staudinger ligation. *Angewandte Chemie International Edition*, *45*(9), 1408-1412. Retrieved from http://www.ncbi.nlm.nih.gov/pubmed/16440394

Weisbrod, S. H., Baccaro, A., & Marx, A. (2008). DNA conjugation by Staudinger ligation. *Nucleic acids symposium series 2004*, (52), 383-384. Retrieved from http://www.ncbi.nlm.nih.gov/pubmed/18776414

Wiener, E. C., Brechbiel, M W, Brothers, H., Magin, R. L., Gansow, O. A., Tomalia, D A, & Lauterbur, P. C. (1994). Dendrimer-based metal chelates: a new class of magnetic resonance imaging contrast agents. *Magnetic resonance in medicine : official journal of the Society of Magnetic Resonance in Medicine / Society of Magnetic Resonance in Medicine*, *31*(1), 1-8.

Wohltjen, H., & Snow, A. W. (1998). Colloidal Metal-Insulator-Metal Ensemble Chemiresistor Sensor. *Analytical Chemistry*, *70*(14), 2856-2859. doi:10.1021/ac9713464

Appendices

Appendix A

a. Nanoparticles with fluorescent isoindole labelled dendrimer core and hydrophilic or hydrophobic shell properties (MA/FII, ST/FII)

The size of the nanoparticles with a fluorescent isoindole-dendrimer core and different shell properties (hydrophilic and hydrophobic) were measured after synthesis with DLS. The nanoparticles have been stored in PBS and cell culture medium (RPMI) at 4 °C and were measured in the following week.

DLS–size measurements of the MA/FII and ST/FII NPs showed a size of 420 nm and 480 nm after synthesis. The samples were stored in PBS and RPMI at 4 °C and measured in the following weeks. The results show that the size slightly changed after 4 weeks for almost all samples, whereas the sample ST/FII in RPMI after two weeks increased. In the overall it can be assumed that the size did not change.

The following tables (Table 3.2 – 3.4) and figures (Figure 3.4 -3.5) show the results of the DLS -analyses of MA/FII and ST/FII NPs.

Table a.1: DLS – measurement of MA/FII and ST/FII NPs in PBS after synthesis.

After synthesis		MA/FII	ST/FII
PDL		0.807	0.783
Interrupt		0.372	0.740
Peak 1	Size [nm]	419	478.9
	Intensity [%]	100	100
	Width [nm]	48.53	32.51

Table a.2: Size analyses by using DLS of MA/FII and ST/FII in either PBS or RPMI after one week at 4°C

After one weeks		MA/FII		ST/FII	
		PBS	RPMI	PBS	RPMI
PDL		0.308	0.357	0.457	0.307
Interrupt		0.925	0.924	0.932	0.972
Peak 1	Size [nm]	494.4	420.7	405.6	405.6
	Intensity [%]	100	100	100	100
	Width [nm]	84.8	61.92	61.15	175.5

Table a.3: DLS – size measurement after four weeks of MA/FII and ST/FII stored in PBS and RPMI at 4 °C

After four weeks		MA/FII		ST/FII	
		PBS	RPMI	PBS	RPMI
PDL		0.717	0.681	1.000	0.915
Interrupt		0.443	1.03	1.100	1.09
Peak 1	Size [nm]	388.4	451.7	458.7	712.4
	Intensity [%]	85.1	100	100	100
	Width [nm]	39.9	19.68	5.59	
Peak 2	Size [nm]	0.632			
	Intensity [%]	14.9			
	Width [nm]	0.0311			

b

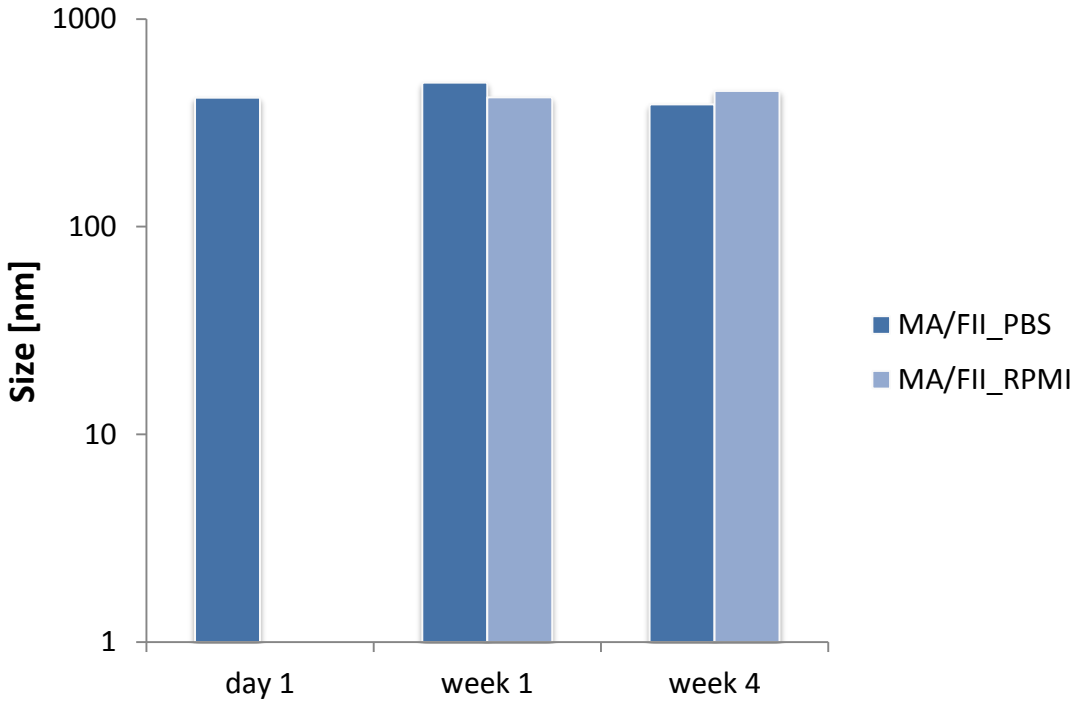

Figure a.1: DLS – size measurements of the MA/FII NPs stored in PBS and RPMI at 4°C

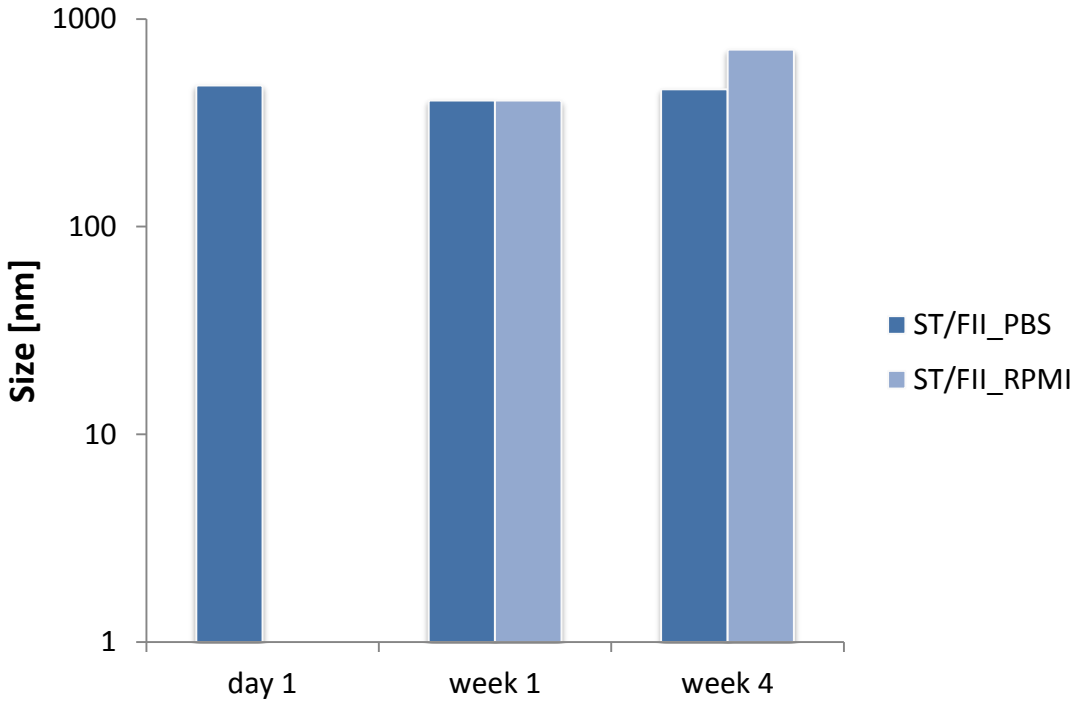

Figure a.2: DLS – size measurements of the ST/FII NPs stored in PBS and RPMI at 4°C

b. Nanoparticles with fluorescent Isothiocyanate labelled dendrimer core or polymeric shell (MA/FITC-core, AMAH/FITC-shell)

The size of the synthesised nanoparticles with a dendrimer core and either fluorescent isothiocyanate labelled dendrimer core (MA/FITC-core) or fluorescent isothiocyanate labelled polymeric shell (AMAH/FITC-shell) were analysed by using DLS. The particles were stored in PBS and cell culture medium (RPMI) at different temperature (4 °C, 24 °c, 37 °C) and their hydrodynamic diameter was measured once per week.

The DLS-size analyses showed that the NPs are having different sizes. Whereas the size of the AMAH/FITC-shell NPs ranged around 240 nm, showed the analysis of the MA/FITC-core NPs a size around 550 nm.

Table b.1: DLS size measurement of the AMAH/FITC-shell and MA/FITC-core NPs after synthesis in PBS.

		AMAH/FITC – shell	MA/FITC - core
PDI		0.453	0.661
Intercept		0.907	1.04
Peak 1	Size [nm]	242.6	550.9
	Intensity [%]	93.9	100
	Width [nm]	59.16	51.22
Peak 2	Size [nm]	44.02	
	Intensity [%]	6.1	
	Width [nm]	7.208	

The DLS analysis of the AMAH/FITC-shell and MA/FITC-core NPs gives information of their behaviour in different solutions and at different temperatures over time. In general it could be observed that the size changed due to the storage temperature and the storage solution. However this observation was not valid for all samples.

AMAH/FITC – shell NPs

Starting from a size of around 240 nm the size was stable after one week stored in PBS at 4 °C and 24 °C and in RPMI at 37 °C, whereas the size increased in the samples stored at 37 °C in PBS and in RPMI at 4 °C and 24 °C. In the following weeks the size of almost all NPs in the different samples increased. Nevertheless the sample stored in PBS at 4 °C showed after three week a size at around 200 nm after it increased before. It was also observed, that in the first week smaller particles in the size of around 1 nm were measured.

MA/FITC – core NPs

Interestingly after the MA/FITC – core NPs have been stored for one week under different conditions, the size of the NPs in PBS at 4 °C, 24 °C and 37°C as well as the sample in RPMI at 4 °C decreased, while the NPs of the RPMI sample stored at 24 °C and 37 °C almost doubled their size. Furthermore the sample in RPMI at 4 °C contained smaller particles at around 100 nm. In the following weeks the size of the NPs in almost all samples increased. The samples stored in RPMI at all temperatures contained smaller and larger particles.

The following tables (Table 3.3-3.8) and graphs (Figure 3.4-3.7) show the hydrodynamic diameter changes over three weeks of the NPs placed at different temperatures.

Table b.2: DLS-size measurement after one week of the NPs AMAH/FITC-shell stored in PBS and RPMI at different temperature (4 °C, 24 °C, 37 °C)

AMAH/FITC- shell week 1		PDI	Intercept	Peak 1			Peak 2			Peak 3		
Solution	Temperature			Size [nm]	Intensity [%]	Width [nm]	Size [nm]	Intensity [%]	Width [nm]	Size [nm]	Intensity [%]	Width [nm]
PBS	4 °C	0.604	0.818	260.9	100	34.81						
PBS	24 °C	0.663	0.902	274.6	100	42.83						
PBS	37 °C	0.331	0.924	598.7	100	93.84						
RPMI	4 °C	0.600	0.708	346.7	93.4	54.8	0.6579	6.6	0.04749			
RPMI	24 °C	0.554	0.754	509.9	100	65.05						
RPMI	37 °C	0.637	0.481	252.6	78.1	46.73	0.8526	21.9	0.1387			

Table b.3: DLS-size measurement after two weeks of the NPs AMAH/FITC-shell stored in PBS and RPMI at different temperature (4 °C, 24 °C, 37 °C)

AMAH/FITC- shell week 2		PDI	Intercept	Peak 1			Peak 2			Peak 3		
Solution	Temperature			Size [nm]	Intensity [%]	Width [nm]	Size [nm]	Intensity [%]	Width [nm]	Size [nm]	Intensity [%]	Width [nm]
PBS	4°C	0.683	0.751	435.1	100	144.8						
PBS	24°C	0.361	0.907	769.6	100	107.7						
PBS	37°C	0.277	0.953	682.3	100	113.4						
RPMI	4°C	0.710	0.651	461.9	100	50.97						
RPMI	24°C	0.243	0.764	519.9	100	83.08						
RPMI	37°C	1.000	1.14	460.8	100	42.68						

Table b.4: DLS-size measurement after three weeks of the NPs AMAH/FITC-shell stored in PBS and RPMI at different temperature (4 °C, 24 °C, 37 °C)

AMAH/FITC- shell week 3		PDI	Intercept	Peak 1			Peak 2			Peak 3		
Solution	Temperature			Size [nm]	Intensity [%]	Width [nm]	Size [nm]	Intensity [%]	Width [nm]	Size [nm]	Intensity [%]	Width [nm]
PBS	4°C	1.000	0.523	208.0	100	14.76						
PBS	24°C	0.618	0.980	517	100	34.21						
PBS	37°C	0.396	0.977	592.4	100	37.32						
RPMI	4°C	0.402	0.835	559.8	100	39.82						
RPMI	24°C	0.431	0.965	807.3	100	56.98						
RPMI	37°C	0.890	0.925	611.6	100	16.81						

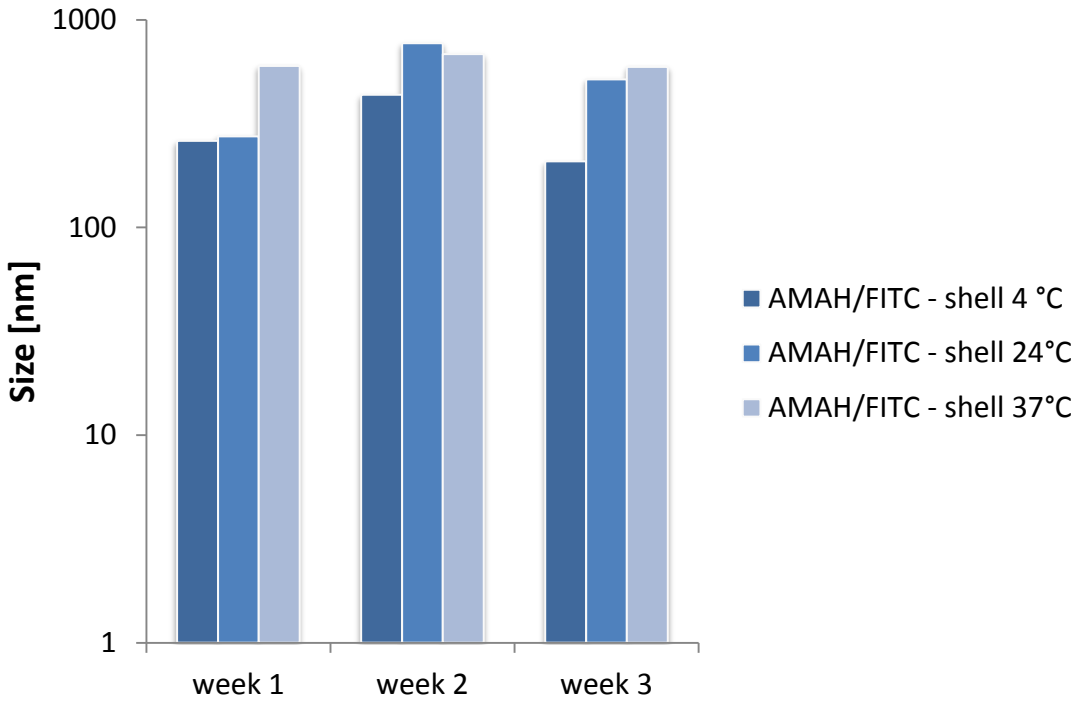

Figure b.1: Size change of AMAH/FITC-shell NPs stored in PBS at different temperature over time

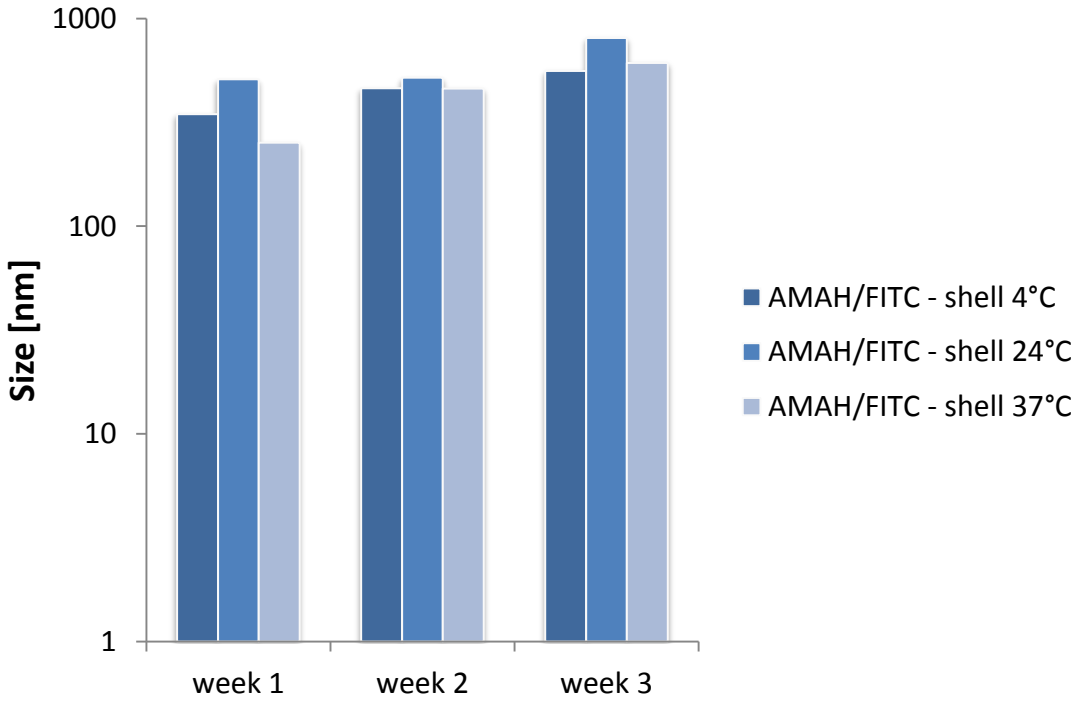

Figure b.2: Size change of MA/FITC – core NPs stored in RPMI at different temperature over time**.**

Table b.5: DLS-size measurement after one week of the NPs MA/FITC-core stored in PBS and RPMI at different temperature (4 °C, 24 °C, 37 °C)

MA/FITC- core week 1		PDI	Intercept	Peak 1			Peak 2			Peak 3		
Solution	Temperature			Size [nm]	Intensity [%]	Width [nm]	Size [nm]	Intensity [%]	Width [nm]	Size [nm]	Intensity [%]	Width [nm]
PBS	4°C	0.702	0.783	424.9	100	55.41						
PBS	24°C	0.769	0.886	437.0	100	40.58						
PBS	37°C	0.689	0.930	450.2	100	47.56						
RPMI	4°C	0.447	0.954	357.4	61.9	167.9	1934	32.7	94.0	4867	5.4	579.8
RPMI	24°C	0.653	0.961	1079	100	121.1						
RPMI	37°C	0.550	0.998	1049	100	79.91						

Table b.6: DLS-size measurement after two weeks of the NPs MA/FITC-core stored in PBS and RPMI at different temperature (4 °C, 24 °C, 37 °C)

MA/FITC- core week 2		PdI	Intercept	Peak 1			Peak 2			Peak 3		
Solution	Temperature			Size [nm]	Intensity [%]	Width [nm]	Size [nm]	Intensity [%]	Width [nm]	Size [nm]	Intensity [%]	Width [nm]
PBS	4 °C	0.648	0.714	707.4	100	101.3						
PBS	24 °C	0.441	0.921	757.0	100	102.7						
PBS	37 °C	0.413	0.947	656.4	100	95.72						
RPMI	4 °C	0.494	0.957	302.2	49.7	138.5	1554	42.8	781.8	4599	7.5	749.4
RPMI	24 °C	0.432	0.961	1299	93.9	310.3	127.7	6.1	16.39			
RPMI	37 °C	0.346	0.965	1813	96.4	505.1	5423	3.6	291.8			

Table b.7: DLS-size measurement after three weeks of the NPs MA/FITC-core stored in PBS and RPMI at different temperature (4 °C, 24 °C, 37 °C)

MA/FITC- core week 3		PdI	Intercept	Peak 1			Peak 2			Peak 3		
Solution	Temperature			Size [nm]	Intensity [%]	Width [nm]	Size [nm]	Intensity [%]	Width [nm]	Size [nm]	Intensity [%]	Width [nm]
PBS	4 °C	0.577	0.888	404.9	100	21.80						
PBS	24 °C	0.271	0.953	728.7	100	39.63						
PBS	37 °C	0.382	0.943	584.1	100	43.32						
RPMI	4 °C	0.462	0.943	914.6	65.4	284.0	211.5	32.1	42.32	5216	2.5	465.3
RPMI	24 °C	0.478	0.950	909.3	52.9	221.4	3794	38	898.3	208.4	9.1	26.65
RPMI	37 °C	0.645	0.959	1249	92.1	111.7	127.2	7.9	8.642			

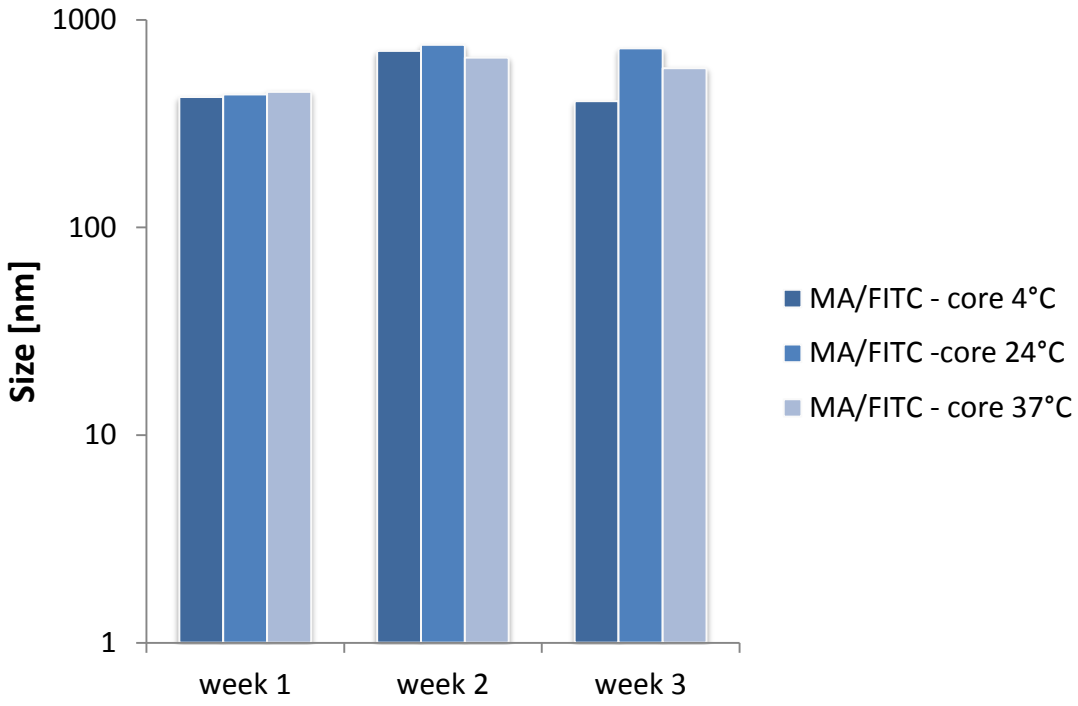

Figure b.4: Size change of MA/FITC-core NPs stored in PBS at different temperature over time

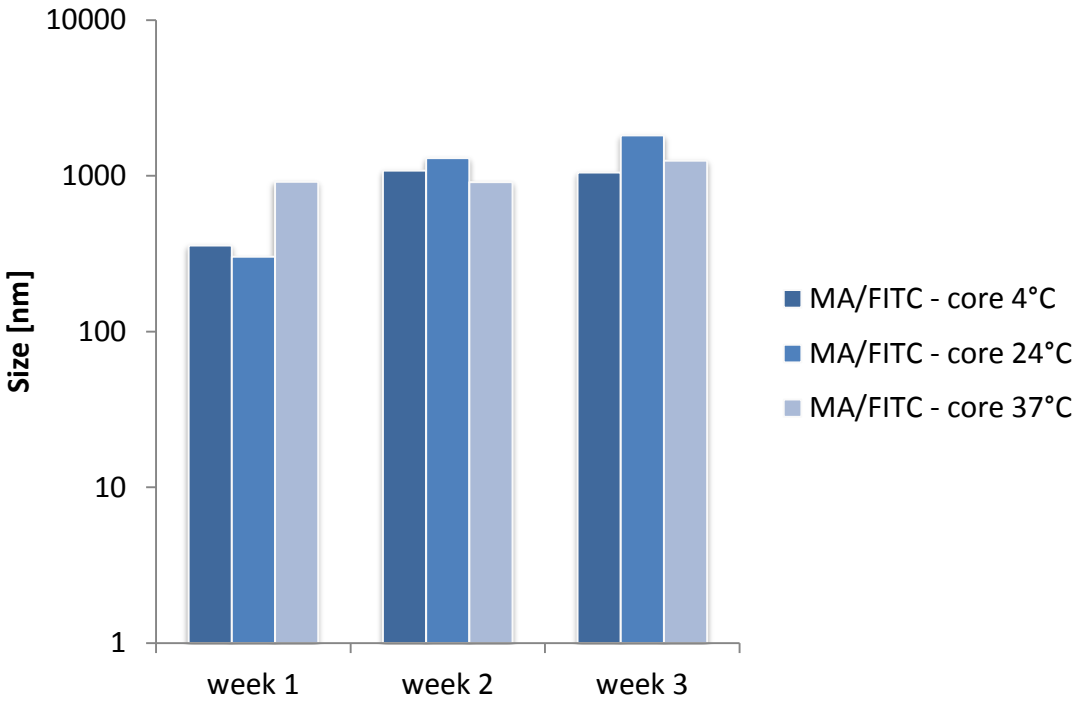

Figure b.5: size change of MA/FITC-core NPs stored in RPMI at different temperature over time

m